An-Najah National University

Faculty of Graduate Studies

SURFACE MODIFICATION OF n-GaAs SEMICONDUCTOR WITH METALLOPORPHYRIN/POLYSILOXANE MATRICES EFFECT OF MODIFICATION ON: BAND-EDGE POSITIONS, SHORT CIRCUIT CURRENT AND SURFACE STABILITY IN AQUEOUS PHOTOELECTROCHEMISTRY

By:

Muayad Masoud Mahmoud Masoud

Supervisors:

Prof. Hikmat S. Hilal, Ph. D.

&

Dr. Samar Al-Shakshir

Submitted in Partial Fulfillment of the Requirements for the Degree of Master of Science in CHEMISTRY, Faculty of Graduate Studies, at An-Najah National University, Nablus, Palestine.

2001

SURFACE MODIFICATION
OF n-GaAs SEMICONDUCTOR
WITH
METALLOPORPHYRIN/POLYSILOXANE MATRICES
EFFECT OF MODIFICATION ON
BAND-EDGE POSITIONS, SHORT CIRCUIT CURRENT
AND SURFACE STABILITY IN AQUEOUS
PHOTOELECTROCHEMISTRY

By:
Muayad Masoud Mahmoud Masoud

This Thesis was successfully defended on ***Saturday, 24 February, 2001*** *and approved by:*

Committee Members	**Signature**
1. Dr. Najeh Jisrawi	
2. Dr. Musa El-Hasan	
3. Prof. Hikmat S. Hilal, Ph.D.	
4. Dr. Samar Al-Shakshir	

Biographical sketch

Moayyad Masoud Mahmoud (Masoud) was born on September 24, 1973 in Burqa-Nablus, Palestine. In 1992, he graduated from Burqa Secondary School. In 1996, he graduated from Al-Yarmouk University (Irbid-Jordan) with the degree of Bachelor of Science in Chemistry. In 1996, he enrolled in the Graduate School at An-Najah N. University and he has been engaged in research under the supervision of Professor Hikmat S. Hilal and Dr. Samar Al-Shakshir.

Dedication

To those candles who burn themselves to enlighten my road,

to the soul of my father, to my mother, my teachers,

my brothers, my sisters,

my friends, my students,

and

to those who are looking forward to enrich their knowledge.

Muayad M. M. Masoud

Acknowledgements

The author wishes to express his sincere appreciation to his supervisors Professor Hikmat S. Hilal & Dr. Samar Al-Shakshir for their guidance, help and encouragement throughout the course work, research work and writing up.

Great thanks are extended to the teaching staff and to the technical staff in the laboratories in the Department of Chemistry at An-Najah N. University. I thank Dr. Waheed Al-Jundi for earlier help and Mr. Mahmoud Al-Shamali for continued assistance.

The author would like to acknowledge the great technical assistance of each of the following: Dr. Najeh Jisrawi, of the Physics Department of Birzeit University, Dr. Marwan Mahmoud, the director of Renewable Energy Research Centre, Dr. Subhi Kamel, of the Physics Department, and Dr. Mo'tasim Ba'baa', of the Electrical Engineering Department, all of An-Najah N. University.

I wish to express my appreciation to my colleagues at the University, especially Imad A. Harb, Ahed Zyoud & Iyad Sa'adeddin. Last, but in no way least, the patience and encouragement given to me by my family are truly appreciated.

Muayad M. M. Masoud

Nablus- An-Najah N. University

2001 A.C. – 1421 H.

LIST OF CONTENTS

CHAPTER THREE: EXPERIMENTAL

CHAPTER FOUR: RESULTS

LIST OF TABLES

LIST OF FIGURES

LIST OF APPENDICES

ABSTRACT

Semiconductor (SC) surfaces are currently being investigated as catalysts for solar energy utilization. In one of the most important applications of photoelectrochemical (PEC) cells, SCs are used as photocatslysts for water splitting. Unfortunately, there is no available SC that satisfies all the features of a good SC catalyst for PEC water splitting. Therefore, it is desired that the band edges of SC be shifted, mainly positively, to improve the charge transfer processes at the surface and to enhance the SC surface resistance against deterioration.

We have developed a new technique to tailor the positions of SC band edges. Tetra (-4-pyridyl)porphyrinatomanganese(III)sulfate (MnP), existing in the form of Mn^{III} and Mn^{II} ion mixture, was embedded into a polysiloxane polymer matrix and was attached to the surfaces of n-GaAs wafers. The n-GaAs/polymer/MnP system was annealed under nitrogen and used for photoelectrochemical study in water/$LiClO_4$ and $Fe(CN)_6^{3-}/Fe(CN)_6^{4-}$ as a redox couple. The results indicated a positive shift in the value of the flat-band potential of the SC due to the presence of the MnP. Mott-Schotky plots

indicated positive shift in the value of the flat-band potential. This was also manifested by shifting the values of the dark-current onset potential and the photocurrent open-circuit potential towards more positive values. Unlike earlier reports, the values of the short-circuit currents, measured with time of exposure, were significantly enhanced by modification. The modified surfaces were more stable, to photodegradation, than the unmodified surfaces while using high intensity illumination. The n-GaAs/polymer/MnP electrode showed higher cell efficiency than the unmodified

Chapter One

INTRODUCTION

INTRODUCTION

1.1. OBJECTIVES OF THIS WORKS

The main goal of this work is to enhance the characteristics of n-GaAs at the solid/liquid interface in photoelectrochemical (PEC) systems. The objective is three-fold: (i) to stabilize semiconductor (SC) surface to photodegradation without sacrificing the short-circuit current (I_{sc}) and efficiency, (ii) to control the positions of flat-band potentials (V_{fb}) and (iii) to enhance the current-potential plots. We are trying to innovate a new method to fulfill these enhancements.

Why n-GaAs/H_2O/$K_3Fe(CN)_6$/$K_4Fe(CN)_6$/$LiClO_4$ system ?

n-GaAs is one of the extensively studied semiconducting materials. This is due to the average value for its band gap, ~1.4 eV, and the very high electron mobility [1-2]. Despite the wide applications of n-GaAs in device manufacturing, its applications in PEC is limited by the fact that it corrodes with photocurrent (anodic corrosion) [2]. Such degradation can be lowered by using suitable redox couples. The water/$K_3Fe(CN)_6$/$K_4Fe(CN)_6$/$LiClO_4$ systems are not the best choice and are known to give poor results, in the dark and under illumination. Researchers use alternative systems for the *J-V* measurements of n-GaAs in water. Se^{2-}/Se_2^{2-} redox couples are known to give better *J-V* plots for n-GaAs electrodes. The water/$LiClO_4$/Fe^{2+}/Fe^{3+} system was intentionally employed in this work, so as to see if our modification technique is competent or not. If found to be satisfactory, it may then be employed for other SCs, such as $GaInP_2$. n-$GaInP_2$ which is a good candidate photocatalyst for light-driven water splitting into hydrogen and oxygen.

1.2. HYPOTHESIS

Covering SC surface with a polymer will affect the SC properties at the solid/liquid interface in the PEC cells in different aspects:

(1) If the polymer contains positive charges then the SC flat band potentials will be shifted toward more positive values.

(2) If the polymer contains a suitable redox couple it may behave as a catalyst for charge transfer across the SC-liquid interface. This in turn will improve the short circuit current and lower the resistance.

(3) Furthermore, this redox couple will protect the SC surface from degradation by catalyzing charge (hole) transfer to the electrolyte. The kinetics will therefore speed up hole transfer towards electrolytes rather than to SC degradation.

We expect that these enhancements can be achieved by covering the surface of the SC with thin polysiloxane film containing porphyrinatomanganese (MnP). The MnP is a mixture of complexes of Mn^{II} and Mn^{III}, acting as a redox couple. The polymer matrix will hold positive charges in the bulk. Annealing will strengthen the attachment of the polysiloxane and the positive charges to the SC surface. The resulting coated SC will then be employed in photoelectrochemical cells.

Chapter Two

FUNDAMENTALS & HISTORICAL BACKGROUND

FUNDAMENTALS & HISTORICAL BACKGROUND

World annual consumption of energy is enormous and tends to double every 15-20 years [3]. The main energy sources, fossil fuels are recognized as limited reserves. Thus search for *alternative sources of energy* indeed becomes urgent.

The sun light is usually converted into chemical energy stored and used to synthesize biological materials and a huge amount of energy, about ten times today's energy needs of mankind, is stored every year through photosynthesis in green plants and bacteria.

Chemical means used to convert sunlight into electricity and fuels, offering good opportunities for solving energy problem, are so called *photoelectrochemical* **(PEC)** methods. They can generate electricity directly from sunlight, produce fuels like hydrogen from water or synthesize important industrial chemicals like alcohols, ammonia and amino acids more cheaply using sunlight to drive this synthesis in PEC cells [3].

2.1 FUNDAMENTALS OF PEC

PEC processes can be performed by making a semiconductor (SC) electrode that is in contact with electrolytic solution absorb solar radiation directly. The electrode will thus be excited and will react with the solution. When n-type SC electrode is brought in contact with an electrolytic solution, equilibrium takes place at the interface resulting in space charge layer (SCL) formation. Electronic energy bands are thus bent upward, Fig. (2-1).

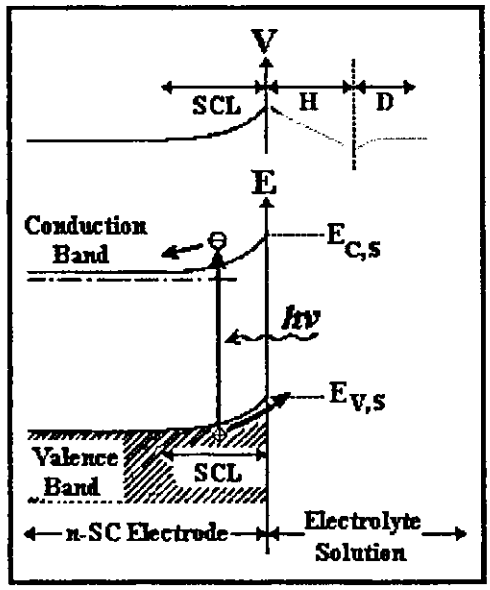

Figure (2-1): Electrical potential drop across SC/electrolyte interface and band bending in n-type SC. The upper curve shows the electrical potential across the interface. SCL = space charge layer; H = Helmholtz layer; D = diffusion layer. $E_{c,s}$ and $E_{v,s}$ mark the surface energies of the conduction and valence band edges respectively.

If the SC electrode receives photons with energy greater than its band gab (E_g), electron-hole (e^--h^+) pair will be generated within the SCL. In the case of n-type SC, the generated electric field drives photogenerated holes toward the interface. The electrons are driven toward the interior (bulk) of the electrode. By joining a SC electrode with a suitable counter electrode a PEC cell is constructed, Fig. (2-2).

Thus, a PEC cell is defined as one *in which the irradiation of an SC electrode/electrolyte system produces a change in the electrode potential (on open circuit) or in the current flowing in the external circuit (under short-circuit conditions)* [4].

If a redox couple (Ox/Red) is present in the electrolytic solution, the holes oxidize the Red to Ox on the SC surface. In contrast, the electron reaching the metal counter electrode may reduce Ox' to Red' of another redox couple (Ox'/Red'). When the redox potential E(Ox/Red) is positive of $E(Ox'/Red')$ the net result of the PEC process: $\text{Red} + \text{Ox}' \rightarrow \text{Ox} + \text{Red}'$ is thermodynamically uphill reaction leading to the storage of chemical energy, Fig. (2-2a).

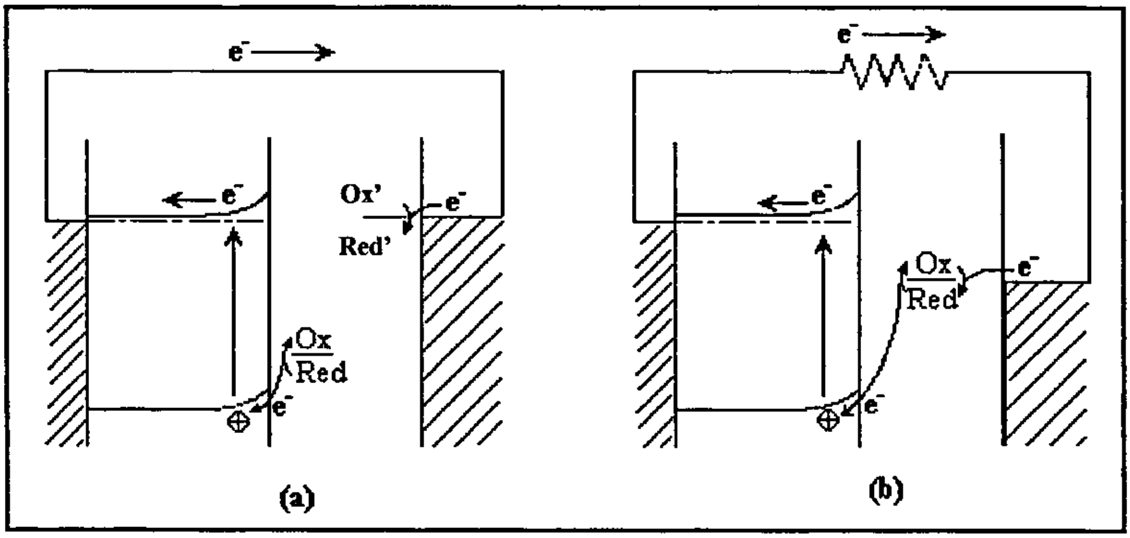

Figure (2-2): Operational principles for the two types of PEC cells: (a) photoelectrolytic cell and (b) regenerative photovoltaic cell.

In contrast, when a common redox couple is reacting at both the photoanode and the metal cathode, no net chemical energy storage occurs, but electrical energy can be withdrawn in the external circuit. This type of PEC cell is called a regenerative cell, Fig. (2-2b) [5]. It is also called photovoltaic (liquid-junction solar) cell. It is like any electrochemical cell in configuration, except that SCs are used as electrode instead of metals. The use of SCs as electrodes in PEC cells for generation of electricity has certain advantages over metals, such as:

(a) Higher quantum efficiencies for electron flow in the external circuit are obtained.

(b) The longer lifetime of the photogenerated electron-hole pairs in SCs allows redox reaction to compete effectively with electron-hole recombinations.

(c) For SCs, the potential drop occurs mainly in the depletion layer and not in the Helmholtz double layer as for metal electrodes.

(d) SCs allow considerable scope for modifications of their conductivity type and behavior by doping, and surface treatment, *etc.*

(e) Metals are not suitable here because they dissipate the light energy they absorb as heat.

2.1.1. How dark current occurs?

The dark current results from the electron transfer from the SC CB to the solution redox couple. At equilibrium, the band bending creates an energy barrier for the electrons to overcome before they transfer. For any given SC and electrolyte, there exists a unique potential for which the potential drop between the surface and the bulk of the electrode is zero (no SCL). This potential is called the flat band potential (V_{fb}), since the band edges do not bend. Thus, for dark current to occur, the n-type SC must be negatively biased to provide the electrons with enough energy to overcome the barrier, equals ΔE_1, Fig. (2-3).

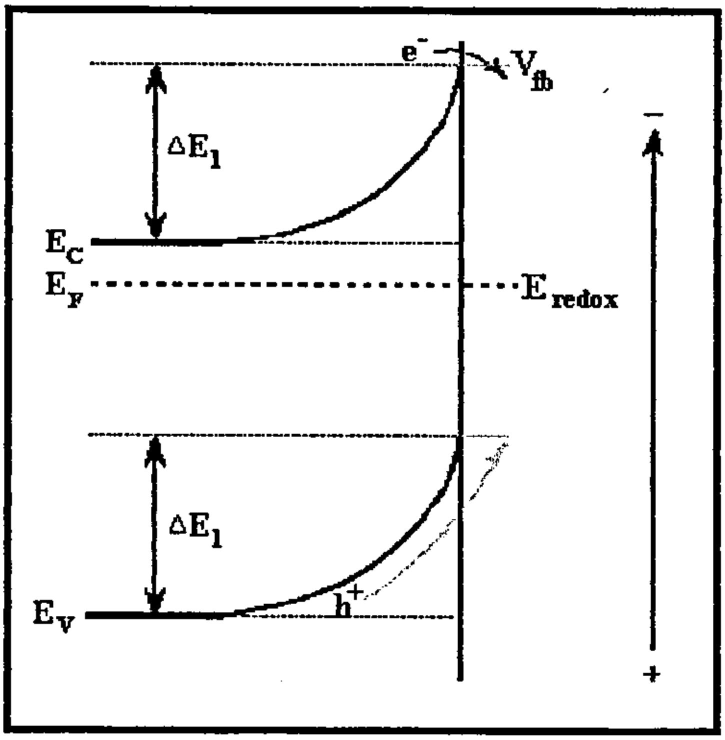

Figure (2-3): Darkcurrent for n-type SC

2.1.2. Photocurrent

When light absorption generates a population of excited holes and electrons, the majority carrier concentration changes relatively little and the minority carrier concentration is greatly enhanced. Hence photo-effects are greatest when minority carriers dominate the electrode response. This occurs when the electrode is biased to form a depletion layer and the photo-generated minority carriers migrate towards the electrode/electrolyte interface.

The SC exhibits a threshold response to photon energy dictated by the band gap energy. The photo-effects switch on as the wavelength of incident light decreases below E_g; above E_g the electrode is relatively insensitive to light. The dependence of the photocurrent or photopotential on excitation wavelength provides information about the E_g. Another important phenomenon to the photo-effect is *recombination*. The excited hole and electron annihilate one another with the evolution of heat or a photon. Recombination can occur directly with the electron descending from the CB to the hole at the VB edge, or indirectly via an intermediate energy level (bulk or *surface state*). The indirect mode of recombination can be particularly effective because the intermediate energy level can capture the hole and electron sequentially, with some delay between the two events. Recombination reduces the magnitude of the photo-effects, and is therefore the bane of solar energy conversion.

When n-type SC electrode is biased sufficiently positive of V_{fb}, the dark currents are very low due to the blocking effect of the depletion layer. Upon irradiation of the SC through the electrolyte with light ($\lambda < \lambda_{bg}$), large anodic photocurrents appear, Fig (2-4).

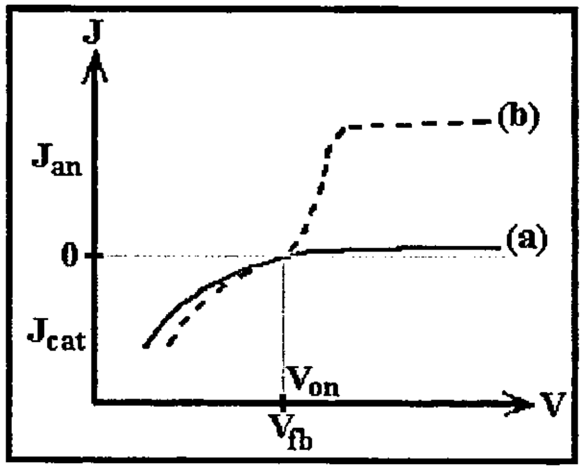

Figure (2-4): Dark and photocurrent voltammogram for an n-type SC. J_{an} = anodic current density; J_{cat} = cathodic current density; (a) dark current density; (b) photocurrent. V_{on} is arbitrarily chosen to equal V_{fb}.

These photocurrents arise from the flux of holes (minority carriers) arriving at the surface. After light absorption generates an electron-hole pair in the depletion layer, the electric field in the depletion layer separates the two charge carriers, with the electron moving toward the bulk of the crystal and the hole migrating toward the surface, Fig. (2-5). Electron-hole pairs generated beyond the depletion layer also diffuse into the electric field and become separated. The holes have an oxidizing power roughly equivalent to the potential of the VB edge at the surface ($V_{v,s}$), and are capable of oxidizing a Red molecule whose formal potential is more negative than $V_{v,s}$, Fig (2-1).

The shape of the photocurrent voltammogram depends on (1) the energy distribution of the incident photons, (2) the absorption coefficient of the SC, (3) the diffusion distance of the excited hole and electron, and (4) the recombination rates.

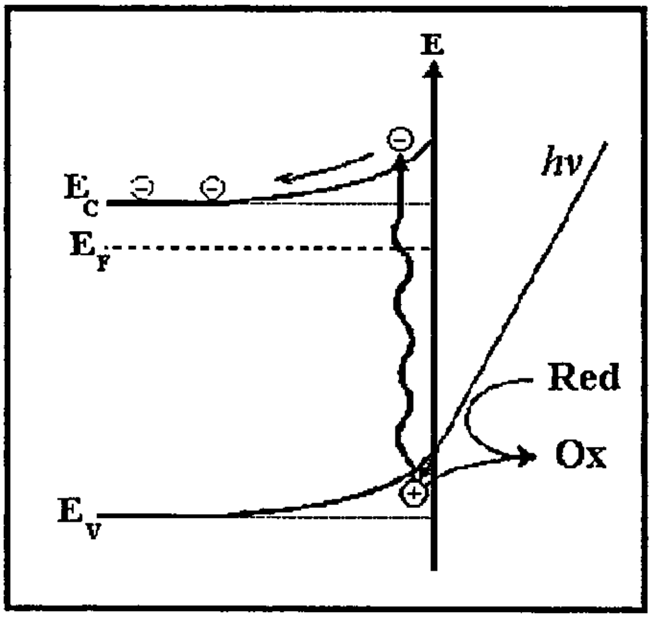

Figure (2-5): Photocurrent generation at an n-type SC. $V > V_{fb}$; a depletion layer is formed. Photogenerated holes move to the surface and oxidize solution reductants.

As the applied potential approaches V_{fb}, the SCL thickness decreases. Recombination rates increase because the holes and electrons are no longer being separated by electric field. The photocurrent drops sharply and merges with the dark current near V_{fb}. At potentials negative of V_{fb} the electrode is no longer blocking, so the dark current increases dramatically. A small cathodic photocurrent is sometimes observed, but the effect is usually minor because photo-excitation does not significantly increase the surface concentration of electrons.

2.1.3 The Mott-Schottky (M-S) plots:

One of the most common methods for measurement of the V_{fb} is the M-S plot. It is based on the capacitance associated with SCL. Each of the regions around the electrode/electrolyte interface [the diffusion layer (D), the Helmholtz layer (Hz), and the SCL, Fig (2-1)] are planes of charge separated by distance, and hence have associated capacitance. The three capacitors are in series, so the smallest one dominates the total capacitance according to the equation:

$$\frac{1}{C_{total}} = \frac{1}{C_{Hz}} + \frac{1}{C_D} + \frac{1}{C_{SC}}$$

In concentrated electrolytes the diffusion capacitance (C_D) is so large that it can be completely ignored. The Helmholtz capacitance (C_{Hz}) is in the order of 10 to 100 $\mu f/cm^2$. The measured capacitance (C_{total}) is small relative to C_{Hz}, and can be assigned to the SCL (C_{SC}). In the depletion region, the space charge capacitance varies with the width of SCL, which in turn is a function of the potential relative to the V_{fb}. The M-S equation incorporates these factors in a convenient linear form:

$$\frac{1}{(C_{SC})^2} = \left(\frac{2}{q N_d \varepsilon \varepsilon_o}\right)\left(|V-V_{fb}| - \frac{kT}{q}\right) \quad \ldots\ldots\ldots\ldots \quad [6-7]$$

where:

C_{sc} : space charge capacitance per unit area ≈ measured capacitance (F/cm^2)

q : electronic charge $=1.6X10^{-19}$ C

N_d : the carrier concentration (practically equals the donor concentration)

ε_o : the permittivity of vacuum $=8.854X10^{-12}\ C^2\ N^{-1}\ m^{-2}$

ε : the dielectric constant of the semiconductor

V : the electrode potential

V_{fb} : the flatband potential

k : Boltzmann constant $= R/N_A = 1.3807X10^{-23}$ (J/K)

T : absolute temperature (K)

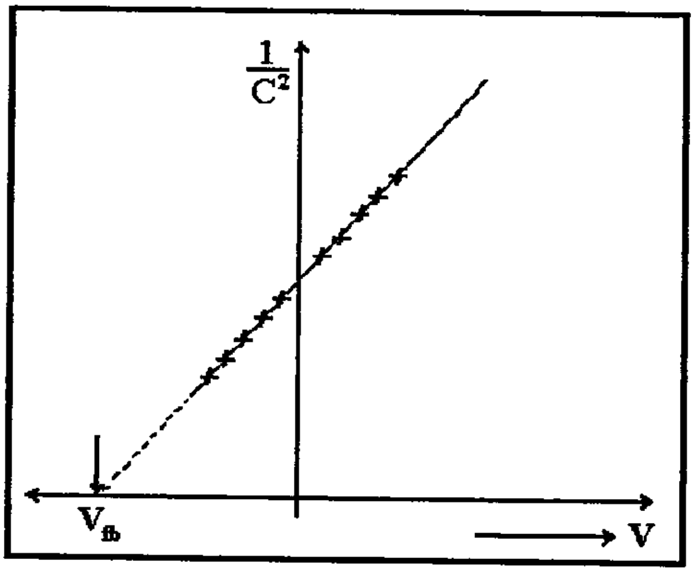

Fig. (2-6): M-S plot, the reciprocal square of the capacitance per unit area is plotted vs. the potential. The intercept is V_{fb} + 0.026 V. The slope contains information about the doping level.

The reciprocal square of the capacitance per unit area is plotted vs. the potential, Fig (2-6). As far as charge carrier concentration is constant a straight line should be obtained in the depletion region. The potential intercept of this line equals V_{fb} + 0.026 V. The accuracy of this technique (±0.05Vfor a series of determinations) is such that kT/q term is frequently ignored. The slope contains information about the doping level; all of the charge is in the depletion layer is assumed to originate from ionized donors or acceptors. The M.-S. plot should remain linear as long as the SCL is a depletion layer.

Special electronic techniques have been developed to measure the value of C_{SC} as shown in literature [6-8]. Details of electronic circuit are beyond the scope of this work.

2.2. APPLICATIONS OF PEC

2.2.1. Light-to-electricity conversion

Electricity is generated in the *photogalvanic* cell from the solar energy either directly or by storage of the energy as chemical energy for subsequent generation of electric power. Lichtin defined *Photogalvanic* cell as *a battery in which photoexcitation of chemical species in a solution results in charge transfer reactions at the electrodes with a subsequent generation of electrical power.*

On the other hand, the *photovoltaic* (PV) cells are most extensively studied as solar energy converters. As shown earlier, the generation of the *photovoltage* here involves the following steps:

a- The absorption of light quanta with energies equal to or greater than E_g.

b- Electron transfer from the *valence band* (VB) to the *conduction band* (CB) leaving a hole in the valance band. Thus, each absorbed quantum of light generates one electron-hole pair.

c- Photogenerated *electron-hole* pair are separated with some built-in electric field within the cell resulting in the photovoltage/photocurrent.

PV cells have many different kinds according to the manner in which the last step is achieved. The common types involve solid-solid (p-n) junctions and solid-liquid junctions that involve PEC cells.

Potentially, there are several advantages for the use of PEC cells for solar energy conversion over conventional PV devices: (a) PEC devices can store energy in the form of conventional fuel and can convert light to electrical energy as well, (b) PEC devices can be fabricated with considerable ease. Contrary to

PV devices, no solid-solid junctions are demanded in PEC. The band bending characteristics of the SC can be conveniently varied by suitable choice of electrolyte and cell variables, (c) PEC cells do not have problems associated with different thermal expansions of solid-solid junction, and (d) unlike PV devices, no antireflection coatings are required in PEC cells. Absorption of light by the electrolyte solutions and reflection losses from the cell however do limit the energy conversion efficiencies in PEC devices in many cases and are shortcomings of PEC systems [9].

2.2.2. Light-driven chemical reactions

We present here two important applications of solar light in driving chemical reactions.

A) Light-Driven Water Purification Processes

Water purification with solar light demands SC materials with certain features, namely: (1) large E_g with high oxidizing power. (2) Inert surfaces. (3) Nontoxic and environmentally nonpolluting. (4) Low cost. Therefore, TiO_2 is an excellent photocatalyst for such purposes, because it exhibits all these features. Table (2-1) lists some examples of photodegradation reactions studied in water purification systems:

Table (2-1): Examples of light-driven water purification systems showing examples of degraded pollutants:

pollutant class	Pollutant example	catalyst	light nature	degradation reaction product	references
haloalkanes	CH_2Cl_2, $CHCl_3$, CH_2ClCH_2Cl, $CH_2ClCOOH$, $CHCl_2COOH$	TiO_2	385 nm, near UV	HCl, CO_2	[10,11]
	bromomethanes	TiO_2 Degussa P25	340-400 nm	formaldehyde, formic acid	[12]
Haloalkenes	trichloroethylene	coated TiO_2 glass beads	365 nm		[13]
	$CHClCCl_2$, CCl_2CCl_2				[11]
Haloaromatics	2-chloro- and 2-nitrophenol	TiO_2 suspension	365 nm	HCl, CO_2, H_2O	[11,14]
Surfactants	sodium dodecylbenze sulfunate (DBS), sodium benzene sulfunate (BS) sodium dodecyl-1-sulfate	TiO_2			[11]
sulfur compounds	2-mercaptoethanol & sodium thiosulfate	soluble metal phthalocyanine complexes, such as zinc(II) 2,9,16,23-phthalocyanine tetrasulfonic acid, zinc(II) 2,9,16,23-phthalocyanine tetracarboxylic acid and zinc(II) 2,9,16,23-tetrakis(8-quinolineoxy-5-sulfonic acid)- phthalocyanine			[15]
	sulfide and ethanethiol	cobalt (II) 2,9,16,23-tetrasulphocyanine and cobalt (II) 2,9,16,23-tetra(chlorosulphonyl)phthalocyanine covalently bonded to a TiO_2 matrix, from $Ti(O^tPr)_4$, by sol-gel processing	halogen lamp	elemental sulfur & thiosulphate	[16]
	sulfur oxoanions ($S_2O_3^{2-}$, $S_4O_6^{2-}$, SO_3^{2-})	water soluble porphyrin complexes (Co 2-TMPyP , Mn 4-TMPyP, Fe 2-TMPyP)	419 nm		[17]
	polynuclear heterocyclic sulfide	TiO_2 suspension acetonitrile	Hg lamp	sulfoxides & sulfones	[18]

Table (2-1): .... Cont.

pollutant class	Pollutant example	catalyst	light nature	degradation reaction product	references
Dyes	rhodamine B (N, N, N', N'-tetra ethylrhodamine, RB)	air-saturated TiO_2 colloidal solution	visible & UV		[19]
	Malachite Green (MG)	Fe^{3+}/H_2O_2 or Fe^{3+}/H_2O_2 system	>470		[20]
phenols	4-nitrophenol	TiO_2 (anatase) supported on TiO_2 (rutile) or Al_2O_3	Xe lamp		[21]
	phenol	aqueous suspension of TiO_2 with: O_2 Ag^+ H_2O_2	near-UV (365 nm)	- Catechol, hydroquinone & 1,2,4-hydroxybenzene - *p*-benzoquinone - obove + ring opening	[22,23]
	phenol	Mixing TiO_2 with activated carbon	340 nm	Hydroquinone, catechol, p-benzoquinone & resorcinol	[24]
	phenol	TiO_2 powder immobilized on solid support substrates (stainless steel, titanium alloy, titanium metal, and tin oxide coated glass) then titanium metal was electrochemically anodisated and annealed to give a thin film of TiO_2 on	>300 nm		[25]
	pentachlorophenol	TiO_2 with oxidants: $S_2O_8^{2-}$ HSO_5^- (oxone) and H_2O_2	UV		[26]
other organic compounds	aniline	TiO_2 Degussa P25	Hg lamp	TOC removal	[27]
	salicylic acid	TiO_2 Degussa P25	300-700 nm		[28]
inorganic pollutant:	nitrate.	titania and humic acids	Xe lamp	nitrite	[29]
	Cr(VI) ion	-ZnO suspension -ZnO, WO_3	UV/vis Hg lamp	Cr(III) ion	[30]
	oxalate ion & copper ion	TiO_2 immobilized on Ti alloy	300-400 nm	CO_2 + Cu	[31]

B) Light-Driven Water Splitting

i) Thermodynamic considerations

The electrolysis of water proceeds by the combination of two half-cell reactions:

$$2H^+_{(aq)} + 2e^- \rightarrow H_{2(g)} \quad \ldots\ldots\ldots\ldots(1)$$

$$H_2O_{(l)} - 2e^- \rightarrow \tfrac{1}{2}O_{2(g)} + 2H^+_{(aq)} \quad \ldots\ldots(2)$$

to result in an overall process of:

$$H_2O_{(l)} \rightarrow H_{2(g)} + \tfrac{1}{2}O_{2(g)} \quad \ldots\ldots(3)$$

In this process, solar light is stored as chemical energy, in the form of H_2 fuel. Such a fuel is environmentally clean and non-polluting. Therefore, PEC driven water splitting is a very important topic for research and application.

This reaction is endothermic, requiring 285.8 kJ to degrade one mole of water. In the electrochemical scale, the difference in free energy for Eqs. (1) and Eqs. (2) amounts to 1.23eV per electron. Hence the minimum energy required for the overall process, Eqs. (3), is 2.46 eV per H_2O molecule. Thermodynamically water oxidation proceeds only at E > +0.7V versus SCE (at pH=4.7) [32]. In photoassisted water splitting, the driving force for electrons to transfer is the light energy, Fig. (2-7).

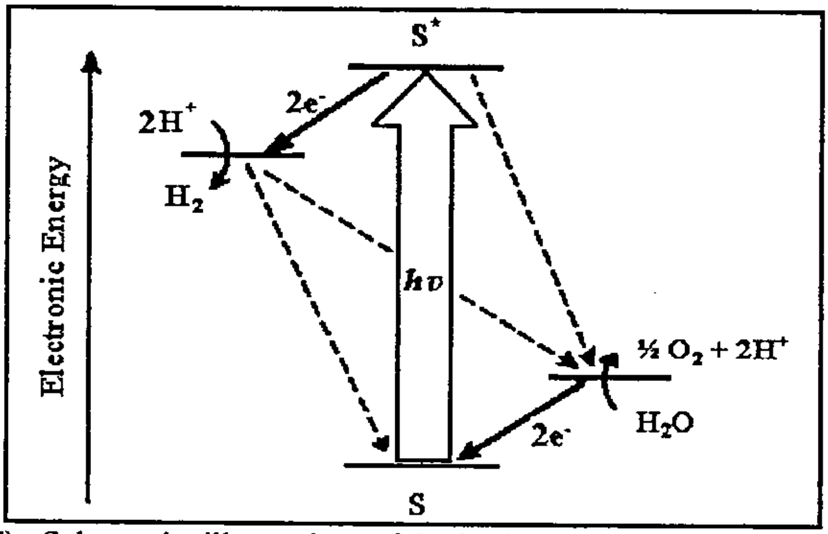

Figure (2-7): Schematic illustration of the basic principle of photoassisted water splitting. The solid arrows represent the vectorial flow to be promoted, whereas the broken arrows denote the recombination paths to be suppressed.

ii) Fundamentals of Light-Driven Water Splitting in PEC

The flow of electrons is mediated by a sensitizer (S), including: (1) SC electrodes, (2) particles, (3) colored redox species such as dyes and metal complexes, and (4) colored redox species adsorbed on SC electrodes. It is important to effectively suppress the energy-wasting electron-hole recombination processes, indicated by the broken lines, Fig. (2-7). Due to the chemical stability of TiO_2 continuous water splitting is possible with such a PEC cell at wavelengths shorter than 415 nm for a very long period (of the order of years).

In SC systems, the initial charge separation is particularly favored by the presence of Schottky barrier or SCL formed at the SC-solution interface, Fig. (2-1). When the SC electrode receives photons with energy greater than its E_g, the electron-hole pair will be generated within the SCL. In n-type SCs, the generated electric field drives the holes toward the interface. Here, in case of water splitting a redox couple $\{(\frac{1}{2}O_2+2H^+)/(H_2O)\}$ is present in the electrolytic solution, the holes oxidize (H_2O) to ($\frac{1}{2}O_2+2H^+$) on the SC surface. In contrast, the electron reaching the metal counter electrode may reduce (H^+) to ($\frac{1}{2}H_2$) of another redox couple $\{(2H^+)/(H_2)\}$. As shown in Figure (2-2a) (noting that Red=H_2O, Ox=$\frac{1}{2}O_2+2H^+$, Ox'=$2H^+$, Red'=H_2). The possibility of solar photoelectrolysis of water was demonstrated for the first time with a system in which n-TiO_2 electrode was connected to platinum black electrode, the former exposed to near-UV light. The photoanodic reaction has been confirmed to be the oxidation of water leading to oxygen evolution:

$$2H_2O + 4h^+ \rightarrow 4H^+ + O_2$$

iii) ***Requirements for Efficient Water Splitting PEC Cells***

Table (2-2) summarizes the semiconducting materials that have been investigated for the photoassisted decomposition of water in PEC systems [33].

Table (2-2): SCs Investigated in PEC cells for water photoassisted decomposition

Semiconductor	Conductivity type	Bandgap (eV)	Bandgap (nm)	Stability
Ge	*n*-, *p*-	0.66	1880	Unstable
Si	*n*-, *p*-	1.1	1128	Unstable
GaAs	*n*-, *p*-	1.35-1.43	868-919	Unstable
CdTe	*n*-, *p*-	1.5	827	Unstable
CuO	*p*-	1.7	730	Unstable
CdSe	*n*-	1.74	713	Unstable
Cu_2O	*p*-	2.2	564	Unstable
Fe_2O_3	*n*-	2.2	564	Fairly stable
V_2O_5	*n*-	2.23	556	Unstable
GaP	*n*-, *p*-	2.25	551	Unstable
CdS	*n*-	2.4	517	Unstable
WO_3	*n*-	2.7	459	Stable
Bi_2O_3	*n*-, *p*-	2.8	443	Unstable
TiO_2	*n*-	3.0	413	Stable
ZnO	*n*-	3.2	388	Fairly stable
$BaTiO_3$	*n*-	3.3	376	Stable
$SrTiO_3$	*n*-	3.4	365	Stable
$KTaO_3$	*n*-	3.5	354	Stable
SnO_2	*n*-	3.7	335	Stable

Suitable SC catalyst for photochemical splitting of water must have the following important features:

542652

(a) Extreme resistance to photocorrosion. Many SCs are known to behave as photoanodes on which oxygen evolution occurs. The oxygen gas should not come from the decomposition of the photoanode itself. A redox reaction having a more negative redox potential will occur by the action of holes in precedence to a redox reaction that has more positive redox potential. Materials that have good stability in PEC cells such as TiO_2, $SrTiO_3$, WO_3, SnO_2, $BaTiO_3$, $KTiO_3$, Fe_2O_3, ...etc. electrodes have more positive decomposition potential than water oxidation. In contrast, in the case of ZnO electrode, the potential for water oxidation is more positive than of the decomposition of potential of the SC. Hence, ZnO undergoes dissolution under illumination.

(b) An optimum value of the band-gap energy corresponding to the most efficient use of sunlight, ~ 1.5 - 2.0 eV. Even when photons are completely absorbed a portion of the photon energy ($E > E_g$) is not utilized because vibrational relaxation takes place in the excited state before charge separation. Thus the fraction $(E-E_g)/E$ of the photon energy is dissipated as heat. Materials such as GaAs (1.4 eV), CdTe (1.5 eV), CuO (1.7 eV), and CdSe (1.74 eV) have close to ideal band-gap values, but they are not stable [34-35].

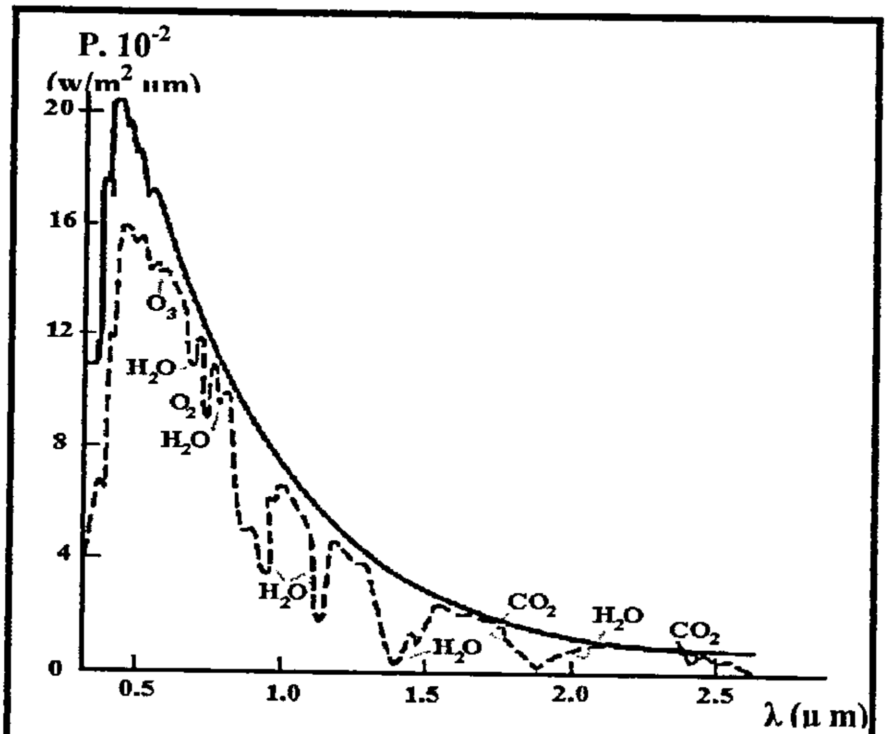

Figure (2-8): Spectrum of sunlight Solid line-beyond the terrestrial atmosphere; dashed line-at the earth's surface. The components of the earth's atmosphere responsible for the strong absorption of light are shown on the curve [34].

Figure (2-8) provides primary information about the solar energy spectrum available of conversion.

(c) Suitable bandedge position: With regard to an n-type SC photoanode the more negative CB E_{fb} leads to more efficient output characteristics of a PEC cell. When E_{fb} is situated negative of the hydrogen evolution potential, photogenerated electron reaching the counter-electrode can reduce protons to result in hydrogen evolution under no applied bias. $SrTiO_3$ and $KTiO_3$ satisfy this condition. In the case of TiO_2 photoanode, the E_{fb} is somewhat positive of hydrogen evolution potential. Hence it's necessary to apply an external bias or equivalently a chemical bias provided by a pH difference between the anolyte and catholyte, or by using p-type SC photocathode in place of a metal electrode. On the other hand, the VB E_{fb} must be more positive than water oxidation potential. Therefore, n-GaAs can not oxidize water, where as TiO_2 and CdSe can do so.

(d) High quantum efficiency: In order to construct an efficient PEC cell the quantum efficiency (the number of electrons flowing from the PEC system per one absorbed photon) should be high, ideally 100%, i.e. it is desirable that the incident photon be totally absorbed within SCL, Fig. (2-9).

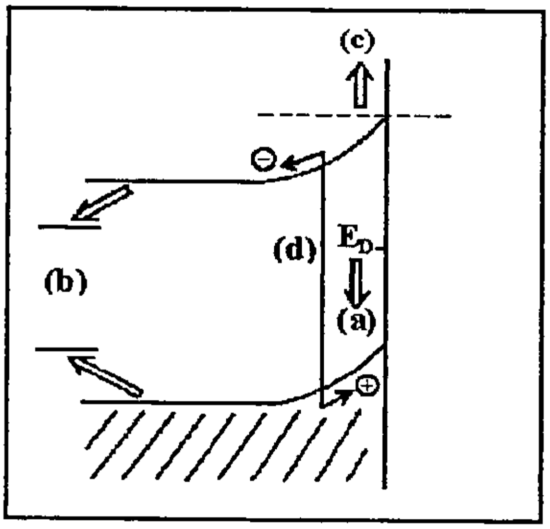

Figure (2-9): Favorable characteristics of a semiconductor photoanode for use in (PEC) cell: (a) long term stability, (b) smaller band gap, (c) Suitable band edges position, and (d) high quantum efficiency.

(e)Rapid charge transfer kinetics to the electrolyte.

2.3. Technical Difficulties of Existing PEC Cells

Until so far, no SC that combines these features has been found. Controlling the SC characteristics at the solid/liquid interface, associated with PEC studies, is one potentially important objective. Shifting the positions of the flat-band potential is important for PEC applications, *viz.* the position of the CB and the VB edges determines the energetics and the kinetics of charge transfer at the solid/liquid interface. This in turn will affect the ability of the SC surface to oxidize or reduce other chemicals in contact with it.

Unfortunately, materials that are stable in PEC cells have band-gaps that are too large. This results in a utilization of only a small portion of the solar spectrum and a consequent decrease in energy conversion efficiency [36]. Attempts to achieve high visible-light response with these stable materials, by doping, suffered principally from low efficiency of minority charge carrier generation. In contrast, materials have close to ideal band-gap values are electrochemically unstable in contact with aqueous electrolytes. Stabilization of the surfaces of these materials, to photodegradation, is a focal area of interest to researchers.

2.4 ENHANCEMENT OF EXISTING PEC CELLS

Researchers look for ways to solve out such difficulties. While doing so, researchers concentrate their efforts on:

(a) Shifting the flat-band potentials of a given SC. This can be achieved by attaching charged ions to its surface. Positive charges should cause a positive shifting in the value of the flat-band potential, whereas negative charges should yield a negative shifting.

(b) Stabilizing the low E_g SC surfaces. CdS, CdSe, CdTe, GaP and GaAs have been stabilized by different techniques. The **stabilization coefficient** for a given SC is defined as *the fraction of the photocurrent associated with the oxidation of the redox couple over the total photocurrent.* This coefficient is light-intensity dependent. The value of this coefficient determines the direction in which the generated holes will go. This in turn will decide the preferences of the competition between the SC-photocorrosion and the photooxidation of redox couples in solution [36].

2.4.1. SC photocorrosion prevention

Different techniques have been suggested to prevent SC photocorrosion. Five examples are listed here [37]:

1) The choice of the best kind SC for the reaction (redox potential relative to band edges): The characteristics of energy levels of the SC and its critical decomposition potential on a common energy scale are shown in Figure (2-10).

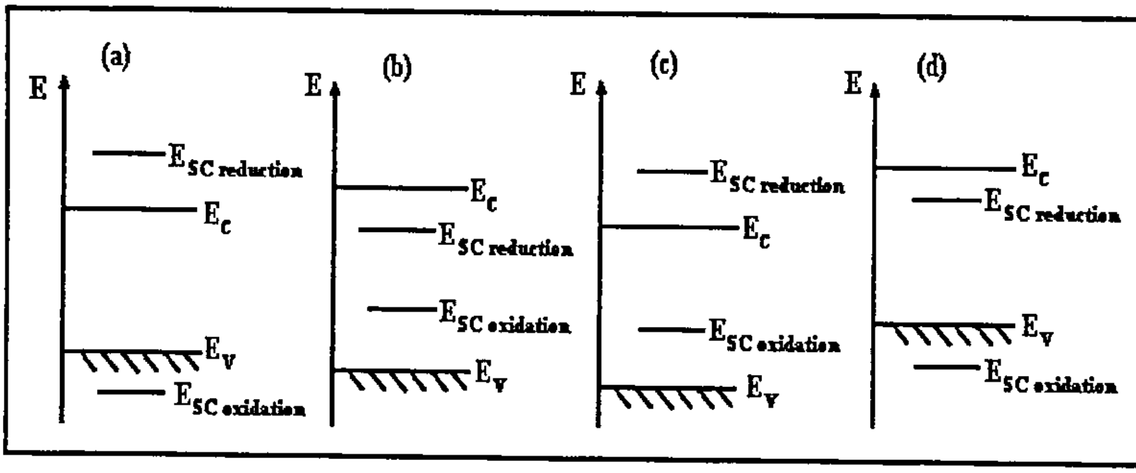

Figure (2-10): The characteristics of energy levels of the SC and its critical decomposition potential.

Figure (2-10) gives an indication of the thermodynamic stability of the electrode system. Figure (2-10a) shows the case when the Fermi energy levels for SC decomposition is located within the energy band of the SC. Decomposition is possible only if the electrode is polarized to such an extent that degeneracy occurs at its surface. Figure (2-10b) illustrates the case where the SC is unstable against both anodic and cathodic decomposition. Figure (2-10c) shows the case where the Fermi level for SC oxidation by holes is located inside the band-gap while the Fermi level for SC reduction is located within the conduction band. In this case the SC is stable against cathodic decomposition (reduction) but will decompose anodically (oxidize) at a certain critical illumination density. This decomposition can be prevented by the addition of electrolyte of a redox couple whose Fermi level is above $E_{SC\ oxidation}$. The redox reaction is effective as long as the concentration of electron donor at the interface remains high enough to capture the holes before they induce the decomposition reaction. This also implies that the rate of hole transfer in the redox reaction has to be fast [38]. In the case of the n-GaAs/1M KOH+1M (Se^{2-}/Se_2^{2-}) cell a high surface state density ($\sim 10^{13}$ cm^2), located at 0.4eV below the conduction band, was responsible for a shift of the band edges under illumination. This reduced the maximum theoretical open-circuit voltage by 300-400mV. It was apparent that the performance (efficiency) of the cell was limited by this shift and by charge transfer kinetics at the SC-electrolyte interface [36,39]. The situation shown in Figure (2-10d) holds for a p-type SC that is stable against anodic photodissolution (oxidation). In this case, cathodic photodecomposition (reduction) can be prevented by a redox couple with Fermi level below $E_{SC\ reduction}$ [38]. In p-type III-V SC electrodes, surface states act as recombination centers for electrons generated by light; surface recombination has been shown to compete effectively with charge transfer from the conduction band to various oxidizing agents in solution. The charge localization in surface states is important, and the considerable changes in Helmholz potential, that result from trapping, help to account to V_{fb} required for the onset of the photocurrent. Surface states also offer an alternative path for electron transfer to the solution. This is especially the case when the standard potential of the redox couple corresponds to the lower part of the SC band gap, even for systems with more negative redox potential, the surface-state contribution to the photocurrent may not be neglected. This is especially the case if charge localization at the surface, as a result of illumination, leads to a displacement of the SC band edges [40].

Figure (2-11) shows the energy diagram for TiO_2 and redox potentials for water oxidation and hydrogen reduction [41].

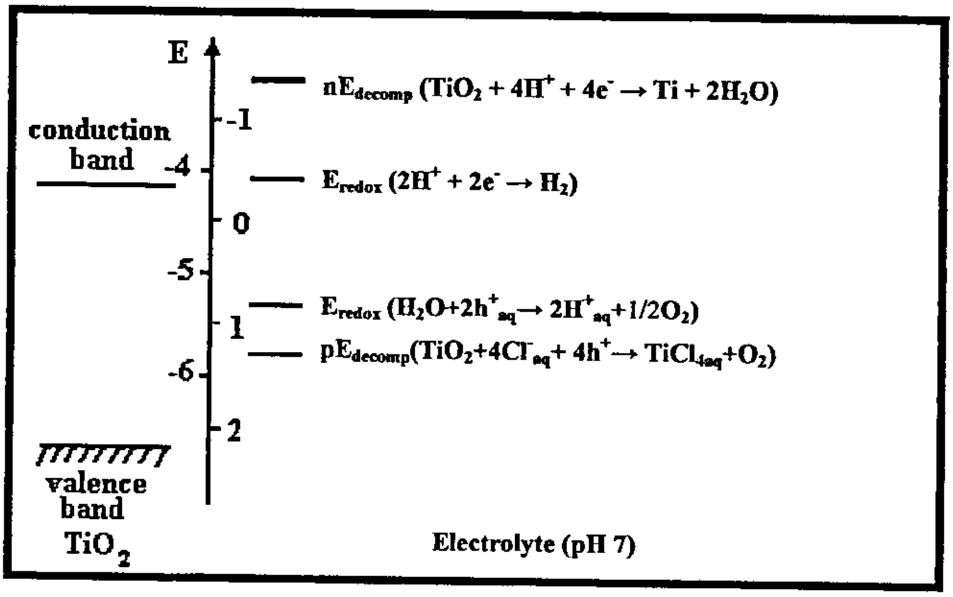

Figure (2-11): Energy correlation between band edges and the Fermi energies of electrode reactions for TiO_2 in aqueous solution of pH=7.

The anodic decomposition potential for crystal is below the energy level for water oxidation. This illustrates the extreme stability of the TiO_2 system and its effectiveness as a photoassistance agent for the decomposition of water. The situation for CdS system is shown in Figure (2-12).

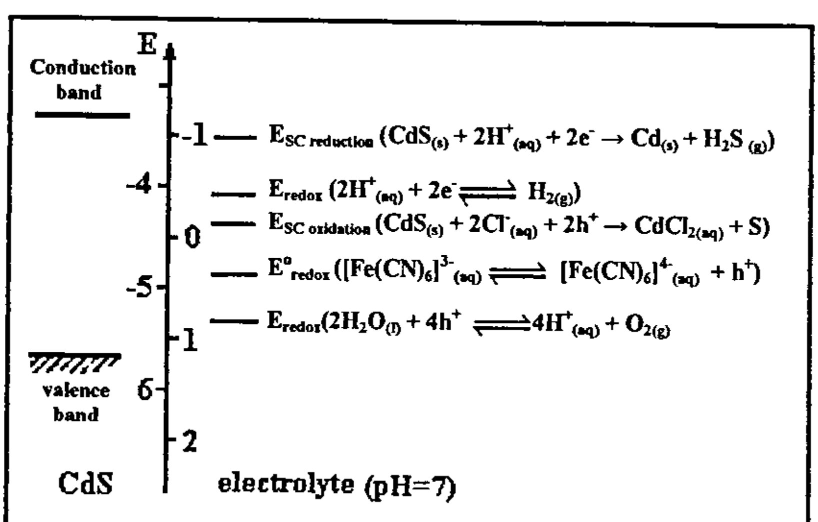

Figure (2-12): Energy correlation between band edges and the Fermi energies of electrode reactions for CdS in aqueous solution of pH=7.

The anodic photodissolution (oxidation) of CdS would occur at low illumination intensity levels. Gerischer proposed kinetic reason for short-term stabilization of CdS photoanodes in terms of the high activation energy of the formation of radical intermediate for the photodissolution process. In contrast to this process, the electron transfer from $[Fe(CN)_6]^{4-}$ to the semiconductor surface was postulated to require low activation energy, and thus favored to decomposition reaction [42].

2) Use of non-aqueous electrolyte: The CH_3CN-dissolved I_3^-/I^- system showed several favorable features. High conductivity, high redox solubility and ability to provide sustained anodic photocurrent on n-GaAs have been observed. However, I_3^- absorbs light and undergoes high degree of polarization of the reaction: $I_3^- + 2e^- \rightarrow 3I^-$ at the counter electrode. This requires (i) cell structure that employs either large or electrocatalytic counter electrodes for I_3^- reduction to minimize the required I_3^- concentration, (ii) a cell with enhanced mixing due to convection or mechanical circulation of the electrolyte, and (iii) a cell employing a back wall design to avoid the light loss problem [43].

3) Concentration of redox system in the electrolyte,

4) Use of electroanalytical modification. Chemisorption of transition metal ions such as Rh^{3+}, Co^{3+}, Ru^{3+} or Os^{3+} onto n-GaAs showed improved photoanode behavior, enhancement of the open-circuit voltage, fill factor and efficiency, in the n-GaAs $|K_2Se\text{-}K_2Se_2\text{-}KOH|$ SC liquid junction solar cell. This effect was interpreted as a reaction with surface chemical entity associated with a surface state near the conduction band, which shunts the cell by allowing electrons to tunnel through the barrier at the junction. Transition metal ions convert the shunting surface state to one to which electrons cannot tunnel. This occurs by

reducing the surface state density, and by catalyzing interfacial charge transfer at the SC/liquid interface [36,44-45]. To date, various attempts have been made to develop the passivation technology, which reduces the surface recombination velocity (SRV) [46]. The first approach followed advances in molecular-beam epitaxial (MBE) growth methods, which suggested that AlAs (2.17 eV, indirect X band) could be used as a crystalline insulator. This was successful provided that the gate voltage swing was limited to small values so as to prevent large leakage currents. An optical coating film of Al_2O_3 was fabricated by oxidizing epitaxially grown AlAs. They have an optically smooth surface morphology and a reflectivity of 6% when used as an antireflection coating on GaAs. Absorption in the Al_2O_3 films is comparable to electron beam evaporated Al_2O_3 films. The capacitance-voltage measurements reveal a reduction in surface state density when compared to electron beam evaporated Al_2O_3 [47-48]. The second approach to finding a suitable heteromorphic insulator for GaAs involved the laser enhanced cleaning of the GaAs surface with de-ionized water. Since elemental arsenic was previously proposed to be responsible for the large interface trap density and the pinning of the Fermi-level at the GaAs surface. The concept is to wash away the arsenic produced as a result of GaAs oxidation, and immediately cap the surface with a layer that is impermeable to oxygen. This work was successful in the short-term unpinning of the Fermi level at the surface. A third, and the most recent, approach to the passivation of GaAs was based on the discovery by Sandroff and co-workers that coating of inorganic sulfides [Li_2S, $(NH_4)_2S$, $Na_2S.9H_2O$, etc.] impart excellent properties to GaAs.

Subsequent studies showed that, in these systems, a gallium-sulfide layer was covalently bonded to the GaAs surface. The disadvantage with this "wet" sulfide approach is that the sulfide films are only temporary after 18 h the SRV return to their pretreatment values. Electronic passivation of n- and p-type of GaAs using chemical vapor deposited GaS was done satisfactorily. The electronic condition of GaS/GaAs interface did not show any deterioration after six-week time period [47]. An ultrathin strained layer deposition of InP-related compounds on a GaAs surface greatly improved the surface band structure properties. Tenfold enhancement in the photoluminescence PL intensity was observed at the GaAs band edges, which indicates a reduction in the surface recombination. Relaxation of the surface pinning, which results in PL intensity enhancement, is observed by x-ray photoelectron spectroscopy (XPS) [46]. Another passivating films were grown on GaAs by direct nitridation with hydrazine at 300-400°C. Analysis showed that the films are primarily gallium nitride with an oxide impurity. Improvements in the band gap PL intensity with nitridation indicate a low surface state density and reflect an improvement of the SC lattice [49].

5) Electrolyte-attack prevention by coating the electrode. An optimal coating material has to show high optical transparency over the solar spectrum, good electrical conductivity, chemical inertness, and has to give low Schottky barrier at the SC / film contact [37].

2.4.2. Dye sensitization

Dye sensitization of photosensitive materials has been investigated from the aspect of improving the visible response of large E_g, but relatively stable, SC electrodes. The mechanism of dye-sensitization can be explained by a simple picture of energy diagram as in Figure (2-13). The dye molecule (D), which has strong absorption properties in the visible, is bonded to the SC surface. The photoexcited dye molecule D^* can act either as a donor or as an acceptor of electrons in the electrolyte. The total reaction scheme may be represented as :

$D + h\nu \rightarrow D^*$

$D^* \rightarrow D^+ + e^-$ (electrode) ...(a) or $D^* \rightarrow D^- + h^+$ (electrode) ...(b)

For reaction (a) to occur, the electronic level of D^* must be above the conduction band edge. For reaction (b), the ground level that is now empty, must be below the valence band edge of the SC. Either of them can be made most effective by suitable polarization of the electrode [positive for (a) and negative for (b)].

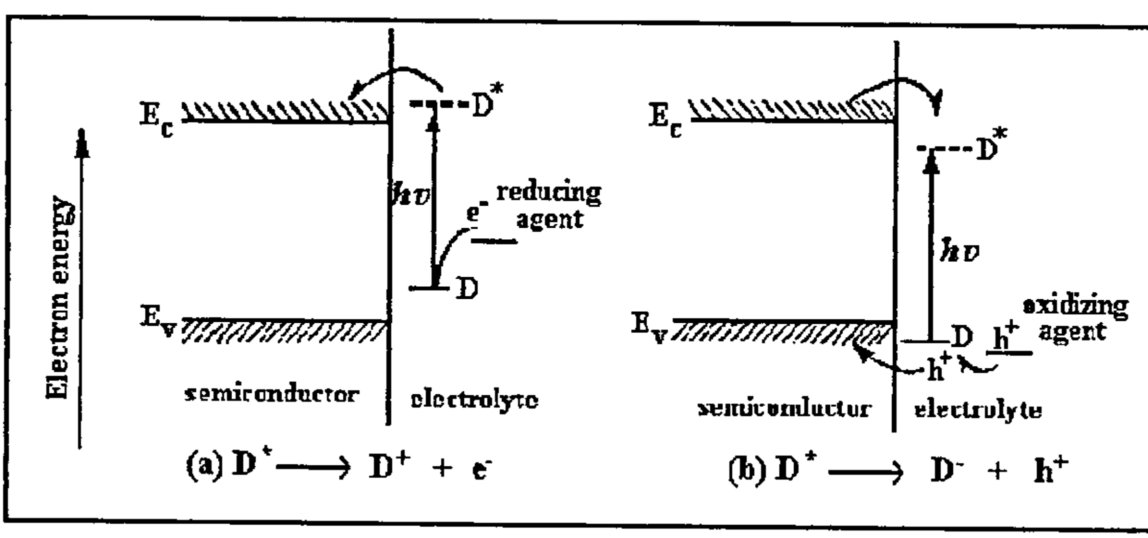

Figure (2-13): Mechanism of dye-sensitization in a SC: (a) excited dye molecule D^* as an electron donor. (b) excited dye molecule D^* as an electron acceptor.

The presence of a reducing agent or oxidizing agent in the solution will enable D^+ and D^- respectively to be restored so that the entire process is regenerative. For water splitting, upon excitation to D^* an e^- is transferred to the SC CB leaving D^+ at the surface. The electron in the SC subsequently reduces H^+

to $\frac{1}{2}H_2$ at a metal cathode, while D^+ oxidizes H_2O to O_2 to regenerate D, Fig. (2-14) [50].

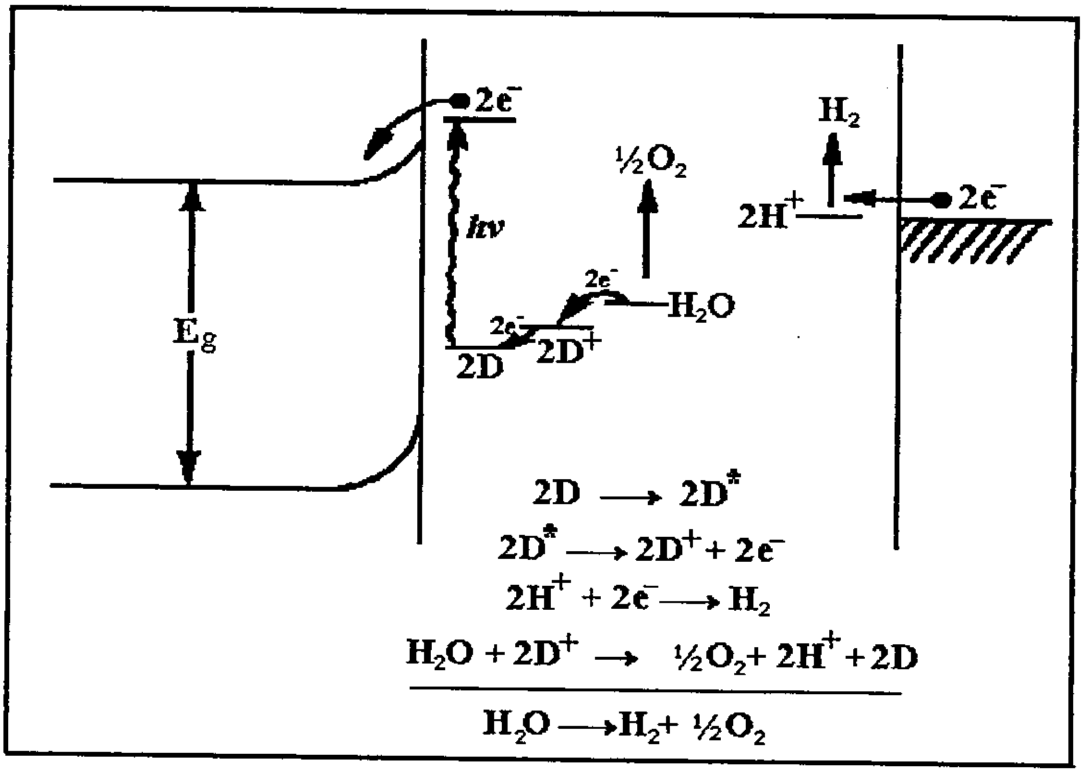

Figure (2-14): Energy level scheme for dye sensitization of n-type SCs

Enhancement of photocurrent by addition of a suitable dye has been observed in ZnO, TiO_2, CdS, GaAs, GaP, SnO_2, Cu_2O and organic SC. The rose bengal, the tris (4,7-dimethyl-1,10-phenanthroline), Rhodamine B, alizarin cyanine, and mesocyanine are examples of used dyes. But unfortunately, dye sensitization approach has many problems such as: (1) the dyes are generally organic species that have relatively poor long term stability and do not survive the repeated oxidation-reduction cycles, (2) the dye layer on the electrode must be very thin to permit charge transfer from the excited dye to the electrode, but this requirement often is in conflict with the dye layer also exhibiting intense optical absorption and this restricts light absorption to the orders of 1-2% since only monolayers of dyes are active for electron transfer, and (3) certain dye-SC electrode combinations show very low quantum efficiencies [50-51].

2.4.3. Examples of enhanced SC in PEC cells

Researchers have been active trying to achieve these goals:

(1) SC surface modification is one way to enhance the characteristics. n-$GaInP_2$ surfaces have been modified with other species, such as 8-quinolinol and cupferron, and flat-band positive shifting was observed [52-53]. In other reports, n-GaAs surface was derivatized using (1,1'-ferrocenedyl) dichlorosilane. Photooxidation occurred at ~0.65V more negative than at Pt. This makes the surface–confined redox active material serves as an effective mediation system for the oxidation of solution species not necessarily oxidized by the naked electrode. But the derivatized electrodes seemed to be as efficient as the naked electrodes in transducing light to electricity in ferricenium/ferrocene liquid junction cells [54]. To stabilize the n-GaAs surface, indium tin oxide (ITO) were deposited onto n-GaAs electrodes produced by the magnetron sputtering technique. Unfortunately, this technique gave extremely poor photovoltaic parameters and the ITO film didn't prevent the direct contact between electrolyte and n-GaAs substrate. This led to corrosion due to the flowing photocurrent because of much higher barrier height at small n-GaAs/electrolyte contact area compared with the barrier height at the n-GaAs/ITO interface [37]. In another attempt, conjugated organic polymers were attached to the SC surface. This class of polymers is oxidized or reduced more easily and reversibly than traditional polymers. The change in oxidation state of polymers affects their electrical, optical, redox, and mechanical properties, as well as their stability. In

many cases, the oxidized or doped state of the polymer displays nearly metallic-like behavior, whereas the reduced or neutral undoped form exhibits insulative or SC-like characteristics. This makes it theoretically possible to have several types of rectifying p-n junctions, when electronic contact is made between either the polymer and a metal or the polymer and a SC [55-63]. Frank *et al* [56-60] attached conjugated polymers, doped and undoped, to different SC surfaces. In the case of n-GaAs, the conjugated polymer matrix significantly stabilized the surface to photodegradation, but the short-circuit current was lowered [60]. In the case of n-CdS a Schottky barrier resulted between the SC and the conjugated electrolytically grown ploy (3-methlthiophene) layer. Improvement of the barrier height by optimization of the synthesis parameters of the films is likely to allow uncorrected conversion efficiencies of 2% and more in white light [60,62].

Metal porphyrins and metal pthalocyanines adsorbed on Nafion a membrane was used for photoinduced electron transfer leading to photoreduction of dioxygen (O_2). H_2O_2 was produced by the reaction of of the semiconducting nature metal porphyrins and pthalocyanines with dissolved oxygen. The back electron transfer reaction between h^+ with $O_2^{\cdot-}$ was prevented by reaction of the hole with other chemicals, such as triethanolamine[64]. 1-naphthol and related phenols were converted to corresponding quinones and oxidative phenol coupled products when reacted with H_2O_2 using 5,10,15,20-tetra(pentafluorophenyl)porphyrinatoiron(III) chlorideas a catalyst [65].

It has been found that n-$GaInP_2$ has suitable band gaps with band edges that are good for water reduction but slightly higher than needed for water oxidation. Therefore it's expected that n-$GaInP_2$ will be the most suitable SC for photoelectrochemical splitting provided that two conditions are met:

(1) The band edges are slightly lowered.

(2) The surface is stabilized without losing short-circuit current

In earlier studies, n-GaAs and n-$GaInP_2$ have been modified with of MnP, at the sub-monolayer coverage level, by chemically attaching the metalloporphyrine with the SC surface through an anchoring ligand via a quaternization reaction [66]. It has been found that the positive charges of the MnP shifted the positions of the SC flat-band edges towards more positive values. However, the surface monolayer coverage did not enhance the surface stability to degradation.

In previous work positively charged species were chemically attached on the surfaces of n-GaAs and n-$GaInP_2$. By this technique, significant lowering in the band edges for the modified SC samples, with respect to the unmodified ones, was observed. And we are still looking forward for further improvement of the n-GaAs surface properties.

Chapter Three

EXPERIMENTAL

EXPERIMENTAL

3.1. MATERIALS

3.1.1. Chemicals & Solvents

$LiClO_4$, $K_3Fe(CN)_6$, $K_4Fe(CN)_6$, and the 5,10,15,20-tetra(-4-pyridyl)-21H,23H-porphine, (H_2TPyP), were purchased from Aldrich. All organic solvents (methanol, dichloromethane, DMF) were obtained from RIEDEL-DE HAEN as a pure form.

3.1.2. Preparation & characterization of MnP

The tetra(-4-pyridyl)porphyrinatomanganese(III)sulfate (MnP) complex, Fig. (3-1), was prepared from H_2TPyP as described in the literature [69]. H_2TpyP (81.7 mg, 0.132 mmol) was vigorously refluxed with excess manganese (II) sulfate (1.53g, 0.91 mmol) in N,N-dimethylformamide, DMF, (60 ml) for 10h. The solution was concentrated by evaporating DMF under reduced pressure. Air was passed through the reaction mixture to oxidize Mn^{2+} to Mn^{3+}. The reaction mixture was then ion-chromatographed over activated neutral alumina using DMF as eluant. Eluate fractions with the characteristic absorption bands at 462, 569 and 620 nm, [68], were stored in the dark.

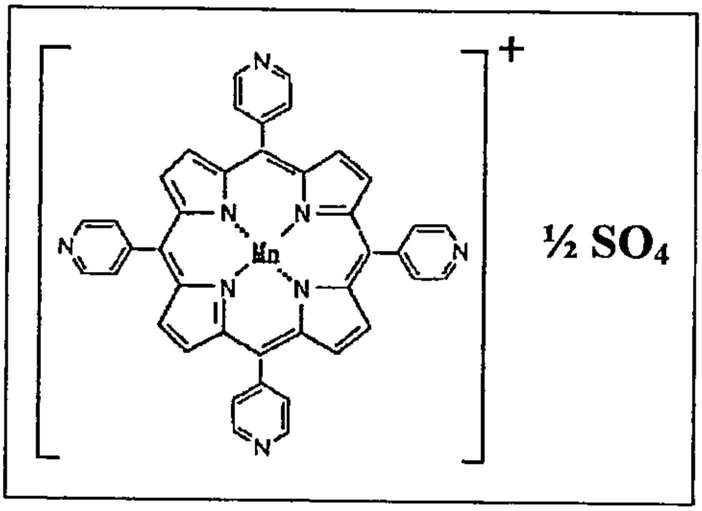

Figure (3-1): the structural formula of MnP

The mixture contained complexes of both the Mn^{II} and the Mn^{III}, as depicted from the electronic absorption spectra in the visible region, Figure (3-2→4). Figure (3-5) shows the electronic absorption spectra for the polysiloxane membrane.

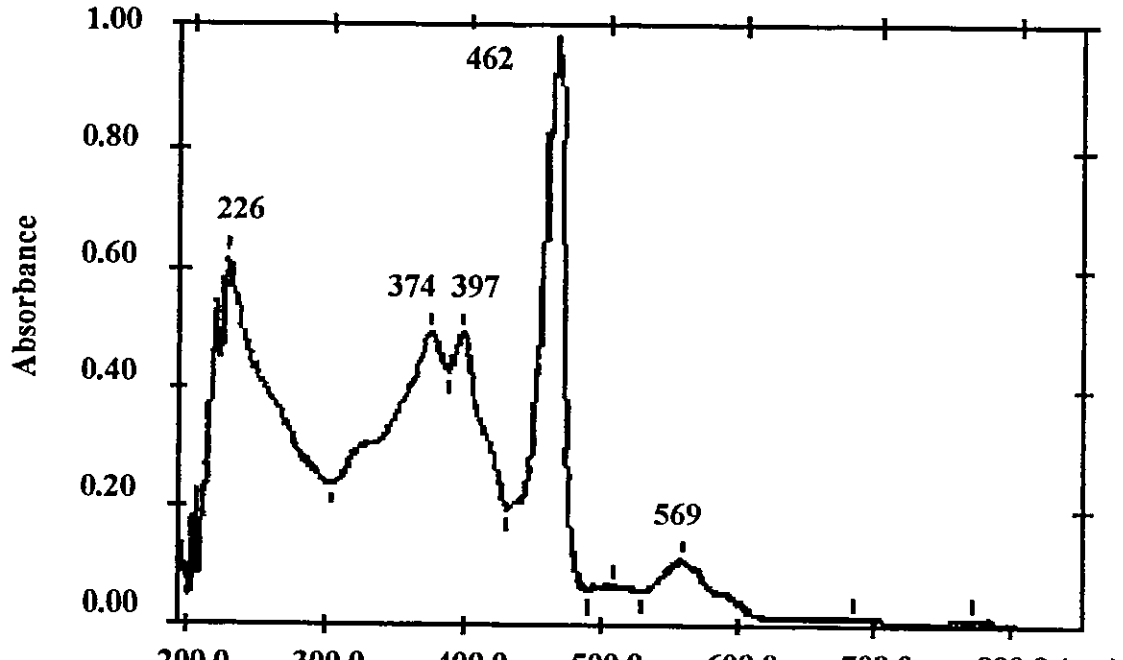

Figure (3-2): The electronic absorption spectra in the UV/visible region for MnP solution in methanol.

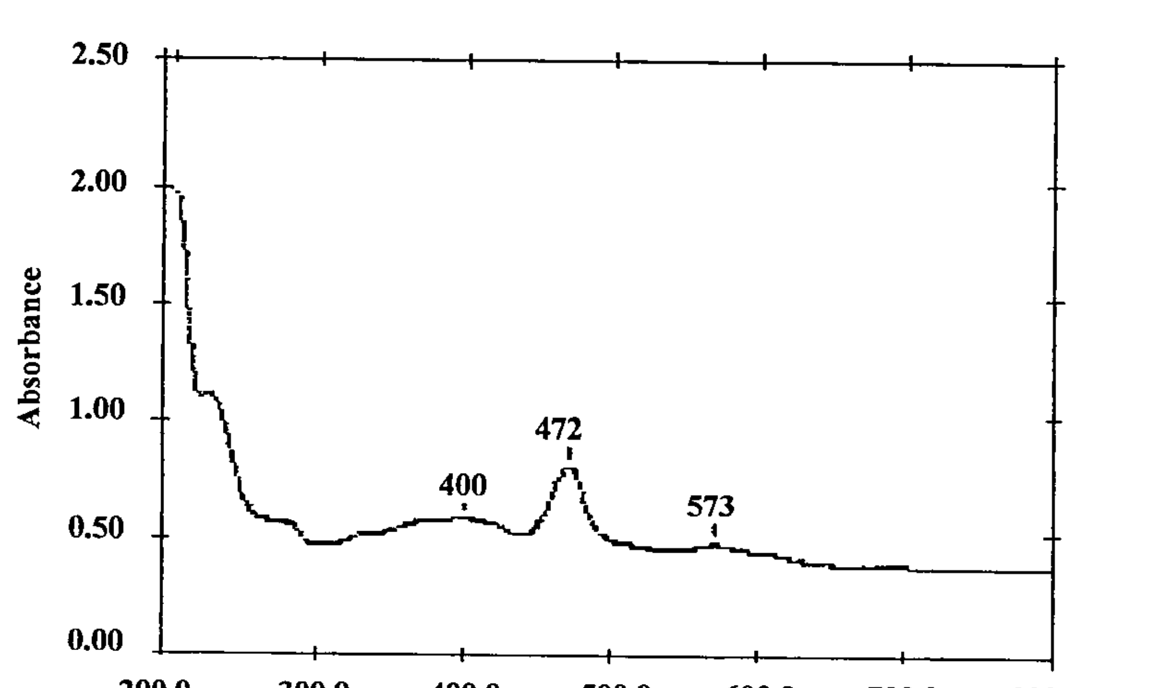

Figure (3-3): The electronic absorption spectra in the UV/visible region for MnP embedded into a polysiloxane polymer solid matrix .

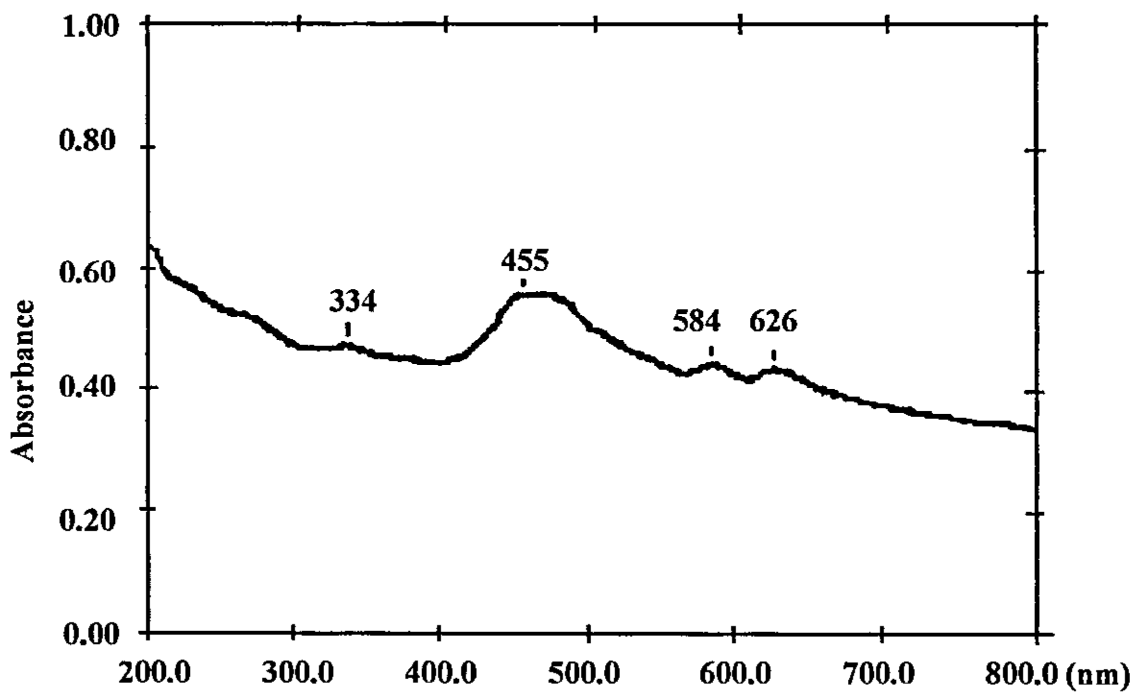

Figure (3-4): The electronic absorption spectra in the UV/visible region for MnP embedded into a polysiloxane polymer solid matrix after annealing at 150°C for 30 min. under N_2 atmosphere.

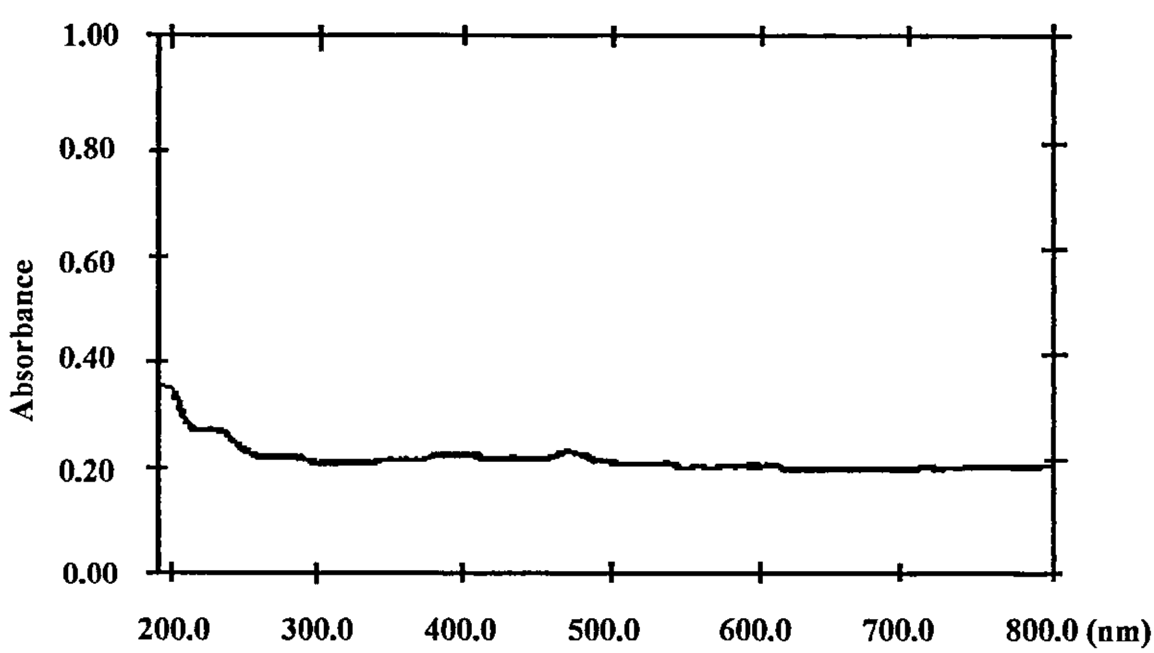

Figure (3-5): The electronic absorption spectra in the UV/visible region for solid polysiloxane membrane.

3.1.3. SC electrodes

A) n-GaAs electrode fabrication

Mono-crystalline single surface mirror polished Si-doped ($3.2X10^{17}$ cm^{-3} for the front and $9.9X10^{17}$ cm^{-3} for the tail) n-GaAs wafers (Crystal Specialties, Intl.) were used. The mono-crystalline plates, 50 mm round-shaped, were measured to be 0.4 mm thick, with <100> orientation. The mobility was $2.8X10^3$ cm^2/V-s in the front and $2.3X10^3$ cm^2/V-s in the tail. The wafer was cut into smaller pieces. Indium metal back contact was made as thin uniform layers. The wafers were then annealed at 350°C under clean pure atmosphere of N_2. The SC electrodes were fabricated as follows: the small square n-GaAs wafer (~0.1 cm^2) was mounted to a copper plate (with a copper wire welded to it) using a thin layer of Ga-In eutectic. The backside and the edges of the electrode, together with the copper wire, were then insulated with a Torr-sealing material. They were allowed to dry overnight, at room temperature, under nitrogen. The dried sealed electrodes were then rinsed repeatedly with methanol to remove away any possible oily solvent contaminants from the Torr seal. It was then dried under slow streams of N_2.

B) Electrode etching

Etching was conducted using a Br_2/methanol (1.0% V/V) solution [69]. The electrode was dipped inside the etching solution for about 5 seconds, which was immediately rinsed with distilled water. The etching procedure was repeated twice or three times, till obtaining a shiny mirror surface. It was then rinsed with water and methanol and dried with nitrogen. In all cases, the wafers and the electrodes were always stored under inert N_2 atmospheres.

C) Electrode Modification

The etched SC electrode surface was modified as follows: A dilute solution of the commercial, R.T.V. made, polysiloxane $(-O-SiR_2-O-)_n$ paste in acetic acid, was prepared by dissolving 0.05g of the paste in 100 mL of dichloromethane. Similarly, methanol solutions of MnP (0.1g, $1.38X10^{-4}$ mol, in 10mL) were prepared. The MnP/Polysiloxane solutions were prepared by adding the MnP solution to the Polysiloxane solution, in a 1:4 V/V ratio, respectively. 0.1 mL of the stock solution (containing $4X10^{-5}$ g polysiloxane and $2X10^{-4}$ g MnP) were pipetted onto the n-GaAs polished surface. The organic solvents were then allowed to evaporate off, leaving a transparent thin layer of the MnP/Polysiloxane matrix on the SC surface. The polysiloxane matrix thickness, excluding the MnP, was calculated to be ~ 4.0 μm, containing $2.0X10^{-4}$ g of MnP. With more thick films, the polymer matrix worked as an insulator and allowed no current to be measured. Therefore, all experiments were conducted using the optimum polymer thickness shown above. For control experiments, n-GaAs surfaces were modified with 4.0 μm thick polysiloxane surfaces without MnP. These n-GaAs/polymer systems were treated similarly.

D) Annealing

Annealing was conducted using a thermostated horizontal tube furnace. The electrode to be annealed was inserted to the middle of a small Pyrex cylinder that was placed in another longer Pyrex cylinder. The heat was raised to 100°C, under a clean atmosphere of N_2 for, 30 min. The system was then left to cool under a continuous flow of N_2, Fig. (3-6).

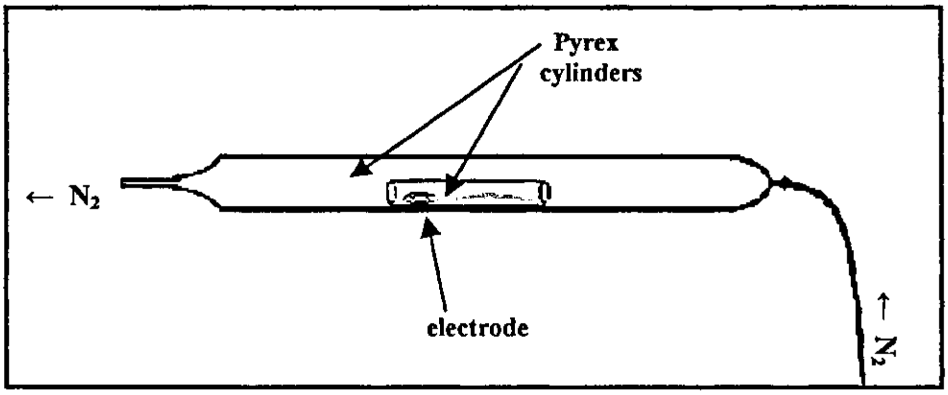

Figure (3-6): The annealing system.

3.2. EQUIPMENTS

3.2.1. Measuring Devices

Solid state electronic absorption spectra were measured on a Shimadzu UV-1601 spectrophotometer, as solid thin films of MnP/polysiloxane on quartz slides. Infrared spectra were measured, as thin films of MnP/polysiloxane, on a Shimadzu FTIR-8201 PC spectrophotometer. Light intensity was measured with Lutron LX-102 light meter. The light meter, which measures the illuminance in lux units, was calibrated against a Kipp & Zonen CM11 pyranometer. The pyranometer measures irradiance in watt.m^{-2}. The calibration was conducted by exposing both light meter and pyranometer sensors to sunlight simultaneously. Original calibration data are located in appendix A1. Therefore, unless otherwise stated, the illuminance used in our experiments was measured in lux and calibrated into irradiance in watt.cm^{-2} units. Current-potential measurements were performed using a Princeton Applied Research

(PAR) Model 263A computer-controlled potentiostat. The Mott-Shottky plots were measured with a SRS 830 DSP lock-in amplifier, a SRS DS345 function generator and a PAR Model 263A potentiostat.

3.2.2. PEC Cell

The n-GaAs electrode was incorporated as a working electrode into a thermostated one-compartment three-electrode electrochemical cell, with a platinum counter electrode and a reference saturated calomel electrode, SCE, Fig. (3-7).

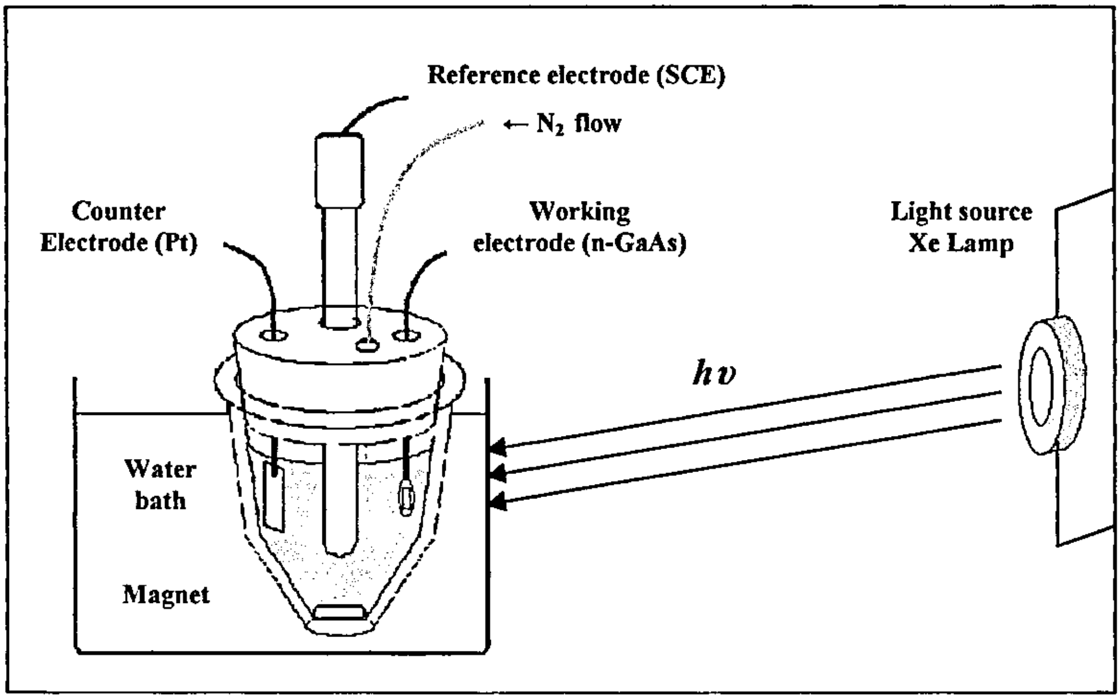

Figure(3-7) : Thermostated one-compartment three-electrode electrochemical cell, with n-GaAs working electrode, a platinum counter electrode and SCE reference electrode.

$LiClO_4$ (0.10 M) was used as a supporting electrolyte, and $Fe(CN)_6^{3-/4-}$ (0.05 M $K_3Fe(CN)_6$, 0.05 M $K_4Fe(CN)_6$) as a redox couple in fresh doubly-distilled water with (pH 6.5). Before each experiment, high-purity nitrogen gas was bubbled through the solution for at least 5 minutes. During measurements, the nitrogen gas stream was kept flowing above the solution to *minimize* contamination with air.

3.2.3. Light source

Illumination was carried out using a 50 W Xenon lamp equipped with housing and a concentrating lens. This lamp has a high stability and an intense coverage of wide spectral range, from about 450 to 750 nm, without any preference [70], Fig. (3-8). The Xenon Lamp was placed at defined distance from the working electrode. A 10-mm thick water filter was placed between the lamp and the electrode.

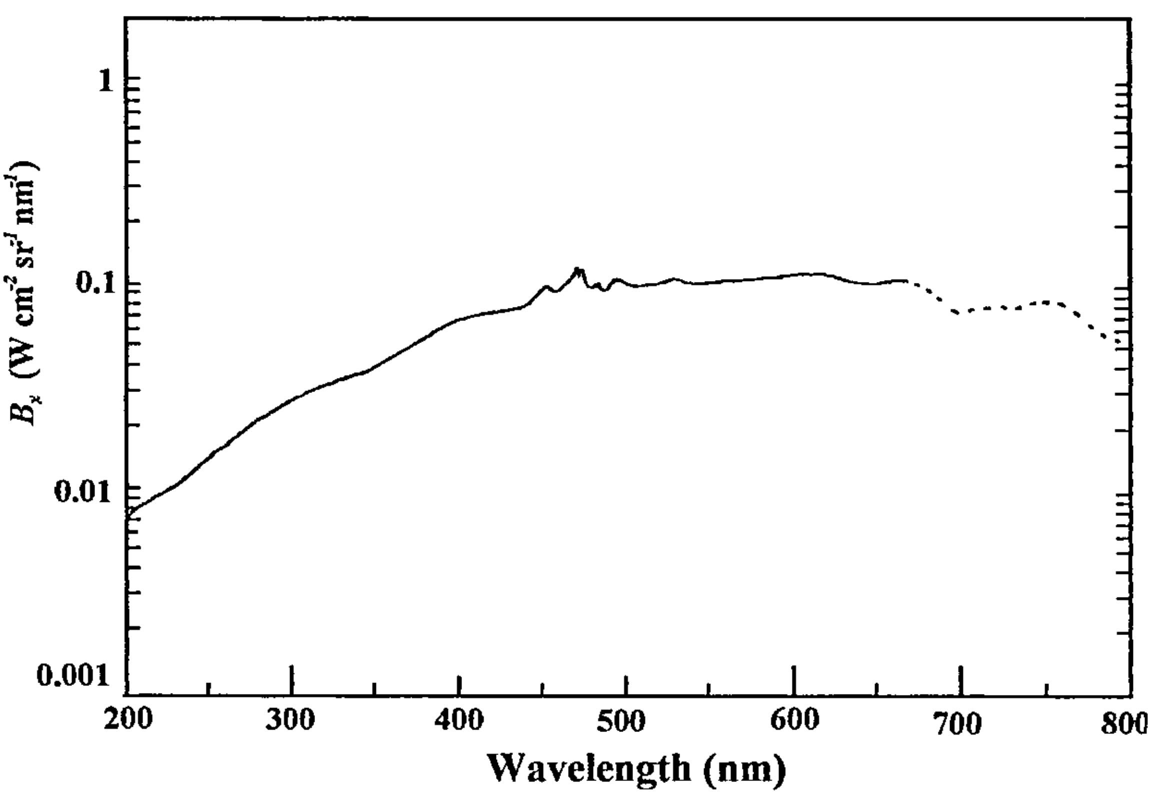

Figure (3-8) : Spectral distribution of high intensity 75-W xenon arc lamp [71].

3.3. MEASUREMENTS

3.3.1. Current-voltage

Current voltage (J-V) plots were measured using a PAR 263A potentiostat. The SC was employed as a working electrode in a one-compartment cell with a platinum counter electrode, SCE reference electrode, under nitrogen atmosphere. $Fe(CN)_6^{3-/4-}$ (0.05 M $K_3[Fe(CN)_6]$, 0.05 M $K_4[Fe(CN)_6]$) was employed as a redox couple in water, using $LiClO_4$ (0.10 M) as a supporting electrolyte. The J-V measurements were done at room temperature, under nitrogen atmosphere. The dark experiments were performed by completely excluding the light. The system was covered with a black cloth while working in a dark room. On the other hand, a 50 W Xenon lamp was used in the photocurrent measurements.

3.3.2. Cyclic voltammometry

Cyclic voltammometry was measured on a PAR 263A potentiostat, in a one compartment cell using platinum counter electrodes, SCE reference electrode, in water/$LiClO_4$, under nitrogen atmosphere, with a scanning rate of 100 mV/s. Thin films of MnP/polymer were cast onto pre-cleaned platinum gauze and used as a working electrode in order to measure the cyclic voltammograms of the MnP. The oxidation peak at -160 mV and the reduction peak at -450 mV, against SCE, were observed Fig (3-8,9).

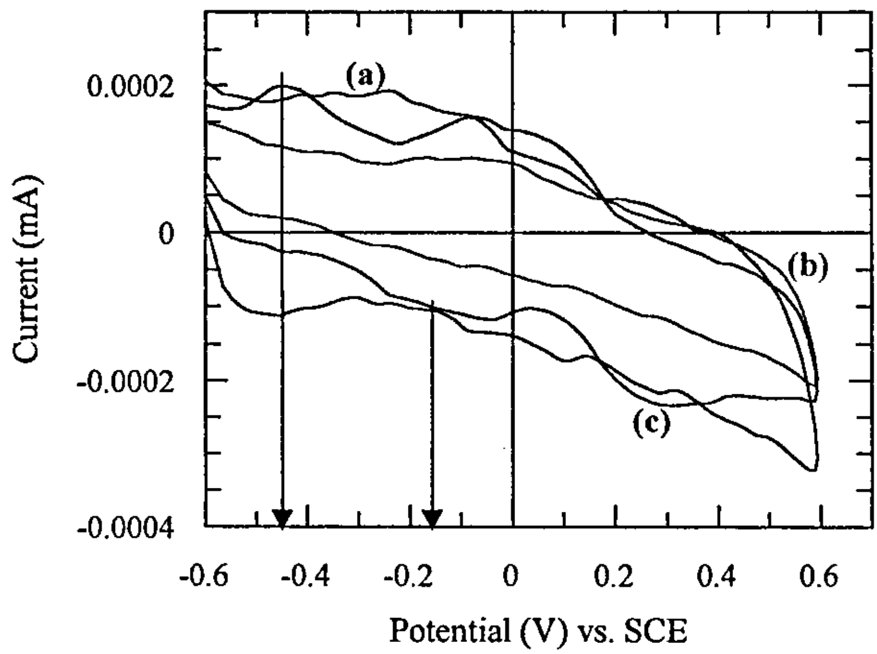

Figure (3-9): Cyclicvolammograms measured in the <u>dark</u> For: a) Platinum, b) Polysiloxane modified Pt, and c) MnP/polysiloxane-modified Pt electrodes. All measurements were taken in aqueous solution under nitrogen atmosphere using $LiClO_4$ supporting electrolyte, a Pt counter electrode and SCE as a reference.

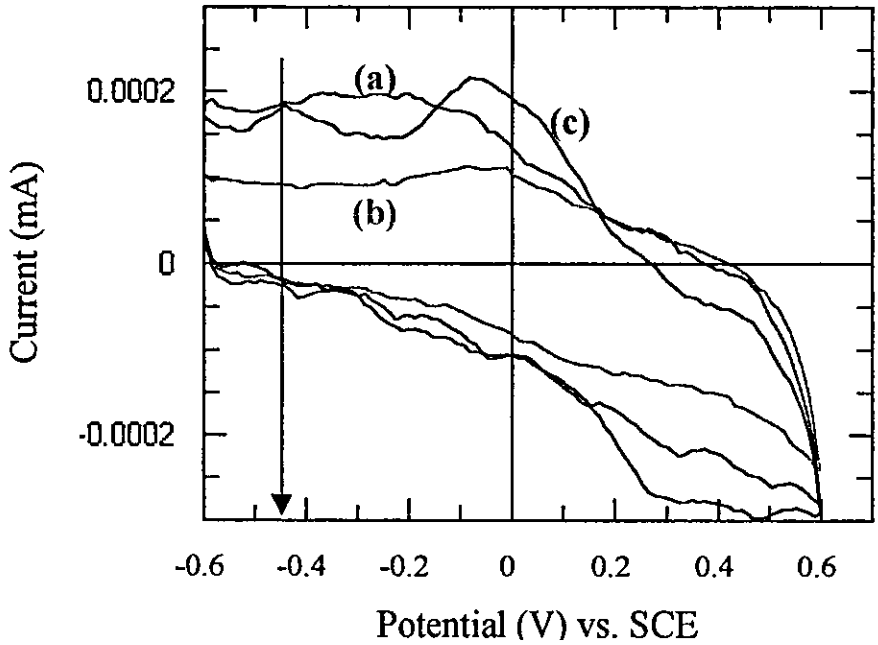

Figure (3-10): Cyclicvolammograms measured under <u>illumination</u> For: a) Platinum, b) Polysiloxane modified Pt, and c) MnP/polysiloxane-modified Pt electrodes. All measurements were taken in aqueous solution under nitrogen atmosphere using $LiClO_4$ supporting electrolyte, a Pt counterelectrode and SCE as a reference.

3.3.3. Capacitance-voltage

Measurements of capacitance *vs.* applied potential were conducted using the same, as described above, electrochemical cell in water/$LiClO_4$/$K_3Fe(CN)_6$/ $K_4Fe(CN)_6$ system. Mott-Schottky (M-S) plots were then constructed, for a potential scanning over a range of -0.5 to +0.5 V (*vs.* SCE) at a scan rate 100 mV/s and 10 KHz frequency.

3.3.4. Stability testing

Experiments were conducted using the same electrochemical cell with the same electrolyte and redox couple. The electrode was kept under illuminance of 140000 Lux (irradiance of 0.10125W.cm-^{2}) for prolonged times using 0.00 V applied potential (*vs.* SCE). The short circuit current I_{sc} was measured with time throughout the experiment. The stability test was conducted over three temperatures (25,35, and 45°C). Temperature was kept constant through the experiment using a water bath connected to a thermostated circulator.

Chapter Four

RESULTS

RESULTS

4.1. GENERAL REMARKS

In this work, n-GaAs surfaces have been modified. Matrices of polysiloxane and polysiloxane/MnP have been attached to the SC surface. The modification method described here has a very important technical advantage over other ones described in the literature [56-63]. Contrary to previous reports, the polymer matrix irreversibly adhered to the polished n-GaAs surface without any need for scratching. When the n-GaAs/MnP/Polysiloxane system was annealed at 100°C the adherence was enhanced and a clear robust glassy solid layer appeared on the surface

The effect of surface modification on SC characteristics at solid liquid interface have been investigated by probing different parameters, namely:

1) Darkcurrent-potential plot shapes and onset-potential value shifts.

2) Photocurrent-potential plot shapes and open-circuit potential value shifts.

3) Mott Schottky plots and flat-band potential shifts.

4) Value of short-circuit current and stability testing.

5) Efficiency enhancement.

4.2. CURRENT-POTENTIAL PLOTS

4.2.1. The effect of polymer matrix thickness

When thick matrices of MnP/polysiloxane were used, the *J-V* plots showed bad current readings, Fig. (4-1a,b). Therefore, thin matrices were made to lower the resistance. Optimum matrix thickness was 4.0 µm. With such thickness, defined *J-V* plots were obtained Fig. (4-1c). Therefore, unless otherwise stated, the 4.0-µm thick polymer matrix was used throughout this work.

4.2.2. Dark current-Potential Plots

Dark *J-V* plots were measured for the naked (etched), polysiloxane-coated (n-GaAs/polysiloxane) and MnP/polysiloxane coated n-GaAs electrodes ***without annealing***.

Figure (4-2) indicates that the attachment of the MnP/Polysiloxane matrix to the n-GaAs surface significantly enhanced the shapes of *J-V* plots when the $K_4[Fe(CN)_6]/K_3[Fe(CN)_6]$ redox couple system in water was used. The naked n-GaAs showed rough *J-V* curve, Fig (4-2a). The polysiloxane-coated electrode showed somewhat better behavior, Fig. (4-2b). The MnP/polysiloxane coated electrode showed acceptably smooth *J-V* curve, Fig. (4-2c).

Figure (4-2) shows also that the MnP-modified SC surface has a shifting in the dark-current onset potential, V_{onset}, compared to the unmodified electrode. The value of the shift was about 160 mV, towards a more positive potential value (positive shift). Such a positive shift is an indicator of a lowering in the value of the flat-band potential (V_{fb}).

In separate experiments, the polysiloxane- and MnP/polysiloxane-modified n-GaAs electrodes were ***annealed*** at 100°C for 30 min. under N_2. Annealing indicates some significant effects on the characteristics of the SC electrode.

Figure (4-3) represents serious enhancements in the shapes of *J-V* plots with the modified surfaces after ***annealing***. The naked n-GaAs showed rough *J-V* curve, Fig (4-3a). The polysiloxane-coated electrode showed somewhat better behavior, Fig. (4-3b). The MnP/polysiloxane coated electrode showed acceptably smooth *J-V* curve, Fig. (4-3c).

The ***annealed*** n-GaAs/MnP/Polysiloxane electrode exhibited a higher shift in the value of the V_{fb}, Fig (4-3). The value of the shift in this case is about 280 mV, which is higher than the value for the not annealed system.

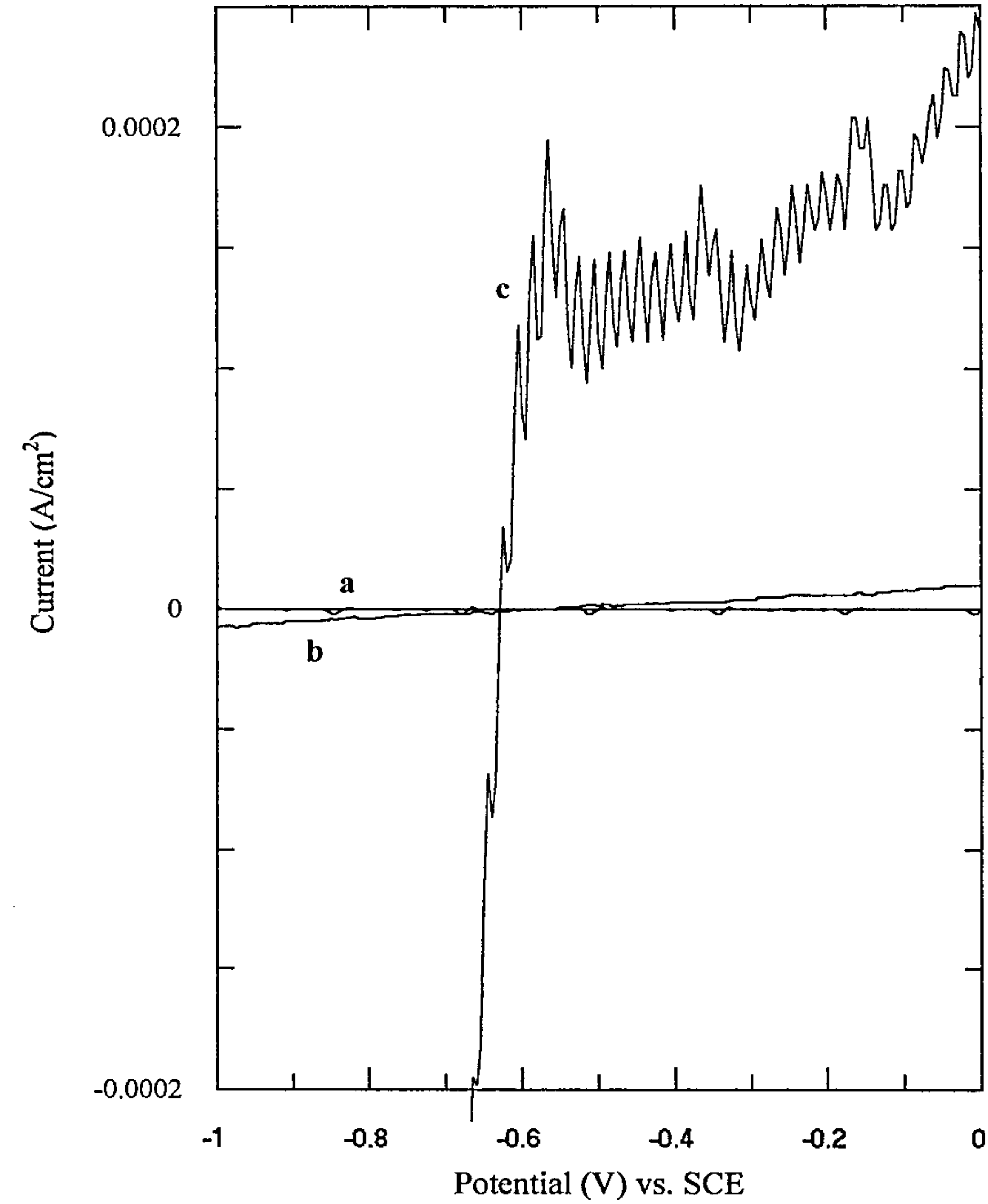

Figure (4-1): The effect of polysiloxane matrix thickness on the current-potential plots measured for polysiloxane- modified n-GaAs electrodes with matrix thicknesses: a) 400 μm, b) 40 μm, c) 4 μm. All measurements were conducted under high intensity illumination with 50 W Xe lamp in water/ $LiClO_4/K_4[Fe(CN)_6]/K_3[Fe(CN)_6]$ at 25°C.

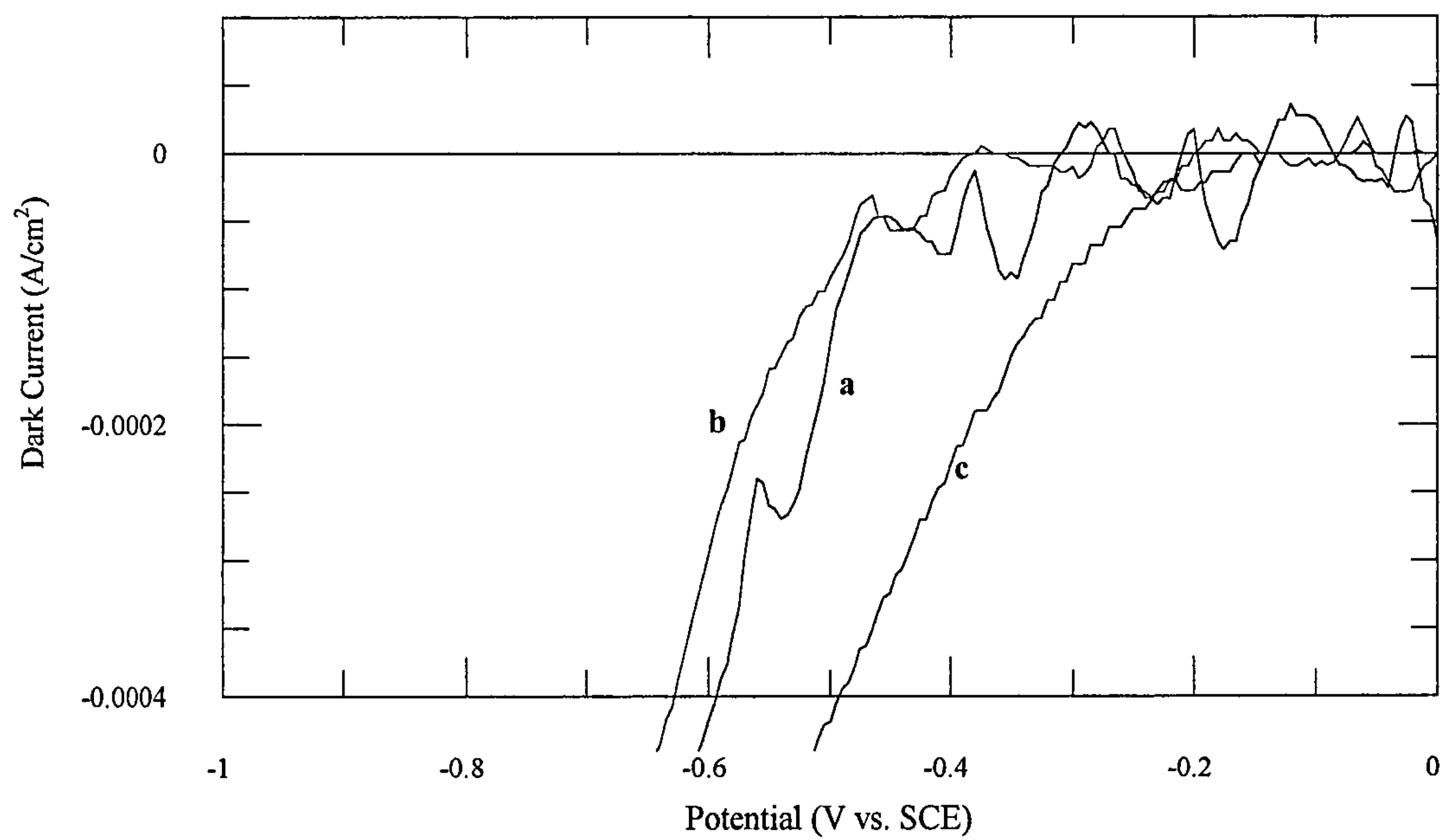

Figure (4-2): Dark-Current reading vs. applied potential measured for: a) unmodified n-GaAs, b) Polymer modified n-GaAs , and c) MnP/Polymer modified n-GaAs. Without annealing. All measurements were conducted in water/ $LiClO_4/Fe^{2+}/Fe^{3+}$ in dark at 25°C.

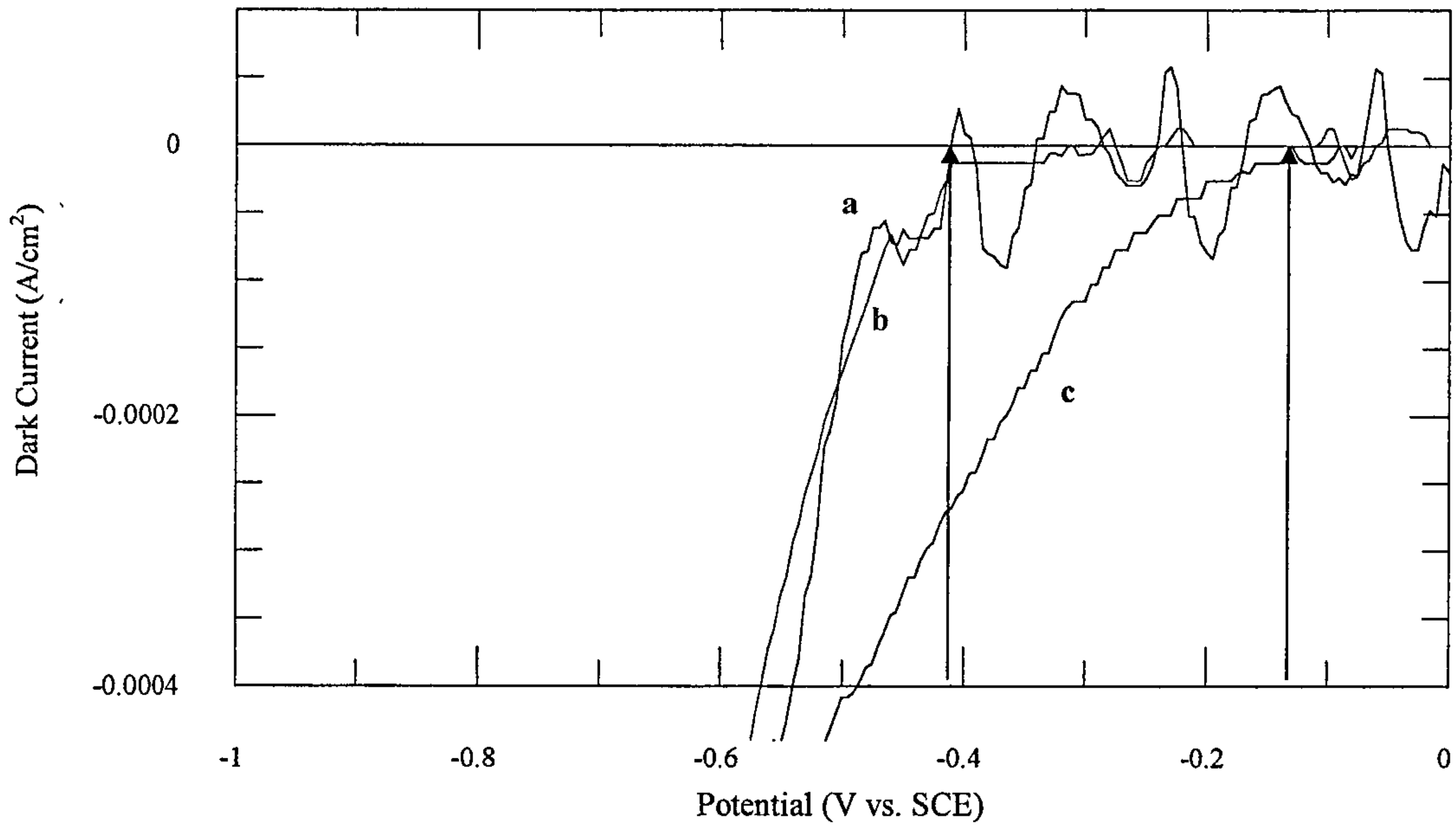

Figure (4-3): Dark-current reading vs. applied potential measured for: a) unmodified n-GaAs , b) Polymer modified n-GaAs , and c) MnP/Polymer modified n-GaAs. After annealing at 100°C for 30 min., under N_2 atmosphere. All measurements were conducted in water/$LiClO_4$/$K_4[Fe(CN)_6]$/ $K_3[Fe(CN)_6]$ in the dark at 25°C.

4.2.3. Photocurrent-Potential Plots

The *J-V* plots were measured for the modified and unmodified n-GaAs surfaces under high intensity polychromatic illumination with a Xe lamp, in the unfavorable water/$LiClO_4$/ $K_4[Fe(CN)_6]/K_3[Fe(CN)_6]$ system described above.

Figure (4-4c) indicates that, before any annealing, the attachment of the MnP/Polysiloxane matrix to the n-GaAs surface significantly enhanced the shapes of *J-V* plots while using the $K_4[Fe(CN)_6]/K_3[Fe(CN)_6]$ redox couple system in water. The naked and the polysiloxane-coated electrode showed rough *J-V* curves, Fig. (4-4a,b).

Without annealing the MnP/Polysiloxane modified n-GaAs surfaces have shown a shifting in the value of the open-circuit potential V_{oc} towards a more positive (lower) position with respect to the naked electrode, Fig. (4-4). The 120 mV lowering in the value of the V_{oc} is a good indication of a lowering in the value of the V_{fb}. In the absence of MnP, no shifting in the value of the V_{oc} was observed.

Figure (4-5c) indicates that, ***after annealing*** at 100°C, the attachment of the MnP/Polysiloxane matrix to the n-GaAs surface significantly enhanced the shapes of *J-V* plots. In contrast, the naked and the polysiloxane-coated electrode showed rough *J-V* curves, Fig. (4-5a,b).

The ***annealed*** n-GaAs/MnP/Polysiloxane electrode has 170 mV shift towards a more positive value of the V_{oc} with respect to the naked electrode, Fig (4-5). This shift was a somewhat higher shifting with respect to the not annealed case.

The lowering in the V_{oc} is smaller than the lowering in the dark-current V_{onset} value.

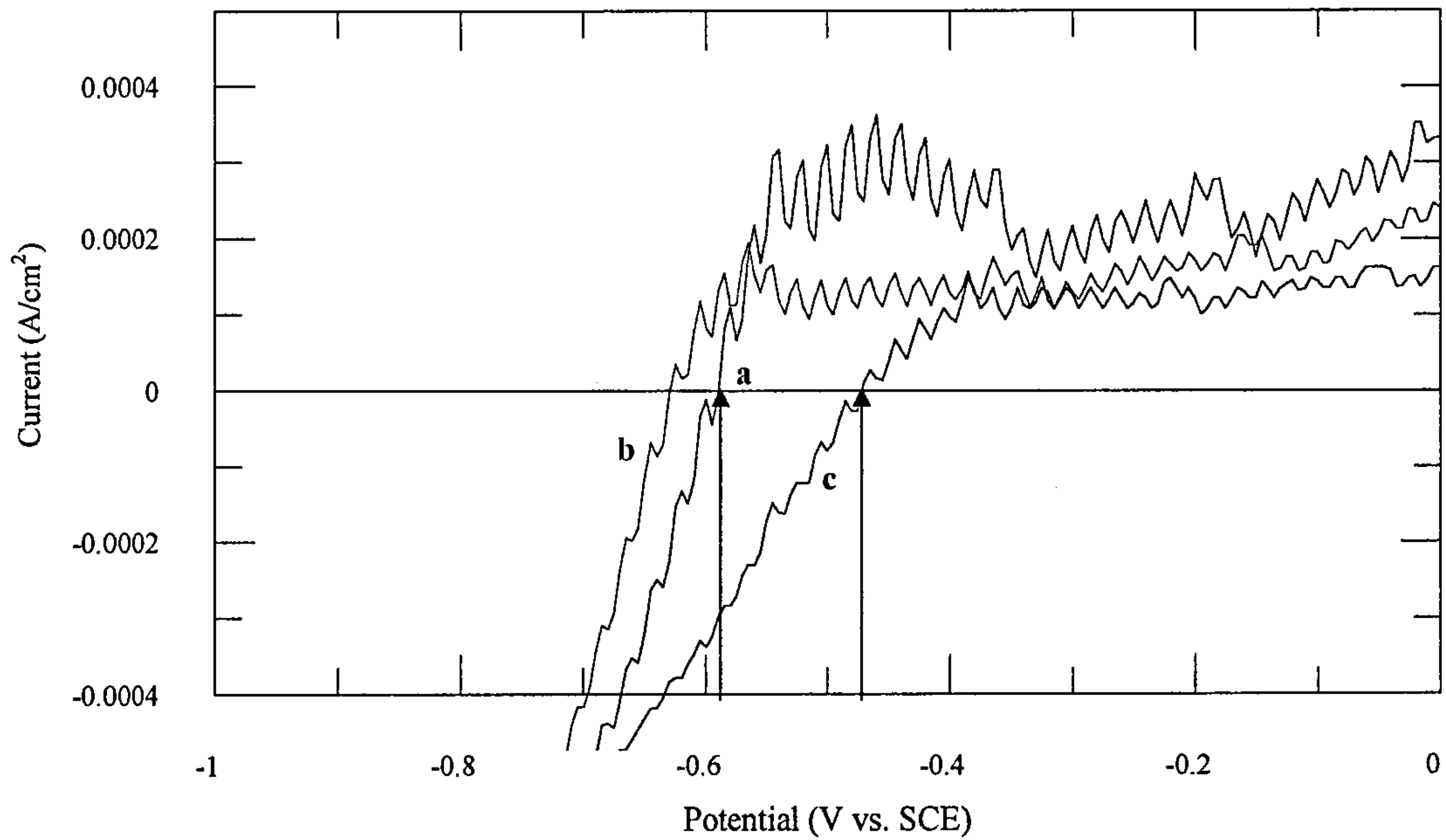

Figure (4-4): Photo-current reading vs. applied potential measured for: a) unmodified n-GaAs , b) Polymer modified n-GaAs , and c) MnP/Polymer modified n-GaAs. Without annealing . All measurements were conducted in water/$LiClO_4$/$K_4[Fe(CN)_6]$/$K_3[Fe(CN)_6]$ at 25°C.

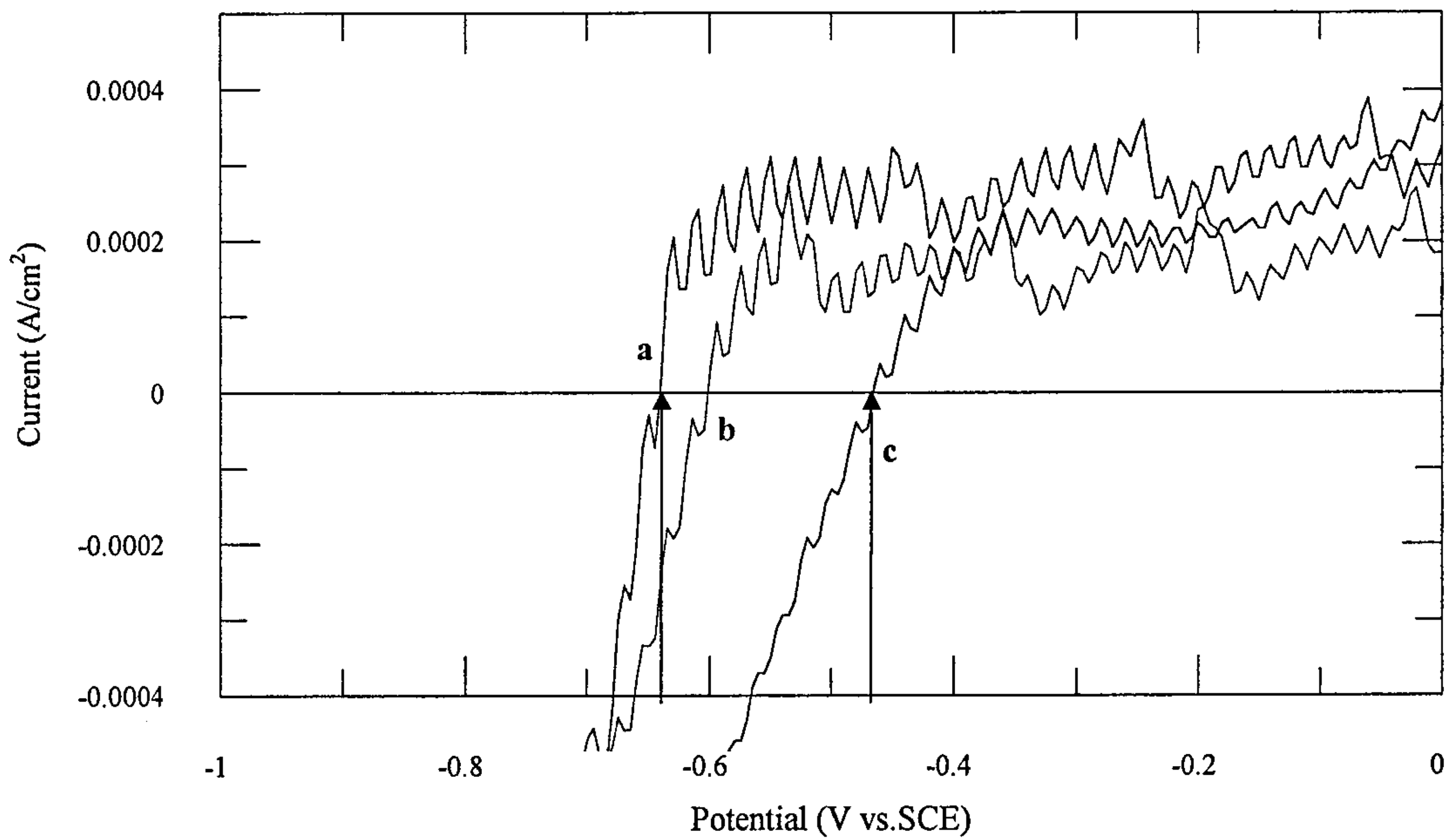

Figure (4-5): Photo-current reading vs. applied potential measured for: a) unmodified n-GaAs , b) Polymer modified n-GaAs , and c) MnP/Polymer modified n-GaAs. After annealing at 100°C for 30 min., under N_2 atmosphere. All measurements were conducted in water/$LiClO_4$/$K_4[Fe(CN)_6]$/$K_3[Fe(CN)_6]$ at 25°C.

Table (4-1): Comparison of V_{onset} and of $V_{open\ circuit}$ for modified and unmodified n-GaAs Electrodes.

		Without annealing	After annealing
Dark-current onset potential (V_{onset})*	Etched n-GaAs	-320	-420
	MnP/polysiloxane/n-GaAs	-160	-140
	The positive shift (ΔV_{onset})	**160**	**280**
	Figure no.	(4-2)	(4-3)
Photo-current open-circuit potential (V_{oc})*	Etched n-GaAs	-590	-640
	MnP/polysiloxane/n-GaAs	-470	-470
	The positive shift (ΔV_{oc})	**120**	**170**
	Figure no.	(4-4)	(4-5)

* Values measured in mV with reference to SCE.

Table (4-1) summarizes a comparison of V_{onset} and of $V_{open\ circuit}$ for modified and unmodified n-GaAs Electrodes.

4.3. MOTT-SCHOTTKY PLOTS & FLAT-BAND POTENTIAL SHIFTS

Values of the V_{fb} were directly measured for the modified and the unmodified n-GaAs electrodes. Capacitance (C) *vs.* potential (V) plots were measured in the water/$LiClO_4$/$K_4[Fe(CN)_6]$/$K_3[Fe(CN)_6]$ systems in the dark and under illumination. Mott-Schottky (M-S) plots of C^{-2} *vs.* V were constructed in order to directly measure V_{fb} values relative to SCE [72].

4.3.1. In the dark

The attachment of the polymer, without MnP, did not cause any shifting in V_{fb}. Figure (4-6) represents M-S plots measured in the dark for the modified and unmodified n-GaAs electrodes ***without prior annealing***. For the n-GaAs/MnP/Polysiloxane electrodes, the value of the V_{fb} was positively shifted by about 240 mV with respect to the naked electrode. With no MnP, no shift in the value of the V_{fb} was observed.

The ***not annealed*** n-GaAs surface modification enhanced the SC surface in another way as appears from Figure (4-6). The MnP/polysiloxane- modified electrodes have different slopes from the unmodified ones. The slope of the modified n-GaAs wafer, Fig (4-6c), gave a value for the measured doping density, **DD**, ($3.26X10^{17}$ cm^{-3}) that is resembles the vendors authentic value ($3.26X10^{17}$ cm^{-3}) of the semiconductor. The naked and polysiloxane- modified surfaces showed rather less accurate values, $3.74X10^{17}$ and $2.76X10^{17}$ cm^{-3}, respectively, Fig. (4-6a,b).

Figure (4-7) shows the Mott-Schottky plots measured in the dark for the modified and unmodified n-GaAs wafers ***after annealing***. The value of V_{fb} in case of n-GaAs/MnP/Polysiloxane is shifted towards a more positive value, by up to 700 mV, relative to that of the unmodified n-GaAs. This value is larger than the corresponding shifting for modified surfaces without annealing.

The n-GaAs surface modification enhanced the SC surface in another way as appears from Figures (4-7). The ***annealed*** MnP/polysiloxane- modified electrodes have different slopes from the unmodified ones. The slope of the modified n-GaAs wafer, Fig. (4-7c), gave a value for the measured doping density, **DD**, (3.26×10^{17} cm^{-3}) that resembles the authentic value (3.26×10^{17} cm^{-3}) of the semiconductor. The naked and polysiloxane- modified surfaces showed rather less accurate values, 3.74×10^{17} and 2.8×10^{17} cm^{-3} respectively, Fig. (4-7a,b).

4.3.1. In the light

Under illumination, M-S plots were measured for the modified and unmodified n-GaAs surfaces in the water/$LiClO_4$/$K_4[Fe(CN)_6]$/$K_3[Fe(CN)_6]$. The effect of n-GaAs surface modification was more pronounced here. The low stability of the unmodified n-GaAs surface made it difficult to measure the **M-S** plots under different degrees of illumination (room light, low intensity light, and high intensity light), Fig (4-8→13) No linear **M-S** plots could be constructed for the unmodified surface. The Polysiloxane-modified surface was also not stable enough to show linear plots. The annealed n-GaAs/MnP/polysiloxane was the only one to show soundly linear **M-S** plots under illumination with room light, 0.0105 W/cm^2, Fig. (4-14b). Without annealing, the modified surface showed, but to a lesser extent, linear **M-S** plots, as shown in Figure (4-14a). These findings dictate that the n-GaAs/MnP/Polysiloxane is shifted towards a more positive value, by up to 700 mV, relative to that of the unmodified n-GaAs. This value is larger than the corresponding shifting for modified surfaces without annealing.

The n-GaAs surface modification enhanced the SC surface in another way as appears from Figures (4-7). The ***annealed*** MnP/polysiloxane- modified electrodes have different slopes from the unmodified ones. The slope of the modified n-GaAs wafer, Fig. (4-7c), gave a value for the measured doping density, **DD**, (3.26×10^{17} cm^{-3}) that resembles the authentic value (3.26×10^{17} cm^{-3}) of the semiconductor. The naked and polysiloxane- modified surfaces showed rather less accurate values, 3.74×10^{17} and 2.8×10^{17} cm^{-3} respectively, Fig. (4-7a,b).

4.3.1. In the light

Under illumination, M-S plots were measured for the modified and unmodified n-GaAs surfaces in the water/$LiClO_4$/$K_4[Fe(CN)_6]$/$K_3[Fe(CN)_6]$. The effect of n-GaAs surface modification was more pronounced here. The low stability of the unmodified n-GaAs surface made it difficult to measure the **M-S** plots under different degrees of illumination (room light, low intensity light, and high intensity light), Fig (4-8→13) No linear **M-S** plots could be constructed for the unmodified surface. The Polysiloxane-modified surface was also not stable enough to show linear plots. The annealed n-GaAs/MnP/polysiloxane was the only one to show soundly linear **M-S** plots under illumination with room light, 0.0105 W/cm^2, Fig. (4-14b). Without annealing, the modified surface showed, but to a lesser extent, linear **M-S** plots, as shown in Figure (4-14a). These findings dictate that the

MnP/polysiloxane modification do indeed stabilize the n-GaAs surface under the un-favored working conditions used here.

Table (4-2): Comparison of the positive shifts in V_{fb}* for n-GaAs Electrodes at different light intensities.

		Dark	Light		
			Room light (0.0105W/cm^2)	**Low intensity** (0.0265W/cm^2)	**High intensity** (0.10125W/cm^2)
Not annealed	Figure no.	4-6	4-8	4-10	4-12
	Shape of the plot	Linear	Curved	Bad	Bad
	V_{fb} shift *	240	-	-	-
Annealed	Figure no.	4-7	4-9	4-11	4-13
	Shape of the plot	Linear	Curved except MnP modified	Bad	Bad
	V_{fb} shift *	700	-	-	-

* Values measured in mV with reference to SCE.

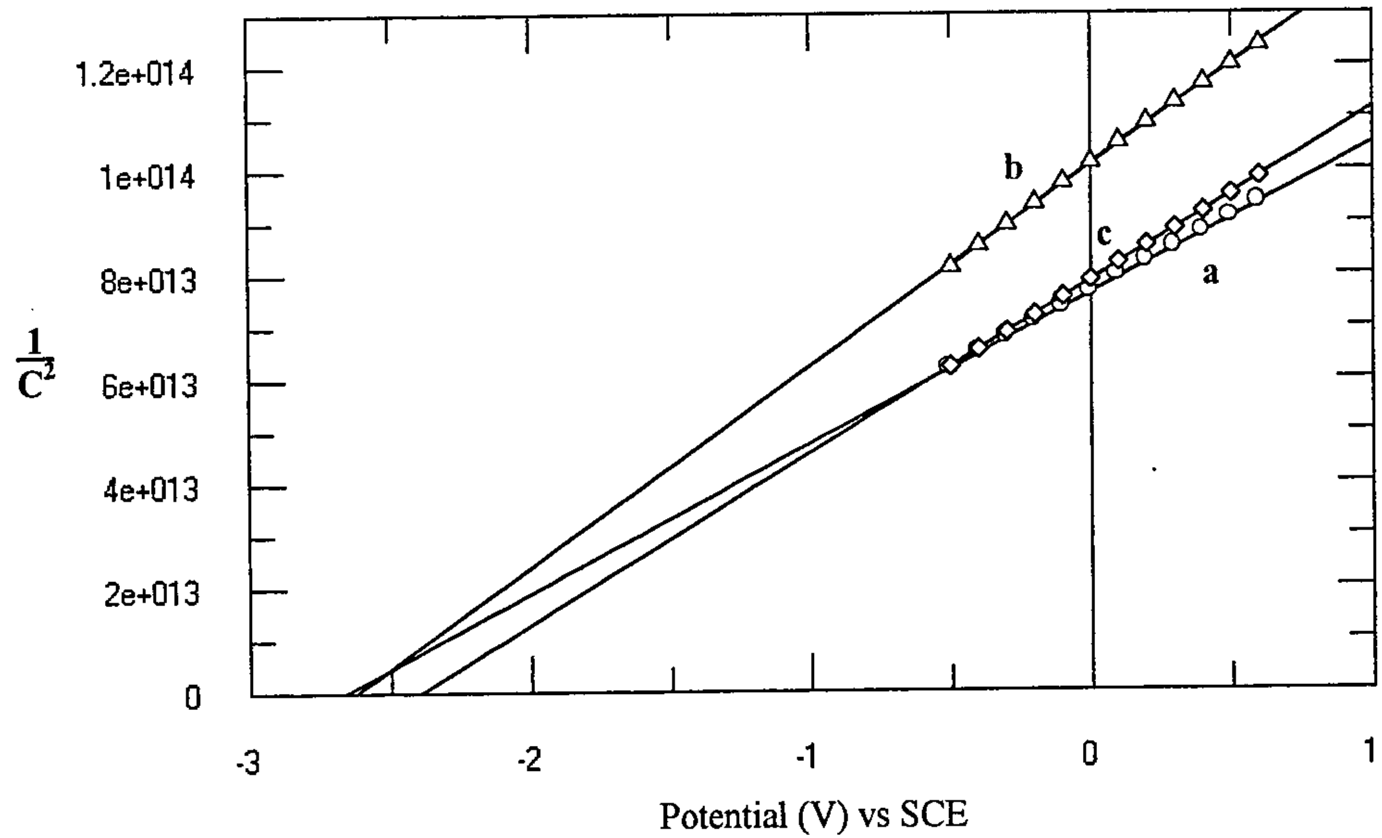

Figure (4-6): Mott-Schottky plots measured for: a) unmodified, b) Polymer modified, and c) MnP/Polymer modified n-GaAs electrodes (without annealing). Measurements were conducted in the dark in water/$LiClO_4$/$K_4[Fe(CN)_6]$/$K_3[Fe(CN)_6]$ at pH=6.5, 25°C.

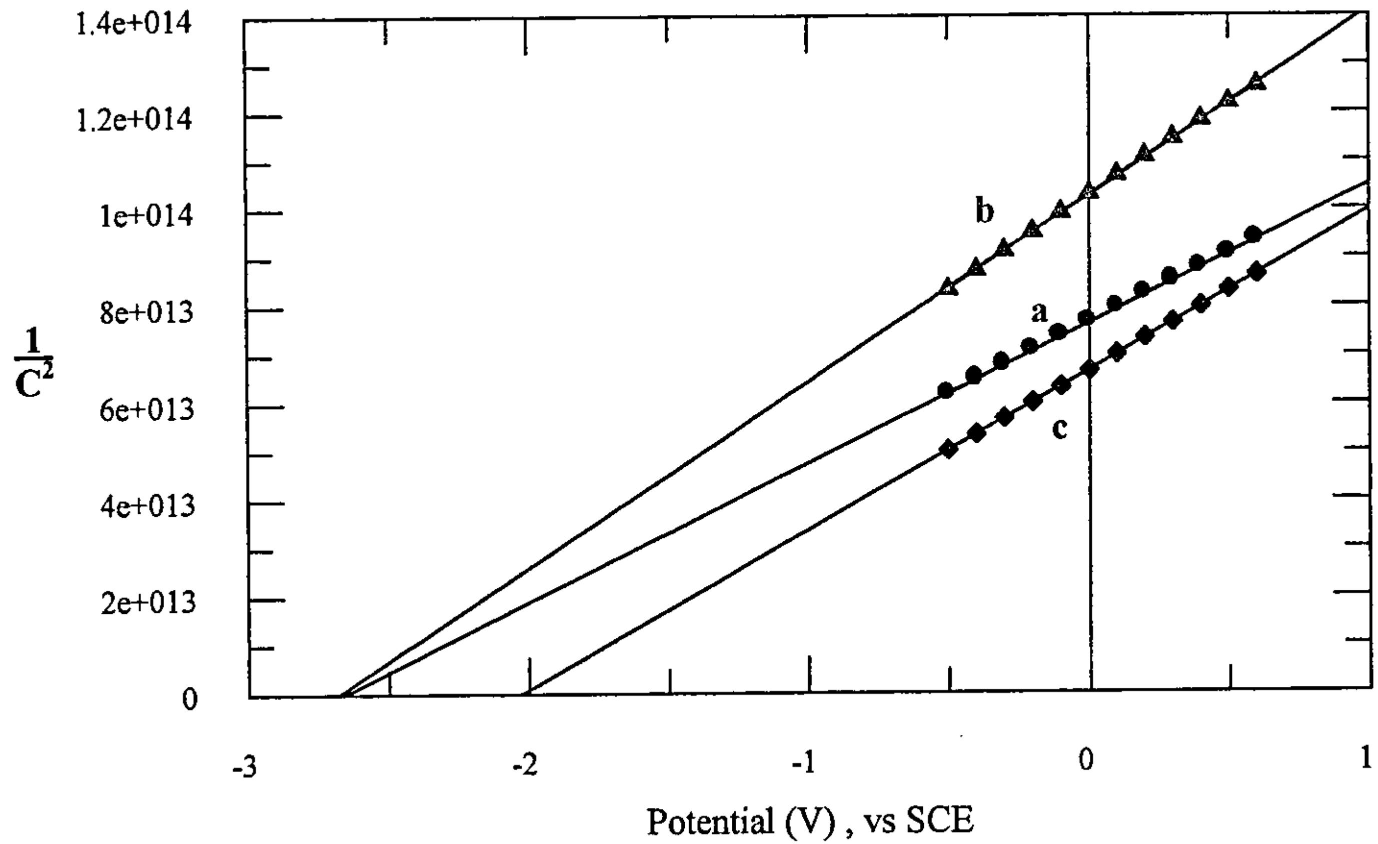

Figure (4-7): Mott-Schottky plots measured after annealing at 100°C for 30 min. under N_2 for: a) unmodified , b) Polymer modified , and c) MnP/Polymer modified n-GaAs electrodes. Measurements were conducted in the dark in water/$LiClO_4$/$K_4[Fe(CN)_6]$/$K_3[Fe(CN)_6]$ at pH=6.5, 25°C.

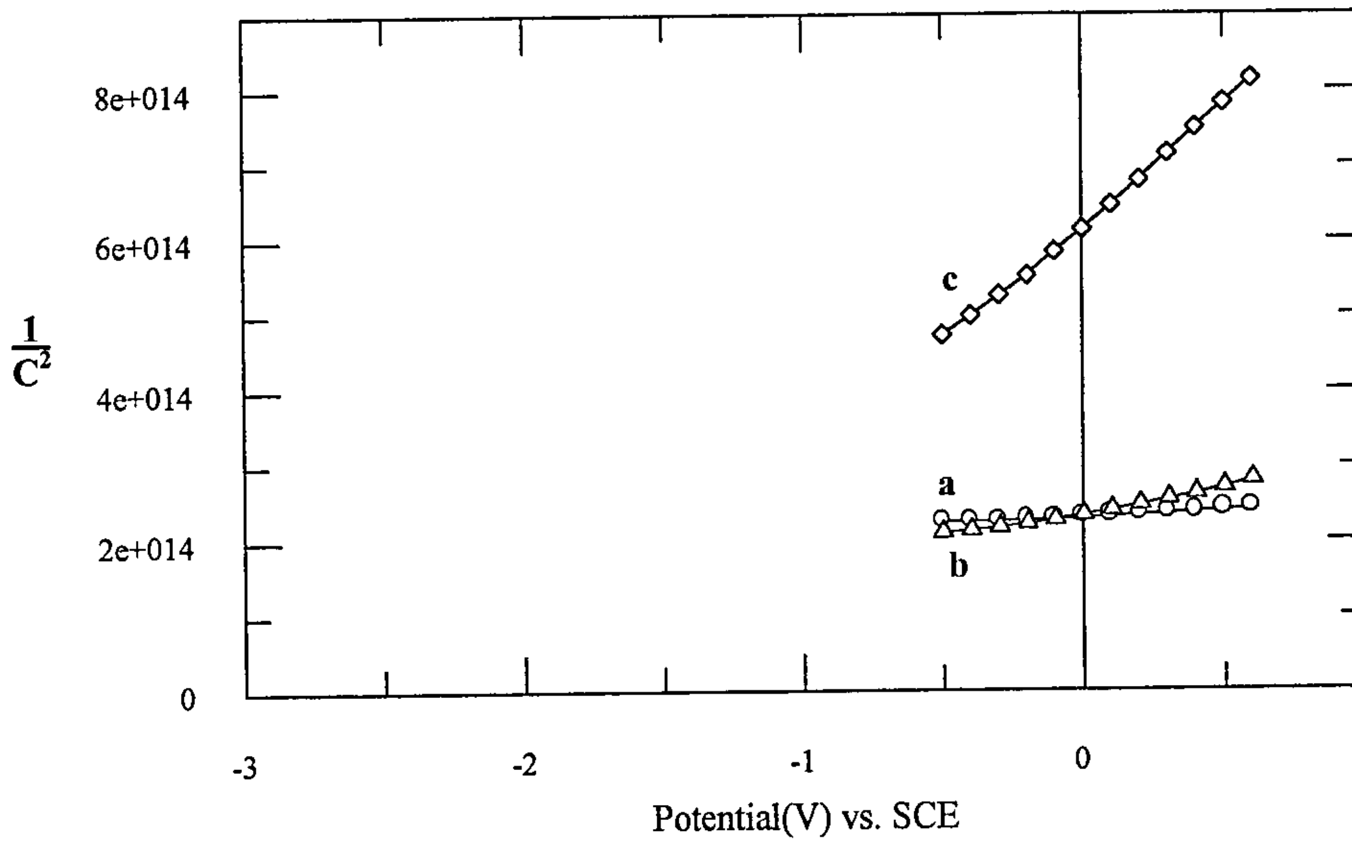

Figure (4-8): Mott-Schottky plots measured for: a) unmodified , b) Polymer modified , and c) MnP/Polymer modified n-GaAs electrodes (without annealing). Measurements were conducted at room light (0.0105 W/cm^2), in water/$LiClO_4$/$K_4[Fe(CN)_6]$/$K_3[Fe(CN)_6]$ at pH=6.5, 25°C.

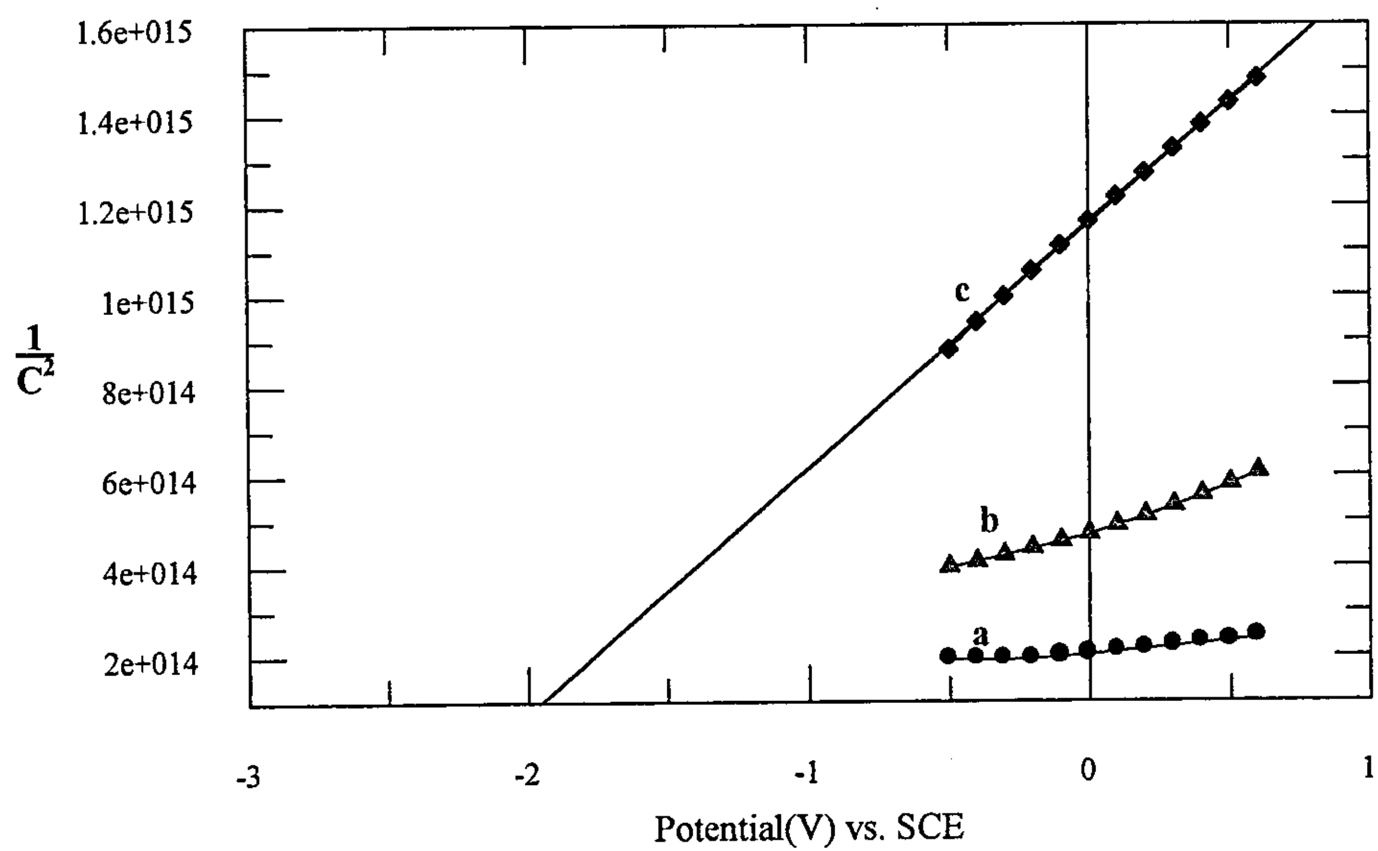

Figure (4-9): Mott-Schottky plots measured after annealing at 100°C for 30 min. under N_2 for: a) unmodified , b) Polymer modified , and c) MnP/Polymer modified n-GaAs electrodes. Measurements were conducted at room light (0.0105 W/cm^2), in water/$LiClO_4$/$K_4[Fe(CN)_6]$ /$K_3[Fe(CN)_6]$ at pH=6.5, 25°C.

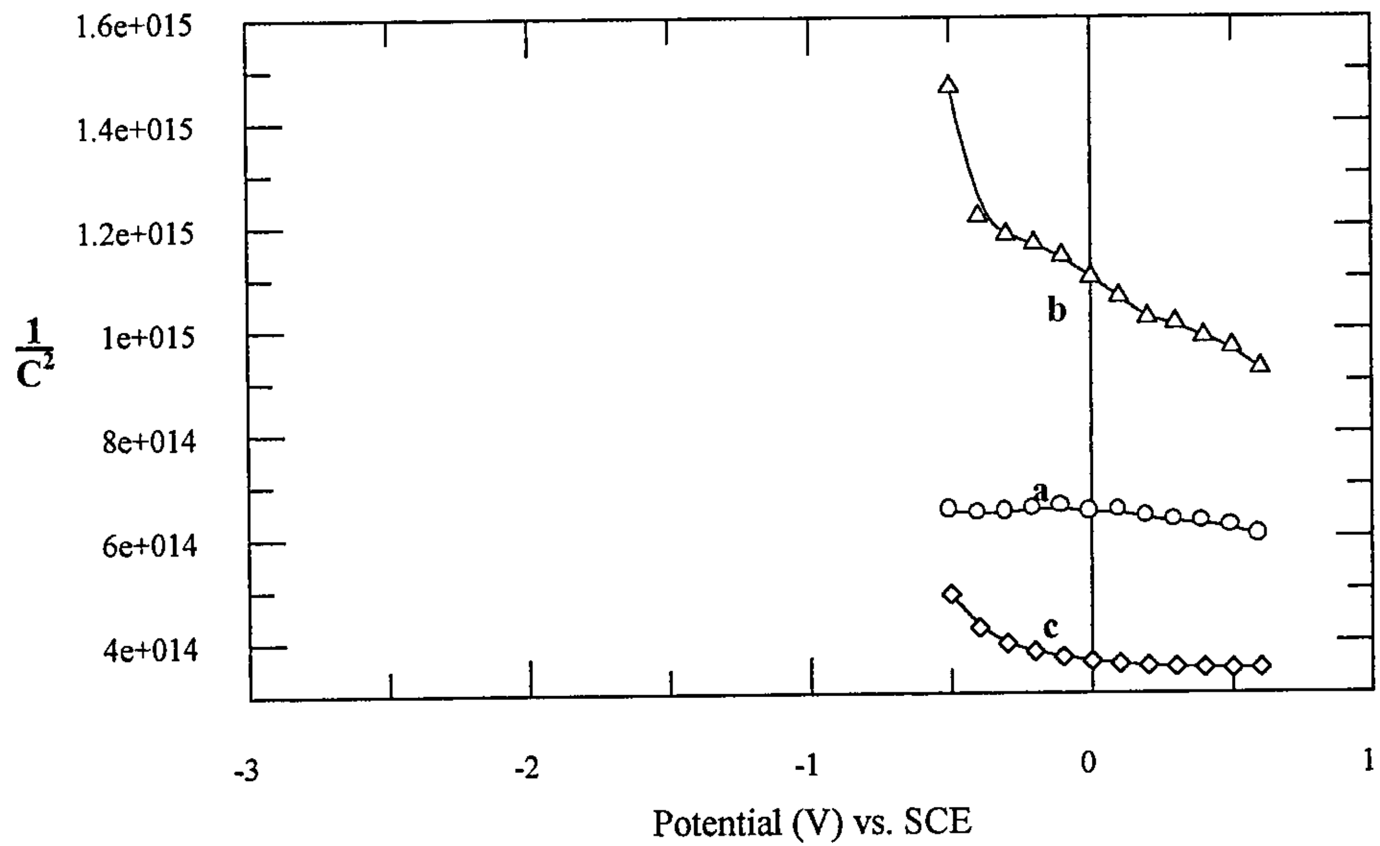

Figure (4-10): Mott-Schottky plots measured for: a) unmodified , b) Polymer modified , and c) MnP/Polymer modified n-GaAs electrodes. (without annealing). Measurements were conducted at low light intensity (0.0265 W/cm^2), in water/$LiClO_4$/$K_4[Fe(CN)_6]$/$K_3[Fe(CN)_6]$ at pH=6.5, 25°C.

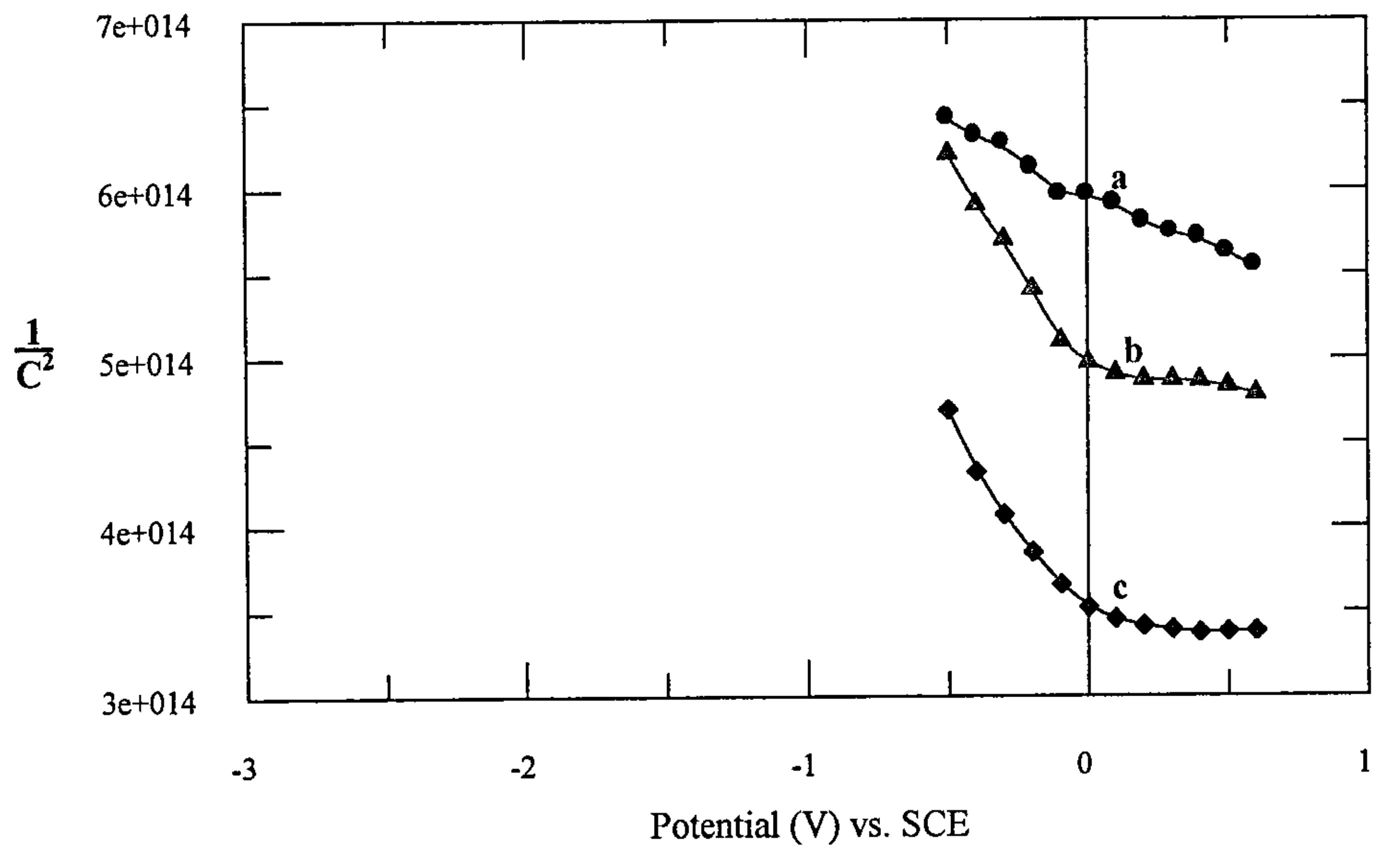

Figure (4-11): Mott-Schottky plots measured after annealing at 100°C for 30 min. under N_2 for: a) unmodified , b) Polymer modified , and c) MnP/Polymer modified n-GaAs electrodes. Measurements were conducted at low light intensity (0.0265 W/cm^2), in water/$LiClO_4$/$K_4[Fe(CN)_6]$ /$K_3[Fe(CN)_6]$ at pH=6.5, 25°C.

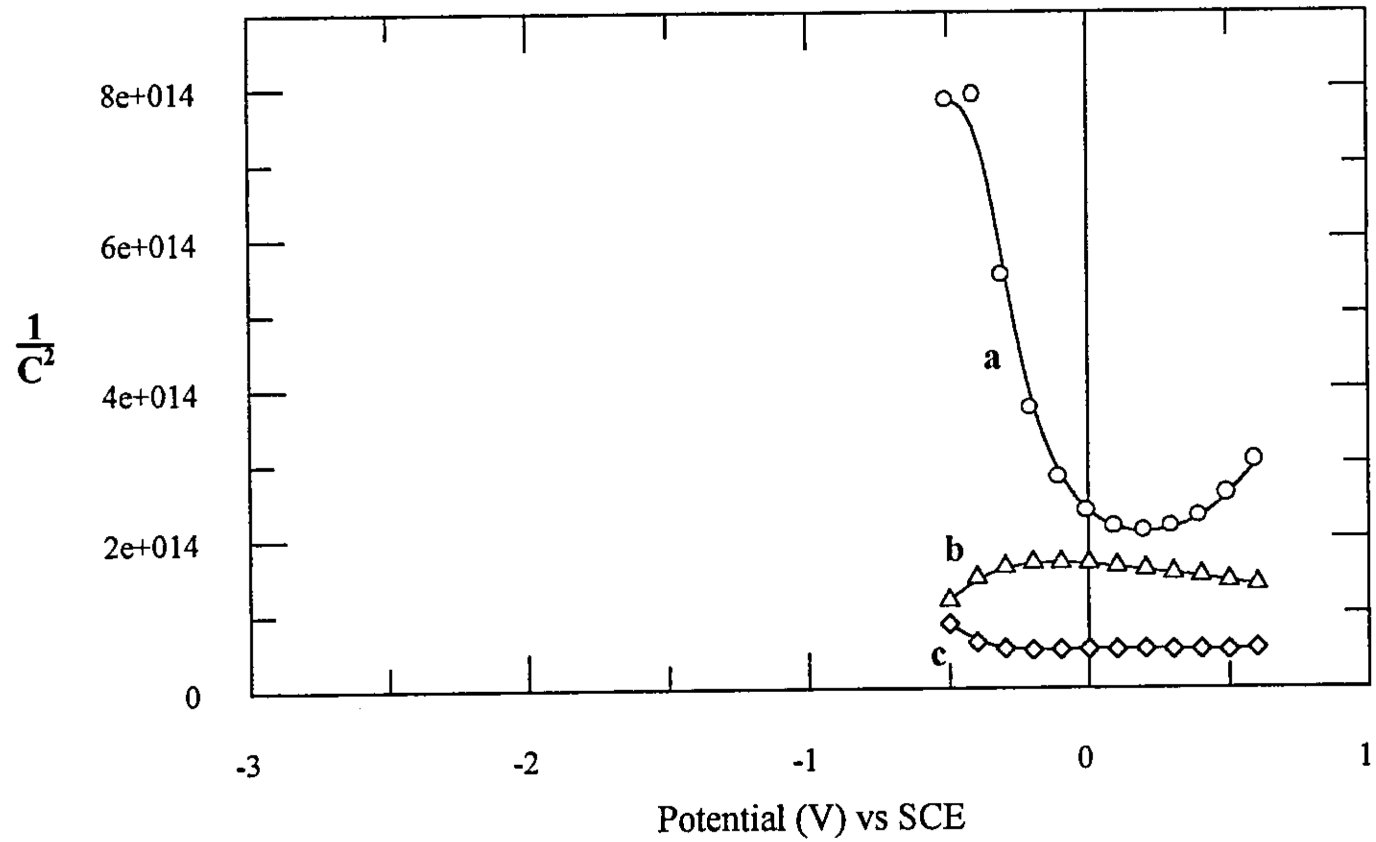

Figure (4-12): Mott-Schottky plots measured for: a) unmodified , b) Polymer modified , and c) MnP/Polymer modified n-GaAs electrodes. (without annealing). Measurements were conducted at high light intensity (0.10125 W/cm^2), in water/$LiClO_4$/$K_4[Fe(CN)_6]$/$K_3[Fe(CN)_6]$ at pH=6.5, 25°C.

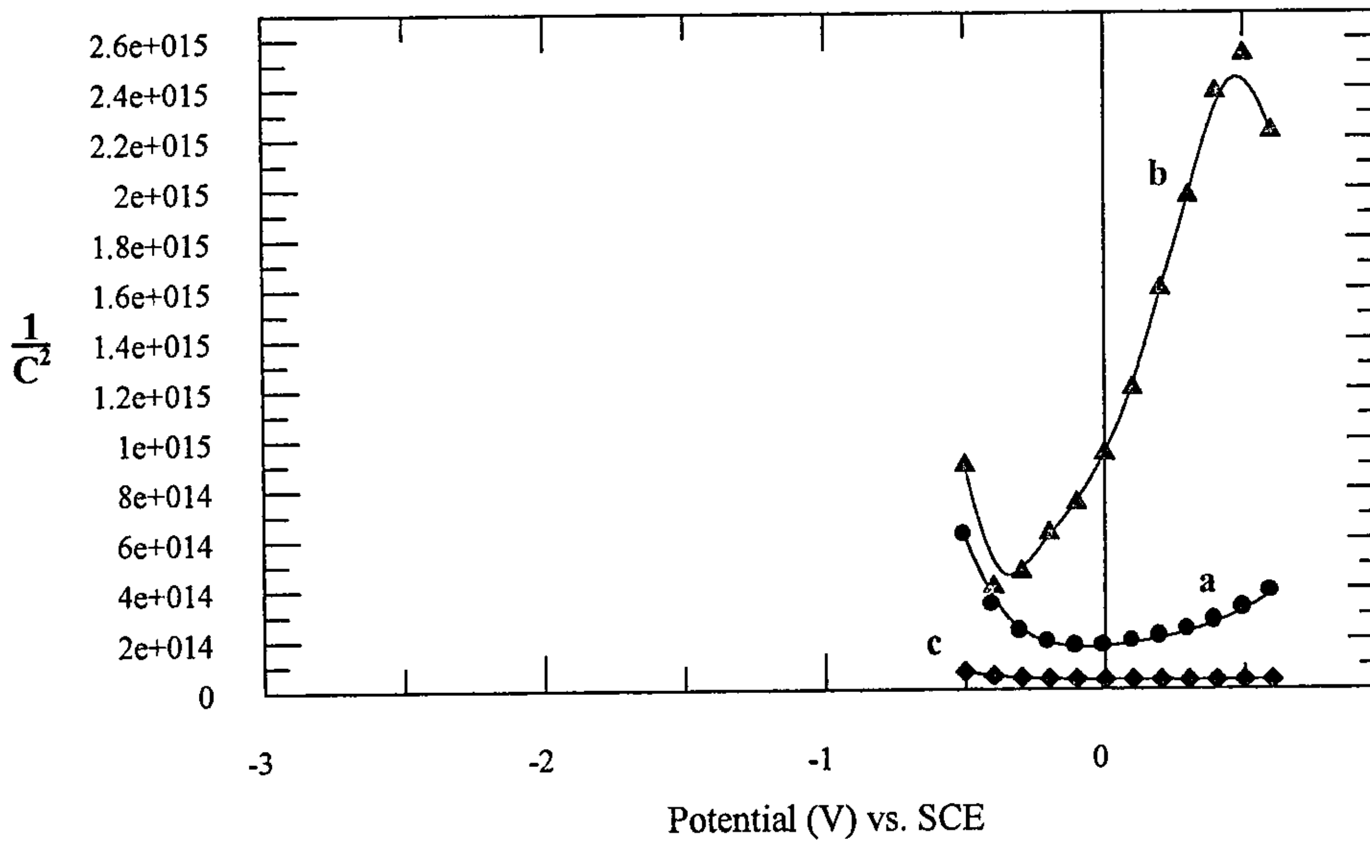

Figure (4-13): Mott-Schottky plots measured after annealing at 100°C for 30 min. under N_2 for: a) unmodified, b) Polymer modified, and c) MnP/Polymer modified n-GaAs electrodes. Measurements were conducted at high light intensity (0.10125 W/cm^2), in water/$LiClO_4$/ $K_4[Fe(CN)_6]$/ $K_3[Fe(CN)_6]$ at pH=6.5, 25°C.

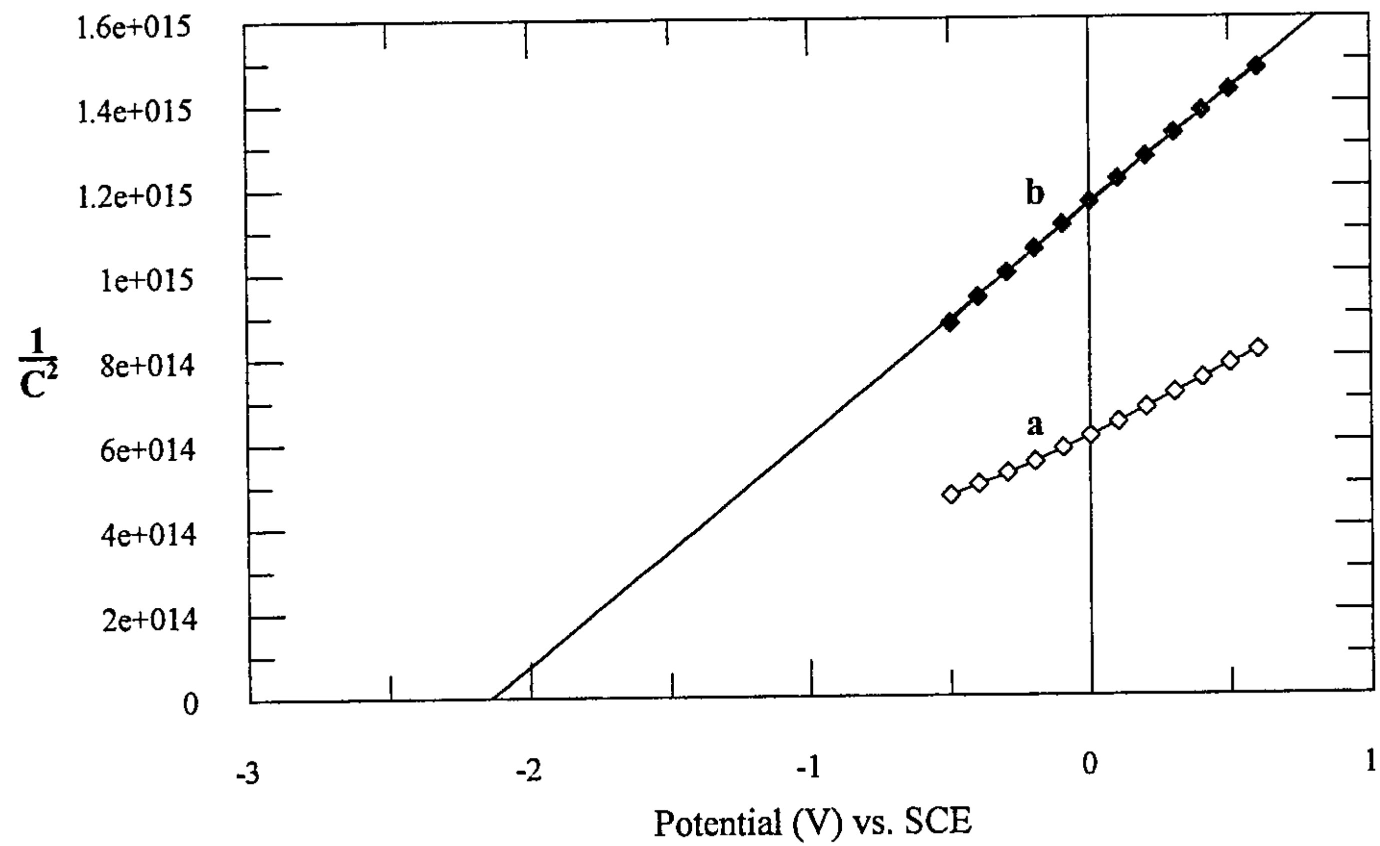

Figure (4-14): Mott-Schottky plots measured for MnP/Polymer modified n-GaAs electrodes: a) without annealing , and b) after annealing at 100°C for 30 min under N_2. All measurements were conducted at <u>room light (0.0105 W/cm^2)</u>, in water/$LiClO_4$/$K_4[Fe(CN)_6]$/$K_3[Fe(CN)_6]$ at pH=6.5, 25°C.

4.4. SC ELECTRODE STABILITY TESTING

The effect of modification on stabilizing the semiconductor surface was studied while using the aqueous $LiClO_4/K_4[Fe(CN)_6]/K_3[Fe(CN)_6]$ system in the dark and under illuminance of 140000 Lux (irradiance of 0.10125 W/cm^2) A nitrogen atmosphere was used to minimize contamination with air.

In the dark, the effect of the MnP/Polysiloxane modification on stabilizing n-GaAs surface was manifested in two ways, as discussed above. The modified surfaces showed enhanced *J-V* plots, and more accurate doping density measurements, than the unmodified surfaces.

Under illumination, the modification effect was even more pronounced. The photocurrent *J-V* plots were also enhanced and better defined than those for the unmodified surfaces, as shown in Figures (4-4,5). In this work, the short circuit current, I_{sc}, value was enhanced by modification with MnP/Polysiloxane. This is one major advantage of this research. In the absence of the MnP ions, the polysiloxane caused some SC surface stabilization, but I_{sc} value was enhanced slightly.

Special experiments were conducted to study the stability of the modified n-GaAs surface to photocorrosion by using the $LiClO_4/K_4[Fe(CN)_6]/K_3[Fe(CN)_6]$ aqueous system with partial contamination with air. A high intensity Xe lamp was used. The SC electrode was exposed to a light with 140000-Lux illuminance, 0.10125-W/cm^2 irradiance, under 0.00 V applied bias (*vs.* SCE). The I_{sc} value was measured with time, throughout 3 hr periods at different temperatures. At the beginning, the value of I_{sc} was too small that no sound comparisons could be made between modified and unmodified electrodes. After some time, better values of I_{sc} were observed.

Figure (4-15) indicates that, ***without annealing***, the modified n-GaAs surfaces exhibited higher I_{sc} values than the unmodified ones. At ***25°C*** the polysiloxane-modified surface has a value of I_{sc} four-fold that for the unmodified surface, when measured after 80-min. exposure time. The MnP/Polysiloxane- modified n-GaAs surface showed a rather higher I_{sc}, with about eight-fold that of the unmodified surface.

After annealing, Figure (4-16) shows that the modification has a somewhat better enhancing effect on I_{sc} values than the not annealed modification. Again at the same temperature, ***25°C***, the polysiloxane-modified surface has a value of I_{sc} four-fold than for the unmodified surface, when measured after 80-min exposure time. The MnP/Polysiloxane- modified n-GaAs surface showed a rather higher I_{sc}, with more than eight-fold that of the unmodified surface.

Effect of modification on the ***annealed*** electrode stabilization was investigated at other higher temperatures. ***At 35°C*** the unmodified n-GaAs surface completely degraded after 200 min. of working time. The n-GaAs/MnP/polysiloxane electrode has a higher stability to photodegradation, causing higher I_{sc} readings for longer times, Fig. (4-17). The stabilizing effect of the MnP/Polysiloxane is therefore pronounced at temperatures in the range 25° to 35°C. At higher temperature, ***45°C***, the modified and the unmodified surfaces showed higher tendency to degrade than at lower temperatures, as shown in Figure (4-18).

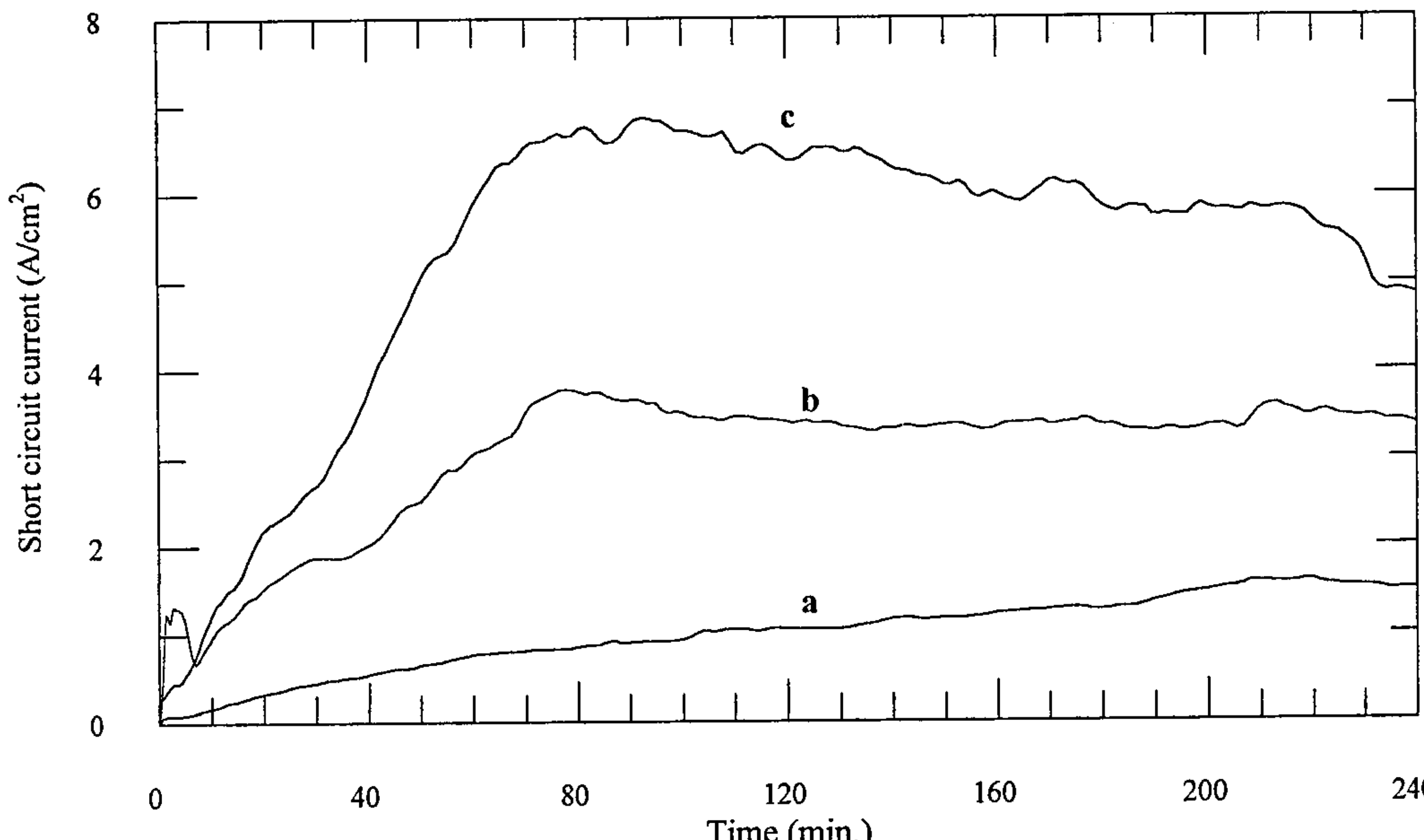

Figure (4-15): Short circuit current vs. time for: a) unmodified n-GaAs, b) Polymer modified n-GaAs , and c) MnP/Polymer modified n-GaAs. Without annealing . All measurements were conducted in water/$LiClO_4$/$K_4[Fe(CN)_6]$/$K_3[Fe(CN)_6]$, pH=6.5, at 25°C, using high intensity illumination Xe lamp (0.10125 W/cm^2).

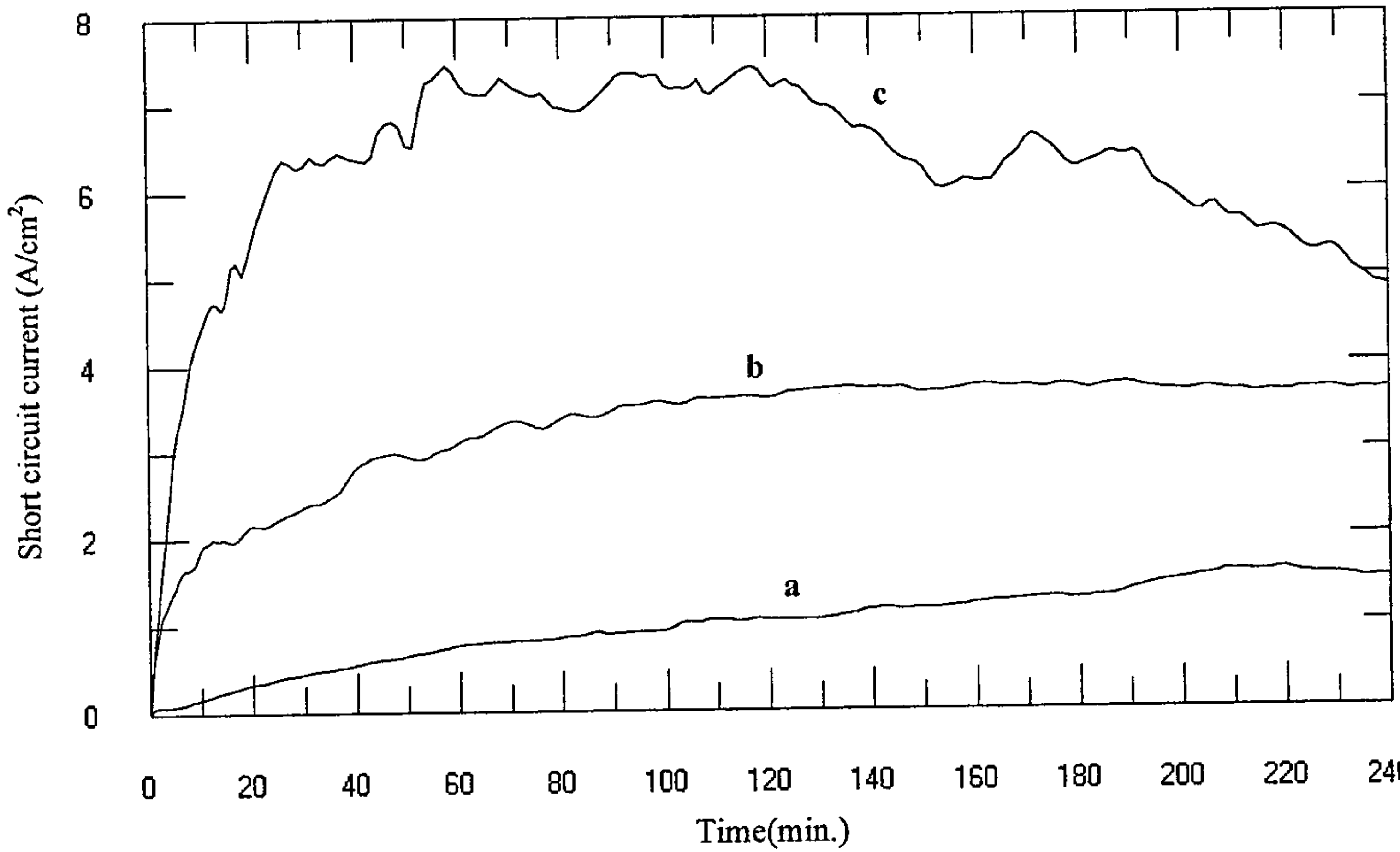

Figure (4-16): Short circuit current vs. time for: a) unmodified n-GaAs , b) Polymer modified n-GaAs , and c) MnP/Polymer modified n-GaAs. All annealed at 100°C for 30 min. under N_2. All measurements were conducted in water/$LiClO_4$/$K_4[Fe(CN)_6]$/$K_3[Fe(CN)_6]$, pH=6.5, at 25°C, using high intensity illumination Xe lamp (0.10125 W/cm^2).

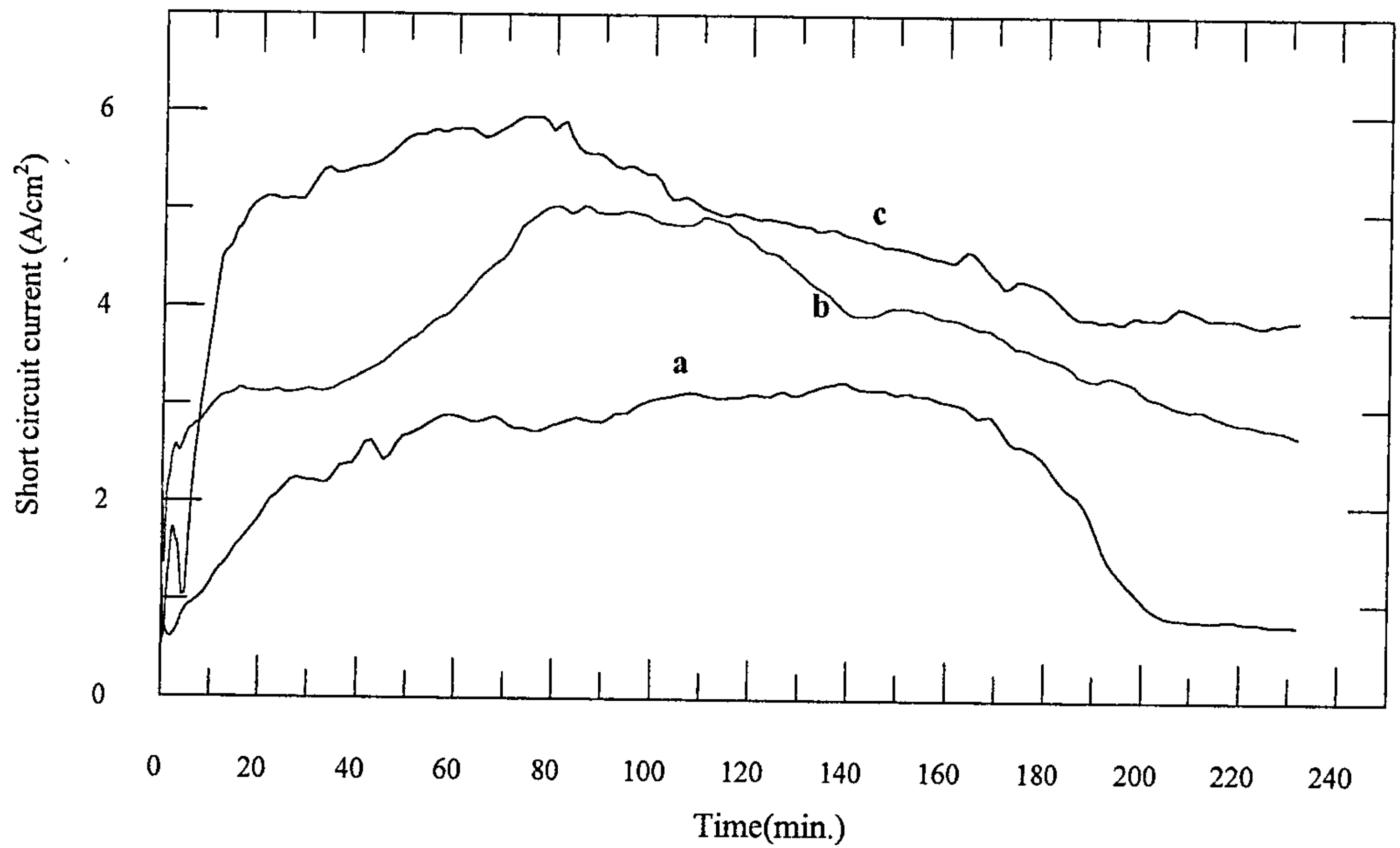

Figure (4-17): Short circuit current vs. time for: a) unmodified n-GaAs , b) Polymer modified n-GaAs , and c) MnP/Polymer modified n-GaAs. Without Annealing. All measurements were conducted in water/$LiClO_4$/$K_4[Fe(CN)_6]$/$K_3[Fe(CN)_6]$, pH=6.5, at 35°C, using high intensity illumination Xe lamp (0.10125 W/cm^2).

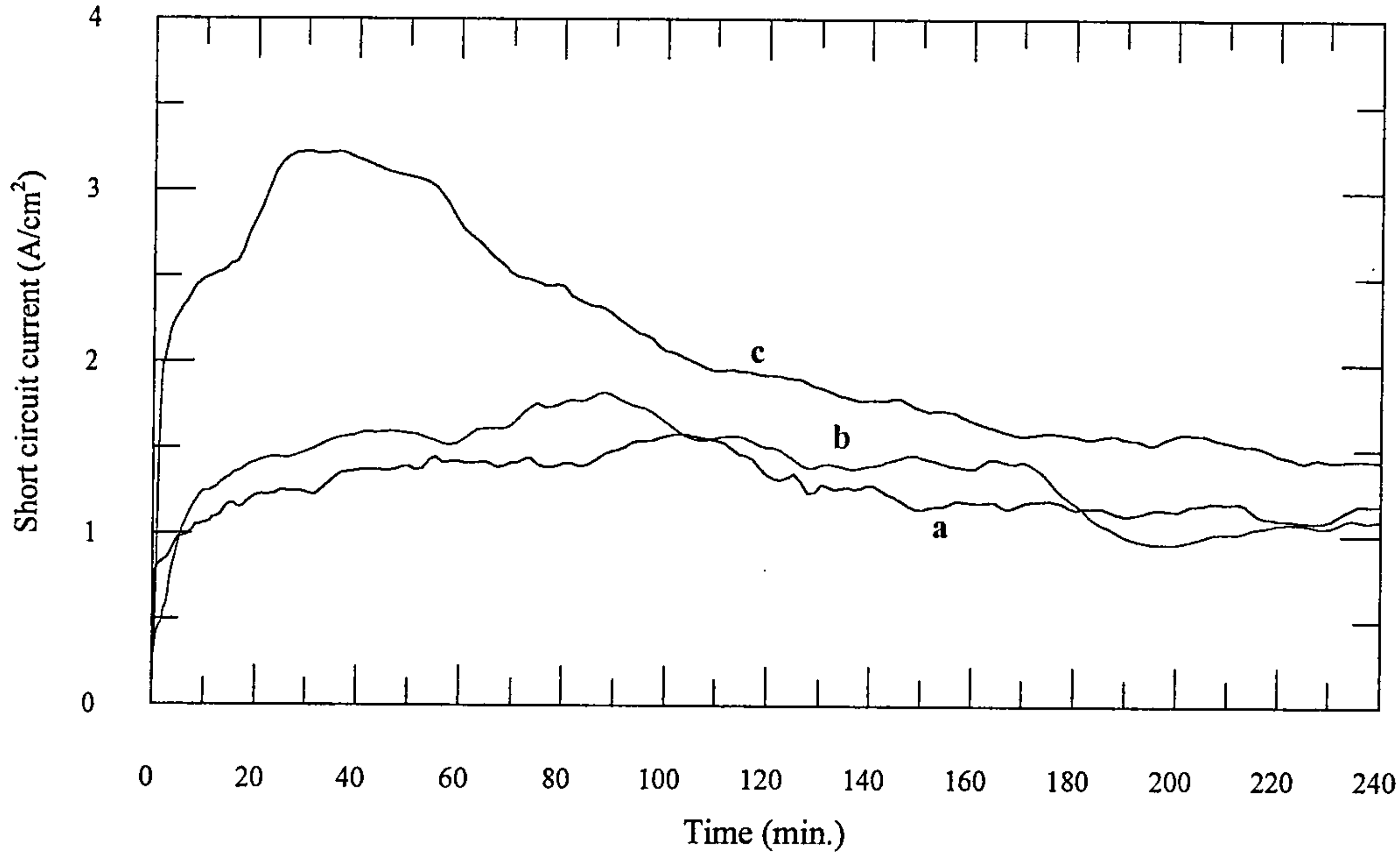

Figure (4-18): Short circuit current vs. time for: a) unmodified n-GaAs , b) Polymer modified n-GaAs , and c) MnP/Polymer modified n-GaAs. Without Annealing. All measurements were conducted in water/$LiClO_4$/$K_4[Fe(CN)_6]$/$K_3[Fe(CN)_6]$, pH=6.5, at 45°C, using high intensity illumination Xe lamp (0.10125 W/cm^2).

4.5. CELL EFFICIENCY STUDIS

The light-to-current-conversion efficiency of the electrode was enhanced by modification. The measured maximum cell power, [current (A cm^{-2}) X potential (V)], measured in W cm^{-2}, was calculated at different exposure times. The cell efficiency, [maximum measured power (W cm^{-2})/lamp power (W cm^{-2})] X 100%, was then calculated for the modified and unmodified n-GaAs surfaces after different exposure times.

Table (4-3): Values of cell conversion efficiency for different n-GaAs electrodes (*without annealing*).

Electrode	Cell Efficiency % at different times (min)					
	40	80	120	160	200	240
Naked n-GaAs	0.31	0.50	0.61	0.72	0.86	0.87
n-GaAs/Polysiloxane	1.24	2.35	2.12	2.08	2.10	2.08
n-GaAs/MnP/Polysiloxane	1.74	3.15	2.97	2.81	2.72	2.26

All measurements were conducted at 25°C in water/$LiClO_4$/$K_4[Fe(CN)_6]$/ $K_3[Fe(CN)_6]$ media, using a 50W Xe lamp, with a 0.10125 W cm^{-2} irradiance at the electrode surface. Cell maximum output power was roughly calculated by multiplying the measured I_{sc} (at 0.0 V) by the corresponding V_{oc} value for the same electrode. Conversion efficiency was calculated by dividing the maximum output power by illumination intensity.

Table (4-3) shows values of cell efficiencies for different ***not annealed*** electrodes measured after different exposure times ***at 25°C***. The results indicate that, after exposure for some time, the efficiency for the MnP/Polysiloxane modified electrode is enhanced. The maximum cell efficiency reached 3.15%, after 80 min, which means up to six- fold enhancement in cell efficiency, Fig (4-19). This efficiency enhancement is due to the short-circuit current enhancement shown earlier for the modified electrode.

Table (4-4) shows values of cell efficiencies for different ***annealed*** electrodes measured after different exposure times ***at 25°C***. The results indicate approximately the same enhancement in cell efficiency, Fig. (4-20). As a net result, the cell efficiency was highly enhanced by modification with Mn/Polysiloxane. The polysiloxane-modified n-GaAs also showed good enhancement in cell efficiency, but a lower extent.

Table (4-4): Values of cell conversion efficiency for different n-GaAs electrodes (*after annealing*).

Electrode	Cell Efficiency % at different times (min)					
	40	80	120	160	200	240
Naked n-GaAs	0.34	0.54	0.66	0.78	0.94	0.95
n-GaAs/Polysiloxane	1.69	2.01	2.14	2.22	2.17	2.19
n-GaAs/MnP/Polysiloxane	2.93	3.20	3.33	2.78	2.70	2.24

All measurements were conducted at 25°C in water/$LiClO_4$/ $K_4[Fe(CN)_6]$/ $K_3[Fe(CN)_6]$ media, using a 50W Xe lamp, with a 0.10125 W cm^{-2} irradiance at the electrode surface.

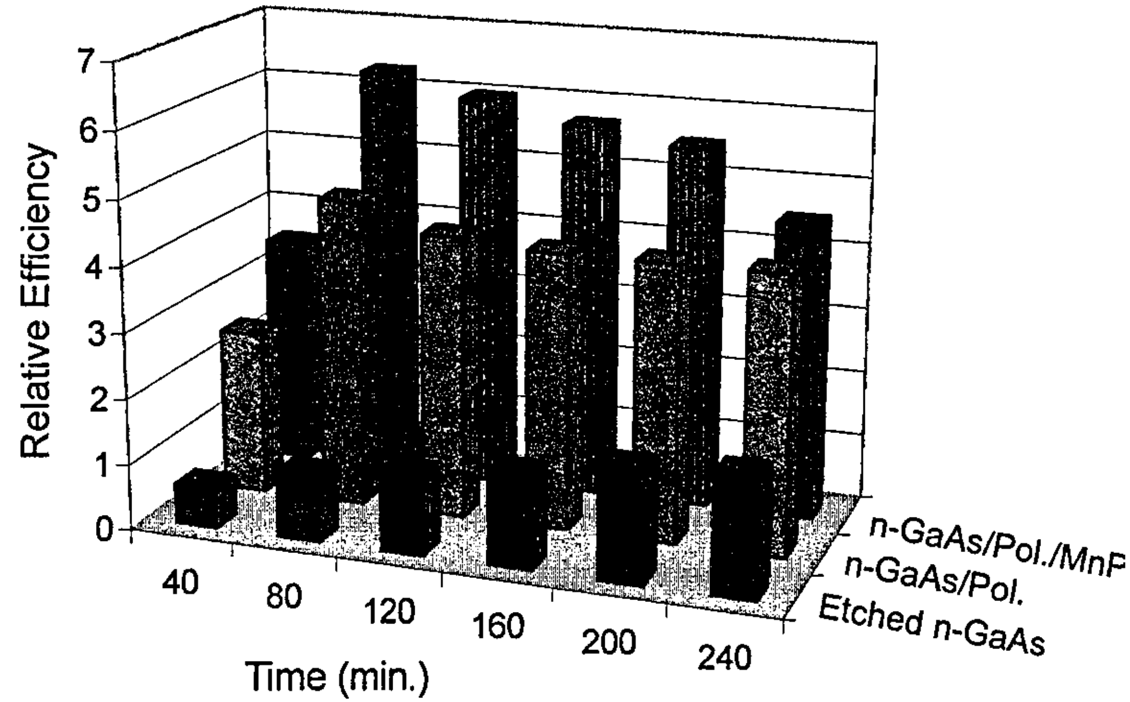

	40	80	120	160	200	240
Etched n-GaAs	0.6	1	1.2	1.4	1.7	1.8
n-GaAs/Pol.	2.5	4.7	4.3	4.2	4.2	4.2
n-GaAs/Pol./MnP	3.5	6.3	6	5.7	5.5	4.5

Figure (4-19): The relative efficiencies for the not annealed electrodes after different time of exposure, at 25°C. All these values obtained by dividing the data in table (4-3) by cell efficiency for the etched n-GaAs electrode after 80 min. of exposure, $0.4974 w/cm^2$.

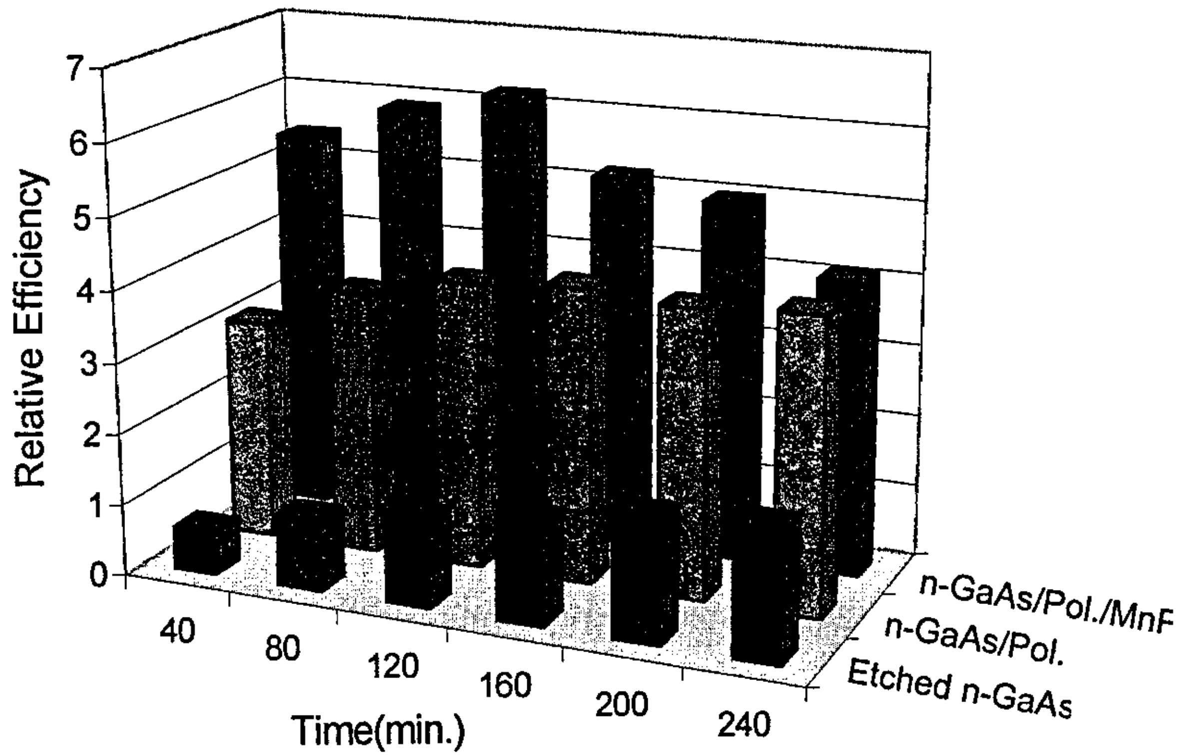

	40	80	120	160	200	240
Etched n-GaAs	0.6	1	1.2	1.4	1.7	1.8
n-GaAs/Pol.	3.1	3.7	4	4.1	4	4.1
n-GaAs/Pol./MnP	5.4	5.9	6.2	5.2	5	4.1

Figure (4-20): The relative efficiencies for the **annealed** electrodes after different time of exposure, at 25°C. All these values obtained by dividing the data in table (4-4) by cell efficiency for the etched n-GaAs electrode after 80 min. of exposure, 0.5396w/cm^2.

Chapter Five

DISCUSSION

DISCUSSION

The V_{fb} is one of the most important experimental parameters to measure on a SC electrode. The position of the band edges on the electrochemical scale, the direction of the band-bending, and in favorable cases the magnitude of the band-bending are determined if V_{fb} is known.

The assumption that positive charges lower the V_{fb} has a reason, since positive charges are known to stabilize energy levels close to it [73]. Our expectation is that positive charges should lower the potential energy only nearby (surface SCL) not bulk values due to distance, Fig. (5-1).

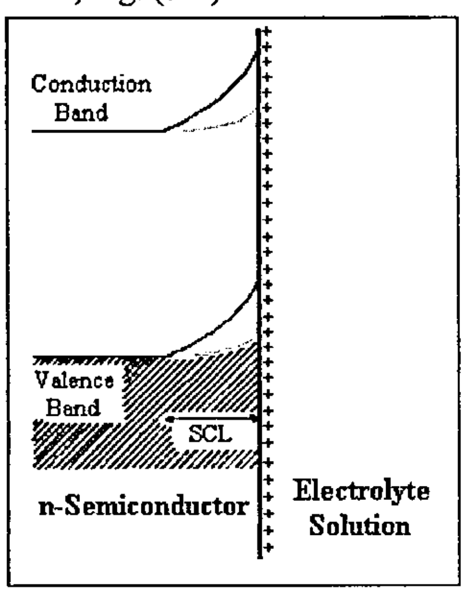

Figure (5-1): Correlation diagram showing band edges: (------) before modification, and (-------) after modification.

Results shown in Figure (4-2→7) validated our assumption. The V_{fb} is positively shifted toward less negative value. This shift was manifested by:

(1) Shifting in V_{onset} (dark).

(2) Shifting in V_{oc} (illumination).

(3) Shifting V_{fb} as directly measured by Mott-Schottky method.

Such a lowering is due to the MnP positive charges residing in a close proximity to the SC surface at the SC/polymer interface. In the absence of MnP, no shifting in the value of the V_{fb} was observed. The lowering in the value of the V_{fb} by attachment of positive charges has already been observed in similar photoelectrochemical systems using sub-mono-layer of MnP chemically anchored to the SC surface [65].

5.1. DARK CURRENT V_{ONSET} SHIFT

The MnP-modified SC surface shwed a shifting in the dark-current onset potential (V_{onset}) compared to the unmodified surface. The shift was towards a more positive potential value (positive shift). Such a positive shift is an indicator of a lowering in the value of the flat-band potential (V_{fb}), Fig. (5-2). The SC band-edge lowering affects the energetics and the kinetics of the charge transfer processes at the SC/liquid interfaces in PEC solar cells.

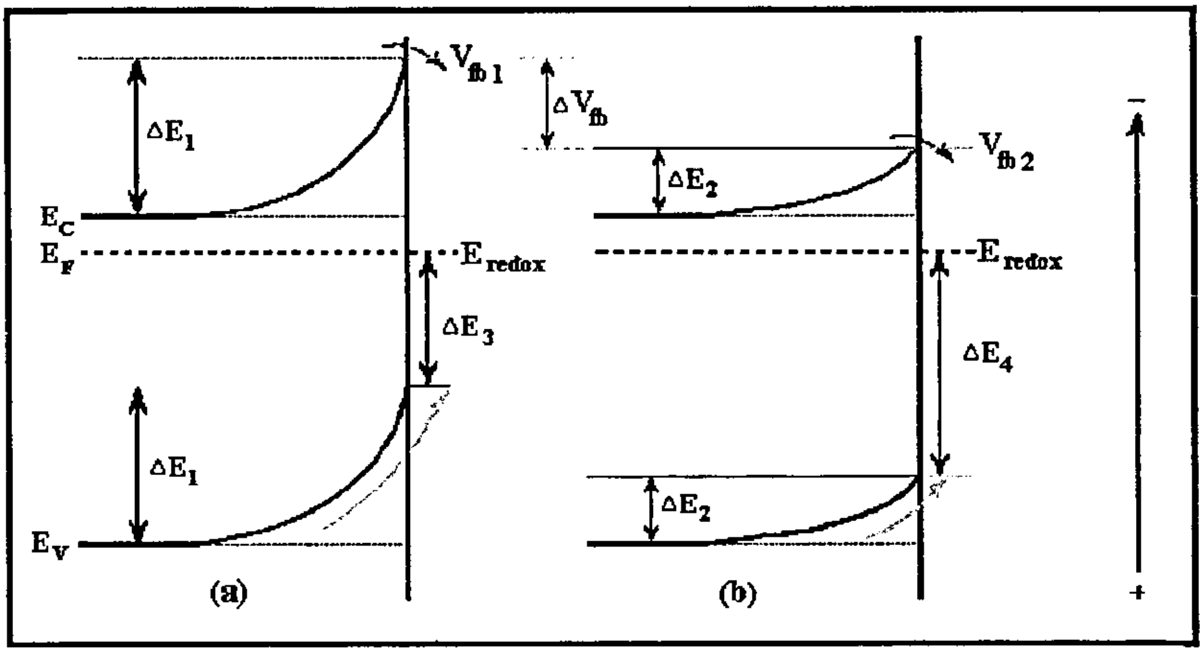

Figure (5-2): Energy correlation between band edges for: a) naked and b) MnP-modified n-GaAs electrodes. The Fermi energy of the redox couple at equilibrium is shown.

In case of n-type SC, negative applied potential is needed to raise the bulk band edges to become flat, in order to have a dark current. In the case of MnP modified n-GaAs, the lowering in the value of the V_{fb} dictates that only a small negative applied potential (ΔE_2) is needed for the dark-current to occur. This applied potential (ΔE_2) is less negative than the one needed in the case of naked n-GaAs (ΔE_1), when using all other conditions the same. In addition to the fact that lowering the SC VB edge, at SCL only, increases the amount of the energy (ΔE) available to drive the hole transfer from the valence band to the solution redox couple. From Figure (5-2) it is shown that ΔE_4 (for the modified electrode) is larger than ΔE_3 (for the naked electrode). Therefore, the hole transfer from the valence band to the redox couple becomes energetically more favored after surface modification. The lowering in the value of V_{fb} is mainly due to the MnP positive charges entrapped inside the polysiloxane matrix adhered to the SC surface. SC surfaces modified with MnP-free polysiloxane matrix did not show a lowering in the value of the V_{fb}. This is apparently due to the fact that the polysiloxane matrix has no positive charges. The fact that positive charge attachment to n-GaAs surfaces yields a lowering in the value of its V_{fb} has been reported [48, 52-53, 74].

Figure (5-2) also explains the effect of the band-edge lowering on the kinetics of the majority carrier (electron) transfer processes at the surface. The dark current results from the electron transfer from the SC CB to the solution redox couple. At equilibrium, the band bending creates an energy barrier. The electrons must overcome this barrier before they transfer. Therefore, for dark current to occur, an applied negative potential is needed to provide the electrons with enough energy to overcome the barrier. When the surface is modified with positive charges, the band edges are lowered, and consequently, the energy barrier is lowered. Thus, a less negative (more positive) potential is needed to create a dark current, in case of modified surfaces. This appears as a positive shift, in the dark current onset potential, toward more positive values.

The polysiloxane matrix is doing its job holding the MnP redox couple enclosed in it. But it should be noted here that the MnP/Polysiloxane modified n-GaAs electrode with no annealing showed a smaller shifting in the value of the V_{fb}. This indicates that annealing process is necessary to permanently bring the MnP positive ions into a close proximity to the SC surface. When the MnP/Polysiloxane modified electrode is annealed the positive ions diffuse through the polysiloxane matrix resulting in increasing its concentration at the SC/Matrix interface.

5.2. PHOTO CURRENT V_{OC} SHIFT

The MnP/Polysiloxane modified n-GaAs surfaces have shown a shifting in the value of the open-circuit potential V_{oc} towards a more positive (lower) position. The lowering in the value of the V_{oc} is a good indication of a lowering in the value of the V_{fb}.

As mentioned earlier, when the applied potential approaches V_{fb}, the SCL thickness decreases and goes to zero (bands are flattened at $V_{oc(1)}$). Recombination rates increase because the holes and electrons are no longer being separated by electric field, and the photocurrent drops sharply. Therefore, to stop photocurrent, a negative potential equal to or higher than ΔE_1 should be applied to the unmodified SC, Fig. (5-3a). Consequently, in case of modified SC photocurrent will occur only when the applied negative potential is less than ΔE_1, equals ΔE_2, Fig. (5-3b). In other words, upon modification, the applied potential must be more positive than $Voc_{(1)}$. Such a positive shift is due to the MnP positive charges in a close proximity to the SC surface, especially after annealing. The lowering in the value of the V_{oc} by attachment of positive charges has already been observed in similar PEC systems [66] using sub-mono-layer of MnP chemically anchored to the SC surface.

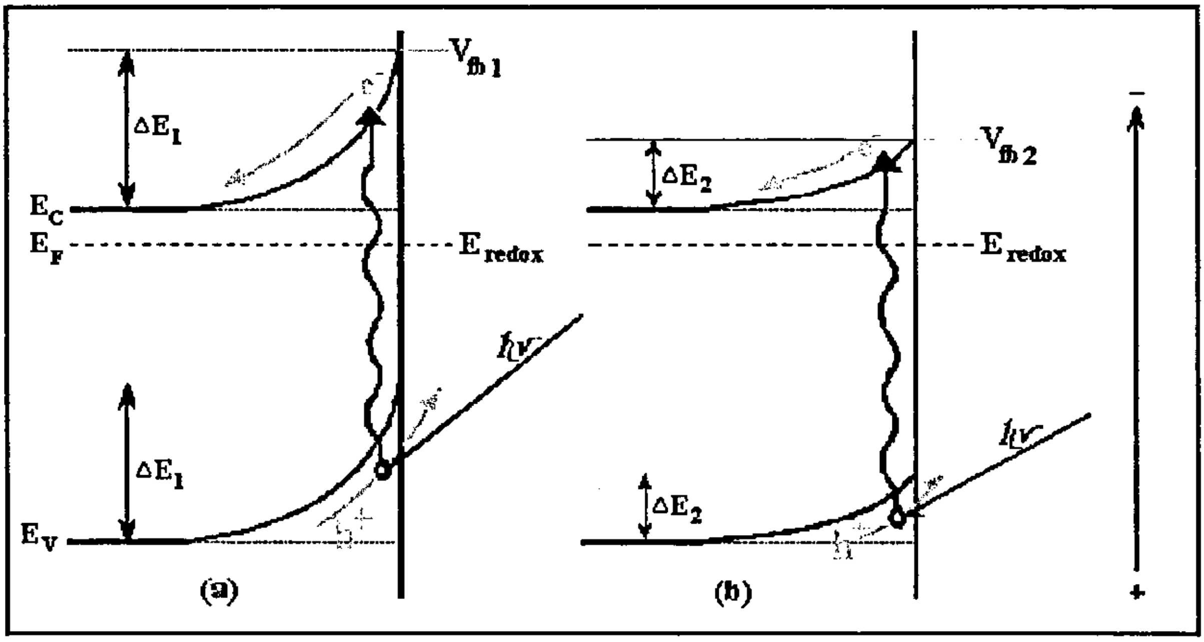

Figure (5-3): Energy correlation between band edges under illumination for: a) naked and b) MnP modified n-GaAs electrodes. The Fermi energy of the redox couple at equilibrium is shown.

As discussed above, the results indicated that the positive shift in V_{oc}, measured for modified surfaces under illumination, is smaller than the dark current V_{on} positive shift. They also indicated that the V_{fb} positive shift measured under illumination is smaller than that measured in the dark. These observations suggest that the band-edge positive shift, resulting from modification, measured in the dark is higher than that measured under illumination. This can be explained using SC surface state charge discussions. Consider the unmodified n-GaAs surface. Illumination of this surface creates electron-hole pairs. In addition to recombination processes, the holes may occupy the surface states, leading to positive charge formation at the surface states. The existence of surface states and surface state charge density, Q_{ss}, has been proposed in the literature. Allongue et al. estimated the surface state density for n-GaAs to be ~10^{13} states cm^{-2} [75]. Therefore, the illuminated naked surface would behave as a positively charged surface. Illumination of the naked n-GaAs surface will therefore produce positive shifts in the value of V_{fb}, with respect to the value of the naked surface measured in the dark. Up to 400 mV positive shifts in V_{fb} resulting from illumination of unmodified n-GaAs surfaces are reported, [75-76].

5.3. CAPACITANCE MEASUREMENTS:

Mott-Schottky (*M-S*) plots of C^{-2} *vs.* V were constructed in order to directly measure V_{fb} values [72].

In the dark, the V_{fb}, in M-S plots for the modified n-GaAs wafers, were shifted towards a more positive value. These results indicated that the positive shift in the value of V_{fb} is a result of only MnP ions. It was clear that annealing n-GaAs/MnP/Polysiloxane surfaces gives better interaction between the SC and the MnP. This was manifested by the larger shift in the V_{fb} value in case of annealing.

The n-GaAs surface modification enhanced the SC surface in another way as appears from Figures (4-6,7). The slope of the modified n-GaAs wafer gave a value for the measured doping density, **DD**, which is close to the authentic value of the SC.

This accuracy in the measured value of the **DD**, for the modified n-GaAs surface, is due to the added surface stability.

Under illumination, V_{fb} were measured for the modified and unmodified n-GaAs surfaces in the water/$LiClO_4$/$[Fe(CN)_6]^{3-}$/$[Fe(CN)_6]^{4-}$ system . The effect of n-GaAs surface modification was more pronounced. The low stability of the unmodified or the Polysiloxane- modified n-GaAs surface made it difficult to measure the **M-S** plots under illumination. Only did the annealed n-GaAs/MnP/Polysiloxane show soundly linear **M-S** plots under illumination by room light. These findings suggest that the MnP/Polysiloxane modification do indeed stabilize the n-GaAs surface under the un-favored working conditions used here.

5.4. STABILITY STUDIES:

The effect of modification on stabilizing the semiconductor surface was studied while using the aqueous $LiClO_4$/$[Fe(CN)_6]^{3-}$/$[Fe(CN)_6]^{4-}$ system. The stabilizing effect of polymer matrices attached to semiconductor surfaces has been reported earlier by other researchers. Attachment of polythiophene matrices to n-type semiconductor surfaces protected the surfaces from photodegradation [55-63]. However, the modified SC surfaces, described in literature, showed a major drawback. The short-circuit current, I_{sc} , was lowered by the polymer matrix. This effect is not favored in the PEC research, because the outcome would be a lowering in the PEC cell efficiency. In this work, the I_{sc} value was enhanced by modification with MnP/Polysiloxane. This is one major advantage of the work described here. In the absence of the MnP ions, the polysiloxane caused some SC surface stabilization, but the I_{sc} value was enhanced to a lesser extent.

At 25°C the polysiloxane-modified surface has a value of I_{sc} four-fold higher than that for the unmodified surface, when measured after 80-min exposure time. The MnP/Polysiloxane modified n-GaAs showed a rather higher I_{sc}, with about eight fold that of the unmodified surface. At 35°C the unmodified n-GaAs surface completely degraded after 200 min working time. The n-GaAs/MnP/Polysiloxane electrode showed higher stability to photodegradation, showing higher I_{sc} readings for longer times. The stabilizing effect of the MnP/Polysiloxane is therefore pronounced at temperatures in the range 25° to 35°C. At higher temperature, 45°C, the modified and the unmodified surfaces showed higher tendency to degrade than at lower temperature

5.5. Cell Efficiency Studies:

The light-to-current-conversion efficiency of the electrode was enhanced by modification. This efficiency enhancement is due to the photocurrent enhancement shown earlier for the modified electrode. Despite the fact that the value of the V_{oc} is shifted positive, which should lower the value of the measured out put power by about 20%, this was compensated for by an eight-fold increase in the value of the short-circuit current. As a net result, the cell efficiency was highly enhanced by modification with Mn/Polysiloxane. The polysiloxane modified n-GaAs also showed some enhancement in cell efficiency, but a lower extent.

5.6. MODE OF ACTION OF MnP IN STABILIZING THE SC:

n-GaAs is unstable to corrosion under PEC conditions in aqueous electrolytic solutions. At pH=7, for example, the expected corrosion half reaction is:

$$GaAs + 6H_2O + 6h^+ \rightarrow Ga(OH)_3 + As(OH)_3 + 6H^+ \qquad E = -0.45V\ (SCE)$$

These particular corrosion products passivate the surface in neutral solution because of the insolubility of the hydroxy compound [77]. Attempts to eliminate surface n-GaAs corrosion have been made. The stabilizing effect of the MnP/Polysiloxane matrices is due to two factors:

Firstly, the polymer matrix stabilizes the SC surface by preventing surface state formation and air oxidation of the surface.

Secondly, the MnP ions stabilize the surface by a different mechanism. Electrode decomposition reactions that are thermodynamically favored compared to electrolyte redox reactions are also generally kinetically favored. This undesirable situation can be alleviated through surface modification. It has been shown that attachment of redox species to SC surface can effect the kinetics of charge transfer across semiconductor-electrolyte junctions such that the less thermodynamically favored reactions predominate over thermodynamically favored reactions [78]. In our work, the presence of the Mn^{II}/Mn^{III} ions in the MnP/polysiloxane matrix furnishes additional redox couple in close proximity with the SC surface. Cyclic voltammometry indicated that the MnP has an oxidation potential at -0.160 V and a reductive potential at -0.450 V (SCE, at pH 6.5 under the experimental conditions). The oxidation potential for the MnP couple is less positive (more negative) than that for the holes generated in the valence band (-0.1 V for the unmodified n-GaAs, and

+0.1 V for the modified n-GaAs surface, *vs.* SCE, pH 7). Therefore, the holes will move upward to oxidize the Mn^{II}/Mn^{III} (MnP) redox couple that is in close proximity with the SC surface. The positive charge will in turn be transferred to the $Fe(CN)_6^{3-}$ $/Fe(CN)_6^{4-}$ redox couple, and current will occur. In this regard, the MnP is behaving as a catalyst that would speed up hole transfer to oxidize $Fe(CN)_6^{4-}$ rather than to the SC surface. In another words, illumination of n-GaAs modified with MnP will not result in the oxidation of n-GaAs but rather will result in the oxidation of $Fe(CN)_6^{4-}$ to $Fe(CN)_6^{3-}$ in the electrolyte. The attached MnP species acts as a hole mediator for n-GaAs, and channels the photogenerated hole to the $Fe(CN)_6^{4-}/Fe(CN)_6^{3-}$ redox reaction rather than to the n-GaAs degradation reaction, Fig. (5-4). Such a process would protect the SC surface from photodegradation, and would enhance the short-circuit current, as depicted in Figure (4-15→18). Similar processes have been suggested for other semiconductor surface. Attachment of ferrocene to n-Si surfaces stabilized it to photodegradation in aqueous $Fe(CN)_6^{3-}/Fe(CN)_6^{4-}$ systems. The ferrocene has been considered as a mediator that kinetically favors the charge transfer to the $Fe(CN)_6^{3-}/Fe(CN)_6^{4-}$ redox couple rather than to the SC surface [79]. This effect can be very useful in stabilizing electrodes in PEC cells.

The role of the MnP redox couple is therefore to kinetically speed up the charge transfer across the SC/liquid interface and consequently to speed up the hole transfer process from the accumulation region to the redox couple. Current enhancement and SC surface stabilization will thus result.

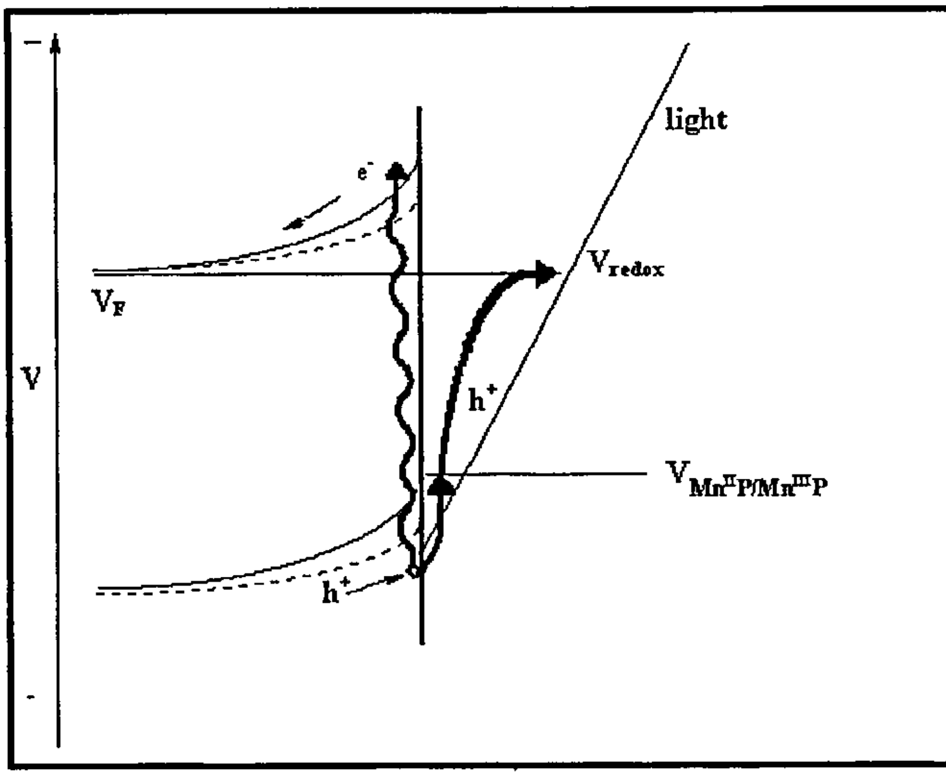

Figure (5-4): Showing how the MnP behaves as a catalyst, by taking the positive charge (hole) and relaying it to the redox couple. In this case the photocurrent will be enhanced and the SC surface degradation will be prevented.

5.7 CONCLUSION & SUGGESTIONS FOR FURTHER WORKS

5.7.1. Conclusions

- n-GaAs wafers, modified with tetra(-4-pyridyl)porphyrinatomanganese(II/III) sulphate encapsulated inside polysiloxane matrices, showed higher stability to degradation under PEC conditions, without sacrificing the value of the short circuit current.
- The values of the V_{fb} of the semiconductor were shifted towards more positive positions by modification.

- These enhancements were achieved, both in the dark and under illumination, using $H_2O/K_3Fe(CN)_6/K_4Fe(CN)_6/LiClO_4$ system, which is known to give poor results.
- Another major advantage of this new modification method is that the polymer layer adhered perfectly to the semiconductor surface without peeling out.
- Annealing the modified n-GaAs surface adds further enhancement to its characteristics.

5.7.2. Suggestions for further work:

Future investigations are to continue in two lines:

a) **The basic research** : which includes the following aspects:

- Controlling the SC band-edge positions by attaching thin films of different kinds of polymers especially conjugated ones.
- Chemically binding thin films of polymers to SC surfaces using different anchoring ligands.
- Studying the reproducibility of the new stabilizing method to other kinds of SC such as: n-$GaInP_2$, n-GaP, or n-InP.
- Applying different PEC experimental conditions such as using methanol as a solvent or using the Se^{2+}/Se_2^{2+} as a redox couple.
- Enhancing SC properties by high doping and trying to improve the SC crystal by controlling the rate of cooling of the annealed SC wafers.

b) **The applied research**: One of the most important applications of our results is the participation in the international efforts aimed at providing alternative energy sources. This can be achieved by utilizing solar energy in producing in producing hydrogen fuel and oxygen from PEC water splitting. This may be possible by applying our new findings to n-$GaInP_2$, which is known to be good candidate photocatalyst for light-driven water splitting into hydrogen and oxygen, Fig. (5-5). The modified n-$GaInP_2$ can be accompanied with other catalysts such as Pt particles and Ru complexes, which improve the hydrogen and oxygen production respectively.

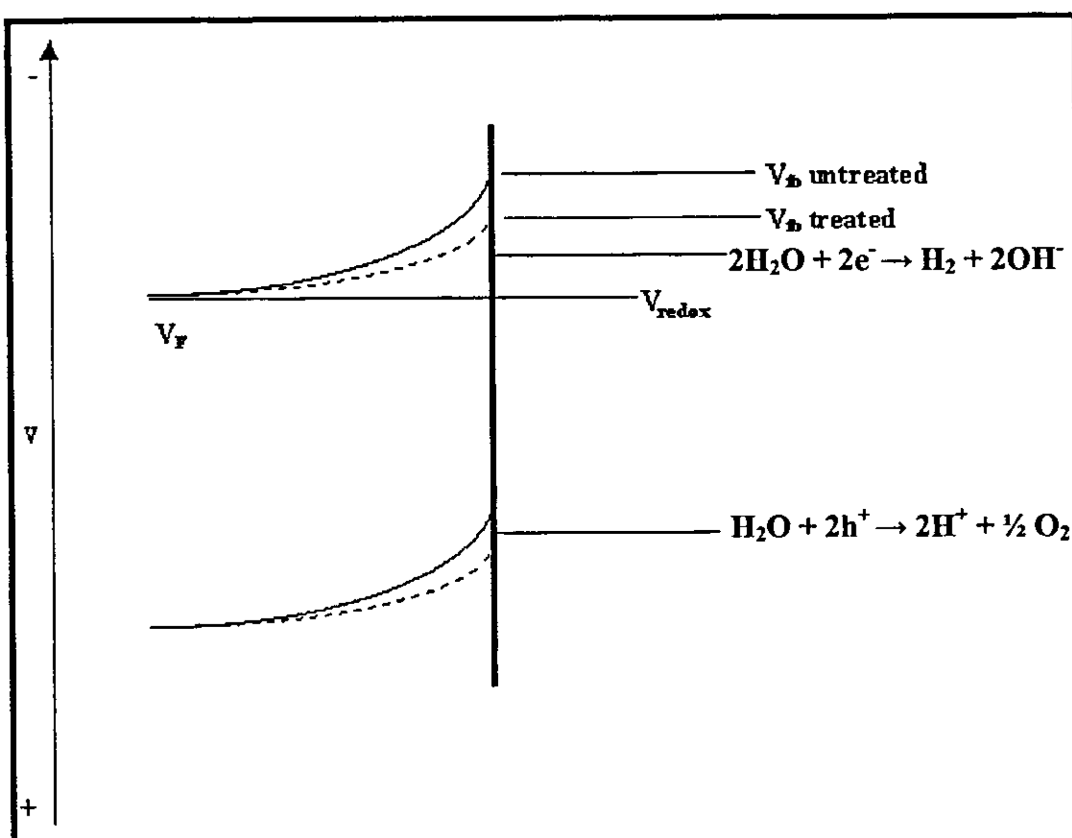

Figure (5-5): Energy correlation between band edges for n-$GaInP_2$ and the Fermi energies of water splitting reactions.

REFERENCES

1] L.Hollman, J.P.Hallais and J.C.Price, in "*Current Topics in Materials Science*", Vol. 5, ed. E.Kaldis, North Holland Publ. Co., (1980), p. 1.

2] K.W.Frese, Jr., in "*Semiconductor Electrodes*", ed. H.Finklea, Elsevier, Amsterdam, (1988), p. 373.

3] K.S.V. Santhanam, in "*Photoelectrochemical Solar Cells*", ed. K.S.V. Santhanam and M. Sharon, Elsevier,Amsterdam, Oxford, N.Y., Tokyo, (1988), pp. 1-14.

4] K. Rajeshwar, P. Singh, and J. DuBow, "*Energy conversion in photoelectrochemical systems – a review*", **Electrochim. Acta,** 23 (1978) 1117.

5] T. Watanabe, A. Fujishima and K. Honda in "*Energy Resources through Photochemistry and Catalysis*", ed. M. Gratzel, Academic Press, N.Y., (1983), pp. 361-362.

6] A. Fujishima, in "*Photoelectrochemical Solar Cells*", ed. K.S.V. Santhanam and M. Sharon, Elsevier, Amsterdam, (1988), pp. 190-195.

7] H. Finklea, in "*Semiconductor Electrodes*", ed. H. Finklea, Elsevier, Amsterdam, (1988), pp. 27-30.

8] S. Chandra, in "*Photoelectrochemical Solar Cells*", Gordon & Breach Science Publishers, New York, (1986), pp. 88-103.

9] K. Rajeshwar, P. Singh, and J. DuBow, "*Energy conversion in photoelectrochemical systems – a review*", **Electrochim. Acta,** 23 (1978) 1118.

12] P. Calza, C. Minero, A. Hiskia, E. Papacostantinou and E. Pelizzetti, "*Photolytic and photocatalytic decompotion of bromomethanes in irradiated aqueous solutions*", **Appl. Catal. B,** 21(1999) 191-202.

13] K.-H. Wang, H.-H. Tsai and Y.-H.Hsieh, "*The kinetics of photocatalytic degradation of trichloroethelen in gas phase over TiO_2 supported on glass bead*", **Appl. Catal. B,** 17(1998) 313-320.

14] K.-H. Wang, Y.-H. Hsieh, M.-Y. Chou and C.-Y. Chang, "*Photocatalytic degradation of 2-chloro and 2-nitrophenol by TiO_2 suspensions in aqueous solution*", **Appl. Catal. B,** 21(1999) 1-8.

15] V. Iliev, V. Alexiev and L. Bilyarska, "*Effect of metal phthalocyanine complex aggregation on the catalytic and photocatalytic oxidation of sulfer containing compounds*", **J. Mol. Catal. A,** 137 (1999) 15-22.

16] T. Sluchinskaya, N. Kundo, L. Gogina, U. Schubert, A. Lorenz and V.Maizlish,"*Cobalt phthalocyanine derivatives supported on TiO_2 by sol-gelprocessing*", **J. Mol. Catal. A,** 140 (1999) 235-240.

17] S.-M. Chen, "*The photocatalytic autoxidation of sulfur oxoanions by water soluble porphyrin complexes*", **J. Mol. Catal. A,** 138 (1999) 1-13.

18] A.-M. A. Abdel-Wahab and A. E.-A. M. Gaber, "*TiO_2-Photocatalytic oxidation of selected hetrocyclic sulfur compounds*", presented , in part, in XI Inter National Conference on Photochemical Conversion and Storage of Solar Energy (IPS-11). Ed, V. Krishnan, July 28-August 2, 1996, Bangalore, India (1996), p.167.

19] P. Qu, J.Zhao, T. Shen and H. Hidaka , "*TiO_2-assisted photodegradationof dyes*", **J. Mol. Catal. A,** 129 (1998) 257-268.

20] K. Wu, Y. Xie, J. Zhao and H. Hidaka, "*Photo-Fenton degradation of a dye under visible light irradiation*", **J. Mol. Catal. A,** 144 (1999) 77-84.

21] V. Loddo, G. Marci, C. Martin, L. Palmisano, V. Rives and A. Sclafani, "*Preparation and characterisation of TiO_2 (anatase) supported on TiO_2 (rutile) catalysts employed for 4-nitrophenol photodegradation in aqueous medium and comparison with TiO_2 (anatase) supported on Al_2O_3*", **Appl. Catal. B,** 20 (1999) 29-45.

22] I. Ilisz, Z. Laszlo and A. Dombi, "*Investigation of the photodecomposition of phenol in near-UV-irradiated aqueous TiO_2 suspensions. I: Effect of charge-trapping species on the degradation kinetics*", **Appl. Catal. A,** 180 (1999) 25-33.

23] I. Ilisz, and A. Dombi, "*Investigation of the photodecomposition of phenol in near-UV-irradiated aqueous TiO_2 suspensions. II: Effect of charge-trapping species on product distribution*", **Appl. Catal. A,** 180 (1999) 35-45.

24] J. Matos, J. Laine, J.-M. Herrmann, "*Synergy effect in the photocatalytic degradation of phenol on a suspended mixture of titania and activated carbon*", **Appl. Catal. B,** 18 (1998) 281-291.

25] J. A. Byrne, B. R. Eggins, N. M. D. Brown, B. McKinney, and M. Rouse, "*Immobilization of TiO_2 powder for the treatment of polluted water*", **Appl. Catal. B,** 17 (1998) 25-36.

26] S. Malato, J. Blanco, C. Richter, B. Braun and M. I. Maldonado, "*Enhancement of the rate of solar photocatalytic mineralization of organic pollutants by inorganic oxidizing species* ", **Appl. Catal. B,** 17 (1998) 347-356.

27] L. Sanchez, J. Peral and X. Domenech, "*Aniline degradation by combined photocatalysis and ozonation*", **Appl. Catal. B**, 19 (1998) 59-65.

28] A. E. Regazzoni, P. Mandelbaum, M. Matsuyoshi, S. Schiller, S. Bilmes, and M. Blesa, "*Adsorption and photooxidation of salicylic acid on titanium dioxide: A surface complexation description*", **Langmuir**,14 (1998) 868-874.

29] B. Bems, F. C. Jentoft, R. Schlogl, "*Photoinduced decomposition of nitrate in drinking water in the presence of titania and humic acids*", **Appl. Catal. B,** 20 (1999) 155-163.

30] L. B. Khalil, W. E. Mourad, and M. W. Rophael, "*Photocatalytic reduction of enviromental pollutant Cr(VI) over some semiconductors under UV/visible light illumination*", **Appl. Catal. B**, 17 (1998) 267-273.

31] J. A. Byrne, B. R. Eggins, W. Byers, and N. M.D. Brown, "*Photoelectrochemical cell for the combined photocatalytic oxidation of organic pollutants and the recovery of metals from waste waters*", **Appl. Catal. B**, 20 (1999) L85-L89.

32] T. Sakata, T, Kawai, in "*Energy resources through Photochemistry and catalysis*", ed. M. Gratzel, Academic Press, N.Y., (1983), pp. 359-364 .

33] K. Rajeshwar, P. Singh, and J. DuBow, "*Energy conversion in photoelectrochemical systems – a review*", **Electrochim. Acta**, 23 (1978) 1132.

34] Y. V. Pleskov, "*Solar energy conversion; A Photochemical Approach*", Springor, N.Y., (1990), p. 46.

35] S. Wagner, in "*Solid state chemistry of energy conversion and storage: Advanced in chemistry series 163*", ed. J. B. Goodenough, and M. S. Whittingham, American chemical society, Washington, (1977), pp. 359-364 .

36] P. Allongue, and H. Cachet, "*Photodissolution kinetics of n-GaAs in 1M KOH and calculation of the stabilization by Se^{2-} effect of the Ru^{3+} surface treatment*", **J. Electrochem. Soc.**, 131 (1984) 2861.

37] A. Kraft, B. Gorig and K.-H. Heckner, "*ITO coated n-GaAs electrodes for photoelectrochemical solar cell*", **Solar energy materials and solar cells**, 32 (1994) 151-158.

38] K. Rajeshwar, P. Singh, and J. DuBow, "*Energy conversion in photoelectrochemical systems – a review*", **Electrochim. Acta**, 23 (1978) 1136-1137.

39] P. Allongue, and G. Horowitz, "*Detailed analysis of a redox stabilized liquid junction solar cells*", **J. Electrochem. Soc.**, 130 (1983) 2352.

40] J. J. Kelly, R. Memming, "*The influence of surface recombination and trapping on the cathodic photocurrent at p- type III-V electrodes*", **J. Electrochem. Soc.**, 129 (1982) 730-738.

41] Y. Pleskov, "*Solar energy conversion; A Photochemical Approach*", Springor, N.Y., (1990), p. 81.

42] R. W. Murray, in "*Electroanalytical Chemistry: A series of advances*", ed. A. J. Bard, Vol. 13, Marcel Dekker, N.Y., (1982), pp. 345-346.

43] M. E. Langmuir, M. A. Parker, and R. D. Rauh, "*Electrochemical photovoltaic cells based on n-GaAs and the Triiodide / Iodide redox couple in acetonitrile*", **J. Electrochem. Soc.**, 129(1982) 1705-1710.

44] B. A. Parkinson, A. Heller, and B. Miller, "*Effect of cations on the performance of the photoanode in the n-GaAs |K_2Se-K_2Se_2-KOH| C Semiconductor liquid junction solar cells*", **J. Electrochem. Soc.**, 126 (1979) 954-959.

45] A. Bansal, M. X. Tan, B. J. Tufts, and N. S. Lewis, "*Distinguishing between buried semiconductor/metal contacts and hybrid semiconductor/metal/liquid contacts at n-GaAs/KOH-$Se^{-/2-}_{(aq)}$ junctions*", **J. Phys. Chem.**, 97 (1993) 7309-7315.

46] Y. Wada, and K. Wada, "*GaAs surface passivation by deposition of an ultrathin InP-related layer*", **Appl. Phys. Lett.**, 63(3) (1993) 379.

47] M. Tabib-Azar, S. Kang, A.N. MacInnes, M. B. Power, A. R. Barron, Ph. P. Jenkins, and A. F. Hepp, "*Electronic passivation of n- and p-type GaAs using chemical vapor deposited GaAs*", **Appl. Phys. Lett.**, 63(5) (1993) 625.

48] E. F. Schubert, M. Passlack, M. Hong, R. L. Opila, L. N. Pfeiffer, K. W. West, C. G. Bethea, and G. J. Zydzik, "*Properties of Al_2O_3 optical coatings on GaAs produced by oxidation of epitaxial AlAs/GaAs films*", **Appl. Phys. Lett.**, 64(22) (1994) 2976.

49] K. W. Voget, and P. A. Kohl, "*Gallium arsinide passivation through nitridation with hydrazine*", **Appl. Phys.**, 74(10) (1993) 6448.

50] A. J. Nozik, in "*Photovoltaic and Photochemical Solar Energy conversion*", ed. F. Cardon, W. P. Gomes, and W. Dekeyser, Plenum Press, N.Y., (1980), pp. 307-308.

51] K. Rajeshwar, P. Singh, and J. DuBow, "*Energy conversion in photoelectrochemical systems – a review*", **Electrochim. Acta**, 23 (1978) 1134-1135.

52] S. S. Kocha and J. A. Turner, "*Displacement of the Bandedges of $GaInP_2$ in Aqueous Electrolytes Induced by Surface Modification*", **J. Electrochem. Soc.**, 142 (1995) 2625.

53] S. S. Kocha and J. A. Turner, "*Impedance Analysis of Surface Modified $Ga_{0.5}In_{0.5}P$-Aqueous Electrolyte Interface*", **Electrochim. Acta**, 41 (1996) 1296.

54] J. M. Bolts, and M. S. Wrighton, "*Chemically derivatized n-type Gallium Arsenide photoelectrodes. Thermodynamically uphill oxidation of surface-attached ferrocene centers*", **J. Am. Chem. Soc.**, 101(21) (1979) 6179-6183.

55] A. J. Frank, in "*Energy Resources through Photochemistry and Catalysis*", ed. M. Graetzel, Academic Press, N.Y., (1983), p. 467.

56] A. J. Frank and K. Honda, "*Visible-Light-Induced Water Cleavage and Stabilization of n-Type CdS to Photocorrosion with Surface-Attached Polypyrrole-Catalyst Coating*", **J. Phys. Chem.**, 86 (1982) 1933.

57] R. Noufi, A. J. Frank and A. J. Nozik, "Stabilization of n-Type Silicon Photoelectrodes to Surface Oxidation in Aqueous Electrolytes Solution and Mediation of Oxidation Reaction by Surface-Attached Organic Conducting Polymer", **J. Am. Chem. Soc.**, 103 (1981) 1849.

58] R. Noufi, D. Tench, and L. F. Warren, "*Stabilization Of n-CdSe Photoanodes in non aqueous $Fe(CN)_6^{3-/4-}$ [Ferro- Ferricyanide] electrolytes*", **J. Electrochem. Soc.**, 128 (1981) 2596.

59] A.J.Frank, "*Photoelectrochemical Solar Cells: Stabilization of Small Band Gap Simiconductor in Aqueous Solution by Surface-Attached Organic Conducting Polymer*", **Mol. Cryst. Liq. Cryst.**, 83 (1982) 341.

60] A. J. Frank, S. Glenis, and A. J. Nelson, "*Conductive polymer-semiconductor junction: characterization of poly(3-methylthiophene):cadmium sulfide based photoelectrochemical and photovoltaic cells*", **J. Phys. Chem.**, 93 (1989) 3818.

61] Fu-Jann Pern, and A.J.Frank, "*Electrochemical and Optical Characterization of Poly(3-methylthiophene) : Effect of Solvent, Anion, and applied Potential*", **J. Electrochem. Soc.**, **137** (1990) 2769.

62] S. Glenis and A. J. Frank, "*schottky barrier formation between poly(3-methylthiophene) and n-type cadmium sulfide*", **Synth. Met.**, 28 (1989) C681.

63] R. Noufi, A. J. Frank, J. White and L. F. Warren, "*Enhanced Stability of Photoelectrodes with electrogenerated Poly Aniline Films*", **J. Electrochem. Soc.**, 120 (1982) 2261.

64] J. Premkumar, and R. Ramaraj, "*Photoreduction of dioygen to hydrogen peroxide at porphyrins and phthalocyanines adsorbed Nafion membrane*", **J. Mol. Catal. A**, 142 (1999) 153-162.

65] S.M.S. Chauhan, B. Kalra, and P.P. Mohapatra, "*Oxidation of 1- naphthol and related phenols with hydrogen peroxide and potassium superoxide catalyzed by 5,10,15,20-tetraarylporphyrinatoiron(III)chlorides in different reaction conditions*", **J. Mol. Catal. A**, 137 (1999) 85-92.

66] S. S. Kocha, M. Peterson, H. S. Hilal, D. Arent and J. A. Turner, "*Photoelectrochemical Based Direct Conversion Systems*", in " Proc. 1994 DOE/NREL Hydrogen Program Rev.", Livermore, Ca., April 18-21, (1994).

67] H. S. Hilal, C. Kim and A. F. Schreiner, "*Preparation &Characterization of Tetra(-4-pyridyl)porphyrinatomanganese Cation Supported Covalently on Poly(siloxane)*", **J. Mol. Catal.**, 64 (1991) 133; "*Preparation &Characterization of Poly(siloxane)-Supported Metalloporphyrins: The Effect of the Support on the Electronic Absorption Spectra*", **Inorg. Chim. Acta**, 189 (1991) L141.

68] N. Kobayashi, H. Seiki, T. Osa, "*Catalytic Electroreduction Of Molecular Oxygen using [5,10,15,20-tetrakis-(1-methylpyridinium-4-yl)porphinato]manganese*", **Chem. Lett.** (1985) 1917.

69] A. Bansal, M. X. Tan, B. J. Tufts, and N. S. Lewis, "*Distinguishing between buried semiconductor/metal contacts and hybrid semiconductor/metal/liquid contacts at n-GaAs/KOH-$Se^{-/2-}_{(aq)}$ junctions*", **J. Phys. Chem.**, 97 (1993) 7309.

70] B. J. Clark, T. Frost, and M. A. Russell, "*U.V. Spectroscopy*", Chapman & Hall, London, (1993), p.p. 18-21.

71] James D. Ingle, Jr. Slanby, R. Crouch, "*Spectrochemical Analysis*", Prentice Hall Englewood, New Jersey, (1988), p. 95.

72] J. A. Turner, "*Energetics of the Semiconductor-Electrolyte Interface*", **J. Chem. Edu.**, 16 (1983) 327.

73] J. E. Huheey, "*Inorganic Chemistry Principles of Structure and Reactivity*", 3rd ed., Harper International si, Cambridge, (1983), pp. 370-371.

74] S. S. Kocha, J. A. Turner and A. J. Nozik, "*Study of the Schottky barrier and determination of the energetic positions of band edges at the n- and p- type gallium indium phosphide electrode/electrolyte interface*", **J. Electrochem. Soc.**, 367 (1994) 27.

75] P. Allongue, H. Cavhet, and G. Horovitz, "*Detailed Analysis of a Redox-Stabilized Liquid Junction Solar Cell*" **J. Electrochem. Soc.: Electrochem. Sci. and Technolo.**, 130 (1983) 2352.

76] H. Hilal, J. Turner, and A. Frank, "*Tailoring The Energetics and Kinetics of Interfacial Charge Transition at The Semiconductor/Liquid Junction: Chemically Modified n-GaAs*", in the course of publication.

77] Karl W. Frese, JR, in "*Semiconductor Electrodes*", ed. H. O. Finklea, Amsterdam, (1988), p.382

78] K. W. Frese, Jr., in "*Semiconductor Electrodes*", ed. H. Finklea, Elsevier, Amsterdam, (1988), p. 373.

79] A. J. Nozik, in "*Photovoltaic and Photochemical Solar Energy conversion*", ed. F.Cardon, W. P. Gomes, and W. Dekeyser, Plenum Press, N.Y., (1980), p.297-280.

Appendix 1

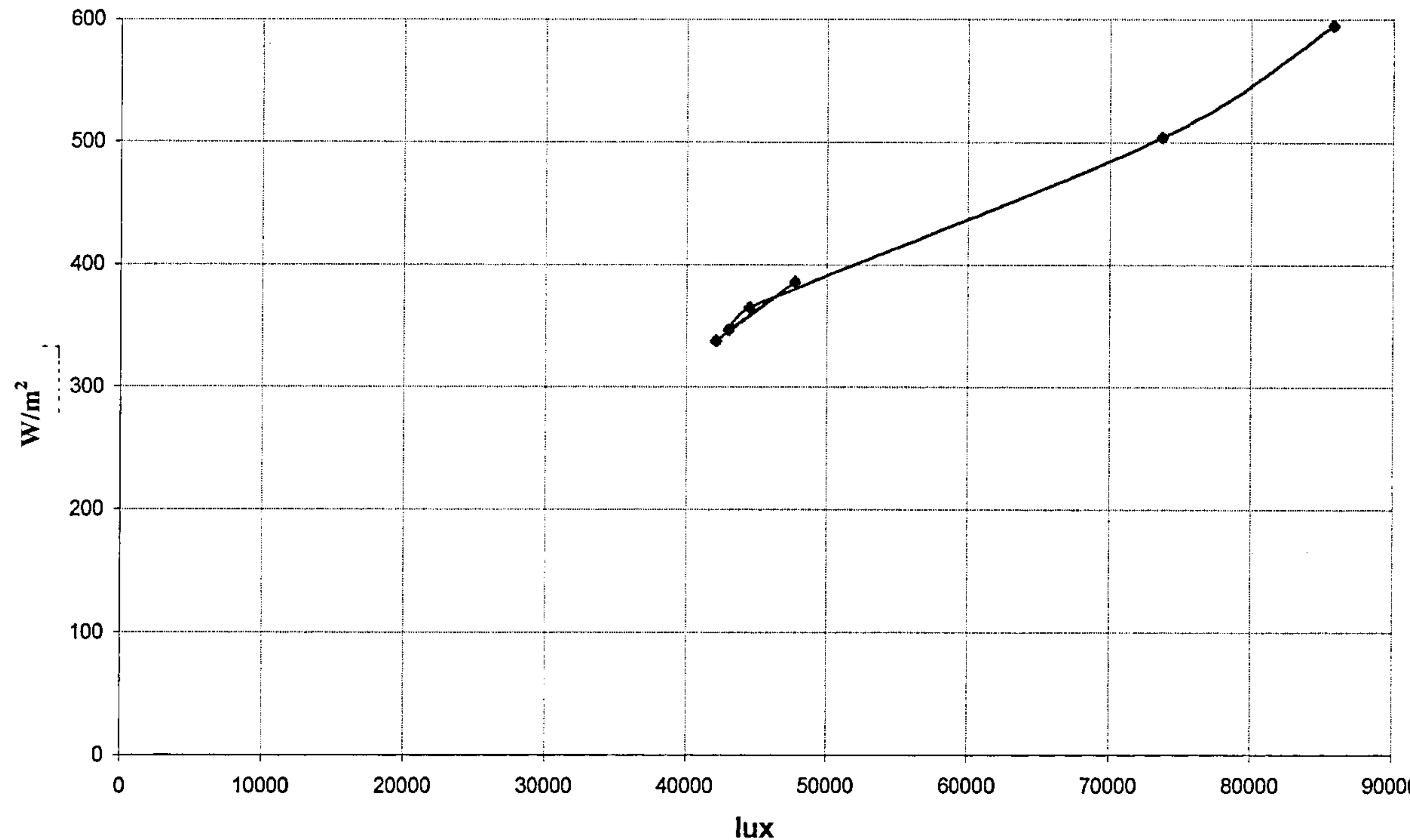

A-1: Calibration curve for lightmeter to exchange the illuminance (in lux) into irradiance (in W/m^2). For details see 2.3.1 Measuring devices, p. 38.

Appendix 2

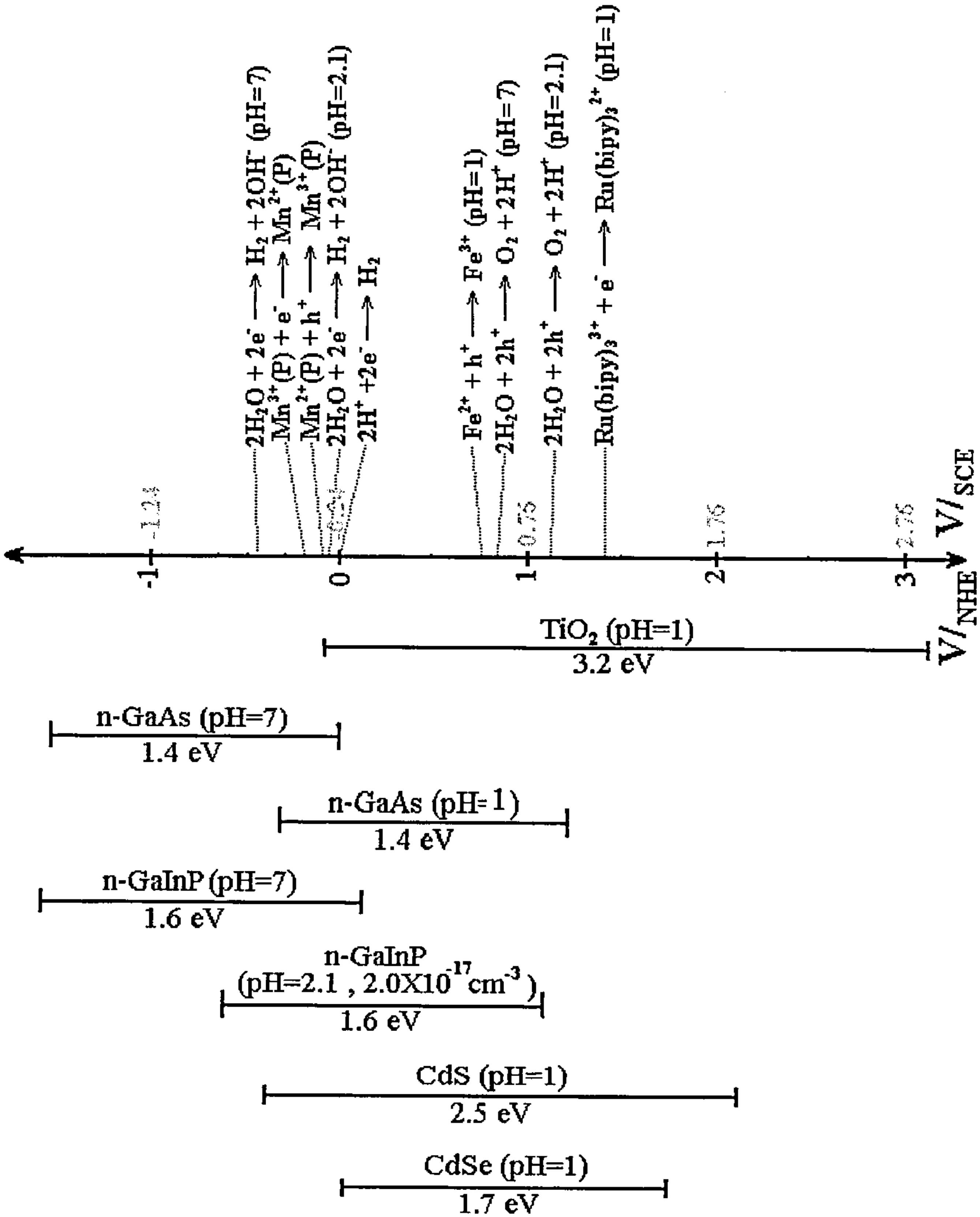

$2H_2O + 2e^- \longrightarrow H_2 + 2OH^-$ (pH=7)
$Mn^{3+}(P) + e^- \longrightarrow Mn^{2+}(P)$
$Mn^{2+}(P) + h^+ \longrightarrow Mn^{3+}(P)$
$2H_2O + 2e^- \longrightarrow H_2 + 2OH^-$ (pH=2.1)
$2H^+ + 2e^- \longrightarrow H_2$
$Fe^{2+} + h^+ \longrightarrow Fe^{3+}$ (pH=1)
$2H_2O + 2h^+ \longrightarrow O_2 + 2H^+$ (pH=7)
$2H_2O + 2h^+ \longrightarrow O_2 + 2H^+$ (pH=2.1)
$Ru(bipy)_3^{3+} + e^- \longrightarrow Ru(bipy)_3^{2+}$ (pH=1)
-1.24
-0.24
0.75
1.76
2.76
$V/_{SCE}$
-1
0
1
2
3
$V/_{NHE}$
TiO_2 (pH=1)
3.2 eV
n-GaAs (pH=7)
1.4 eV
n-GaAs (pH=1)
1.4 eV
n-GaInP (pH=7)
1.6 eV
n-GaInP
(pH=2.1 , $2.0X10^{-17} cm^{-3}$)
1.6 eV
CdS (pH=1)
2.5 eV
CdSe (pH=1)
1.7 eV

Appendix 3: Glossary

Band gab (E_g)	:	The difference between the lower limit of the conduction band and the upper limit of the valence band.
Bulk state	:	An intermediate energy level at the interior (bulk) of the SC.
Conduction band (CB)	:	The lowest empty energy band
Chemical bias	:	Potential resulting from oncoming ionic species.
Chemical vapor deposition	:	A technique used to prepare SC by allowing gaseous reactions to deposit the solid SC.
Diffusion layer (D)	:	The thickness of electrolyte where the ion concentrations deviate from the bulk electrolyte values.
Degeneracy	:	Having relatively high concentration of carriers.
Depletion layer	:	A situation formed when the applied potential moves positive of V_{fb} minority carriers (holes) accumulate at the surface and the majority carriers are removed from the surface.
$E_{c,s}$	:	The energy of the conduction band edge at the surface
$E_{v,s}$	:	The energy of the valence band edge at the surface
Cell efficiency	:	Maximum measured power (W cm^{-2})/ illuminance intensity (W cm^{-2})] X 100%.
Cell output power	:	A quantity calculated by multiplying the measured I_{sc} (at 0.0 V) by the corresponding V_{oc} value for the electrode.
Electron mobility	:	A convenient measurement of speed of motion of electrons in a field, defined as velocity per applied electric field, units (m^2 s^{-1} V^{-1}).

Fermi energy level	:	The energy (E_f) at which the probability of an energy level being occupied by an electron is exactly ½ .
Fill factor	:	Ratio between maximum measured cell power divided by calculated (expected) cell power.
Flat-band potentials (V_{fb})	:	The unique potential for which the potential drop between the surface and the bulk of the electrode is zero (no SCL)
Helmholtz layer (Hz)	:	The region between the electrode surface and the plane of closest approach for ions.
Illuminance	:	The power (Φ) incident per unit area (for visual light)
Irradiance	:	The power (Φ) incident per unit area (concerning energetic aspects of light)
J_{an} = anodic current density	:	The current resulting from the holes flowing per unit area of the electrode.
J_{cat} = cathodic current density	:	The current resulting from the electrons flowing per unit area of the electrode.
Open-circuit voltage	:	The negative applied potential that makes the SCL thickness decreases and goes to zero (bands are flattened) and the photocurrent drops sharply.
Passivation	:	Making the SC inactive
Photodegradation	:	The decomposition of a certain substance utilizing the light energy.
Quantum efficiency	:	The number of electrons flowing from the PEC system per one absorbed photon
Schottky barrier	:	A metal-semiconductor junction that has rectifying characteristics .
Short-circuit current (I_{sc})	:	The current flowing between the two sides of SC while they are connected with a metal wire (the applied potential = 0.00V)

Space charge layer (SCL)	:	The presence of a charge, resulting from the charged doping sites or the accumulation of holes or electrons, occupying the volume near the surface
Stabilization coefficient	:	The fraction of the photocurrent associated with the oxidation of the redox couple over the total photocurrent
Surface recombination velocity (SRV)	:	The velocity at which the excited hole and electron annihilate one another indirectly via a surface state.
Surface state	:	An intermediate energy level at the surface of the SC.
Surface state density	:	Number of surface states per unit area.
Valence band (VB)	:	The highest filled energy band.

لوجود بورفرينات المنغنيز. حيث أشارت منحنيات موت-شوتكي (Mott-Sckotky plots) إلى وجود إزاحة موجبة في جهد الحزمة المستوية. كما أكدت ذلك وجود إزاحة موجبة في قيم كل من جهد الانطلاق (Onset potential) لتيار الظلمة (Darkcurrent) وجهد الدارة المفتوحة (Open circuit potential) للتيار الضوئي (Photocurrent). وعلى النقيض مما أظهرته التقارير السابقة فأن قيمة تيار الدارة المختصرة (Short-circuit current) لشبه الموصل المعالج قد أظهرت تحسنا ملحوظا لدى قياسها بعد زمن من التعرض للضوء. إضافة إلى ذلك فان شبه الموصل المعالج قد أظهر ثباتا أكثر في مقاومة التحطم الضوئي مقارنة بشبه الموصل غير المعالج. كما أن كفاءة الخلية تحسنت بشكل ملحوظ.

ملخص

يجري حاليا البحث في أشباه الموصلات كعوامل مساعدة للاستفادة من الطاقة الشمسية. وفي واحد من أهم التطبيقات للخلايا الكهروكيموضوئية (Photoelectrochemical cells)، حيث تستخدم سطوح أشباه الموصلات كعوامل مساعدة لتحليل الماء إلى غازي الهيدروجين والأكسجين باستخدام الضوء. ولسوء الحظ وحتى الآن، لا يوجد أي شبه موصل تتوفر فيه مزايا العامل المساعد الملائم لتحليل الماء. لذا بات من المرغوب فيه إزاحة حواف حزم الطاقة (Energy Band Edges) في شبه الموصل بشكل إيجابي لتسهيل عبور الشحنات لسطح شبه الموصل، وتحسين مقاومة ذلك السطح للتلف والتآكل.

لقد قمنا بتطوير تقنية جديدة للتحكم بمواقع حواف حزم الطاقة في شبه الموصل. حيث طمرت كبريتات رباعي (٤-بريديل) بورفرينات المنغنيز (٣) (Tetra(-4-pyridyl)porphyrinatomanganese(III)sulfate) والتي تحوي خليطاً من أيونات المنغنيز Mn^{2+} و Mn^{3+}) في نسيج من مبلمر عديد السايلوكسان (polysiloxane) وتم تثبيته على سطح رقائق النوع السالب من أرزينيد الغاليوم (n-GaAs). ومن ثم شوي شبه الموصل المعالج بالمبلمر والبورفرينات في جو من النيتروجين تمهيدا لاستخدامه في دراسة كهروكيموضوئية اِستُخدِم فيها الماء وفوق كلورات الليثيوم بالإضافة إلى سداسي سيانيد الحديد (II) وسداسي سيانيد الحديد (III) كزوج تأكسد-اختزال. أكدت النتائج وجود إزاحة إيجابية (Positive shift) في جهد الحزمة المستوية (Flat band potential) لشبه الموصل نتيجة